UNIVERSIDADE FEDERAL DE SÃO CARLOS
CENTRO DE CIÊNCIAS EXATAS E DE TECNOLOGIA
DEPARTAMENTO DE QUÍMICA
PROGRAMA DE PÓS-GRADUAÇÃO EM QUÍMICA

"Synthesis and characterization of micro-and mesoporous materials for catalytic biomass upgrading"

Erlen Yizenia Cruz Jorge *

Tese apresentada como parte dos requisitos para obtenção do título de DOUTORA EM CIÊNCIAS, área de concentração: QUÍMICA ORGÂNICA.

Orientador: Prof. Dr. Márcio Weber Paixão

*** bolsista CAPES**

São Carlos - SP

2019

UNIVERSIDADE FEDERAL DE SÃO CARLOS

Centro de Ciências Exatas e de Tecnologia
Programa de Pós-Graduação em Química

Folha de Aprovação

Assinaturas dos membros da comissão examinadora que avaliou e aprovou a Defesa de Tese de Doutorado da candidata Erlen Yizenia Cruz Jorge, realizada em 16/05/2019:

Prof. Dr. Márcio Weber Paixão
UFSCar

Prof. Dr. Ernesto Antonio Urquieta Gonzalez
UFSCar

Prof. Dr. Ivo Freitas Teixeira
UFSCar

Profa. Dra. Liane Marcia Rossi
USP

Prof. Dr. Leandro Helgueira de Andrade
USP

This study was financed in part by the *Coordenação de Aperfeiçoamento de Pessoal de Nível Superior* - Brasil (CAPES) - Finance Code 001.

For my dear parents (Angel and Yiliam)

and my husband Orlando

Acknowledgements

First, I want to thank God for giving me strength, health and guiding me every day of my life.

To CAPES for the doctoral program and the Postgraduate Program in Chemistry – UFSCar.

To my advisers Professor Dr. Márcio W. Paixão (UFSCar) and Prof. Dr. Daniel G. Rivera (LPN-FQ-UH) for allowing me to carry out this work in their research group, for transfer of knowledge, advice and teachings not only for the realization of this thesis but also for my growth as a person.

To Dr. Carolina G. S. Lima and Dr. Thiago M. Lima for all the knowledge transmitted both in the laboratory and conceptual, for dedicating me the time they do not have and always be willing to do it no matter the day or time.

Prof. Dr. Arlene G. Corrêa, Prof. Dr. Ricardo S. Schwab and All UFSCar laboratory staff for allowing me to work in a reference center like this one, in which I have been able to train in the field of research.

To the Institute of Science and Technology of Materials (IMRE) and to the Faculty of Chemistry of the University of Havana for giving me the possibility of entering this doctoral program.

To all my IMRE work colleagues for covering me all the time, to give me their help and unconditional support, especially to Lili, Patri, Chava, Juanito that without them I would not be here.

To my friends throughout the university, more than friends are the brothers that life did not give me but thank God I have them: Yaque, Sandri, Alfredo, Dario and the "new acquisitions" Elaine, Noe, Linna, Katia that have demonstrated me that friendship has no limits and that distance is never an impediment to being present and helping each other. I thank them for always being by my side no matter day, time and situations.

To the friends that I have made here in Brazil who have supported me unconditionally and have been helping me all the time my anguish and discomforts day and night: Dianne, Jose, Radell, Fidel, Valeria, Humberto and Juan.

To my doctors in Cuba (Saragilda, Gema, Guilfredo, Alien, Zullin, Sergio) that thanks to all their care, treatments, consultations both in Cuba and in the distance allowed me to finish the PhD thesis when I thought it was impossible.

To my working colleagues in the natural products laboratory and the Center of Excellence for Research in Sustainable Chemistry (CERSusChem) of the UFSCar, especially Markito.

To the post-graduation girls, Cristina Motta, Ariane, Rejiana and Luciani for all the help and guidance provided.

To all the people who in one way or another have been part of this thesis and my training as a professional throughout my life because without their collaboration and support this work would not have been possible.

To my Brazilian family that could not be better to Elsi, Marcos, Camila, Jose and Amelia for their welcome, attention, concern, affection and love.

My whole family, the real one, who throughout my career as a student has been by my side, has supported me, given strength and shown their love. Some of them are no longer there but I know where they are, they continue to take care of me.

To my parents and my husband to whom this thesis is dedicated and my two previous theses for being the most important and precious people in my life. There are no words to express the admiration, gratitude, pride and love I feel for them. Thanks for the patience, for tolerating my bad moments, moods and remoteness, for the sleepless nights, for the continuous teachings, for impelling me to be better every day not only as a person but also as a professional. Thank you for always getting the best out of me even though many times they receive the worst part of me, thanks for making me happy, for being as they are and for being unconditionally by my side.

List of Table

List of Figure

List of Scheme

Abstract

SYNTHESIS AND CHARACTERIZATION OF MICRO- AND MESOPOROUS MATERIALS FOR CATALYTIC BIOMASS UPGRADING. In the last years, biomass, especially lignocellulosic, has emerged as an alternative source of carbon. From the fractionation of lignocellulosic biomass, a series of chemical compounds or platforms can be obtained, having multiple industrial applications: lubricants, solvents, additives for fuels and personal hygiene products. Industrially, the fractionation process uses mineral acids, high temperatures and pressure, which has led to the emergence of solid catalysts such as micro and mesoporous materials. These are separated from the reaction medium more easily and are usually less industrially aggressive. On the other hand, to carry out the fractionation of the lignocellulosic biomass, catalysts with both Brönsted and Lewis sites are needed. So far, to carry out the different steps of this fractionation are used mixtures of catalysts, one that works as Brönsted acid and other as Lewis acid. The objective of this work is to synthesize bifunctional catalysts that are able to perform cascade reactions for the recovery of compounds derived from lignocellulosic biomass. To achieve this, two catalysts were synthesized, characterized and evaluated: zeolite-β magnetically recoverable in its acid form and exchanged with transition metal ions such as iridium, iron and palladium; as well as dendritic silica functionalized with sulfonic acid. Despite the enormous industrial importance of zeolites, their applications in technological processes in which high added value products are obtained and involving large molecules are limited due to the small size of their pores. The need of materials with a pore size greater than a nanometer boosted research in the field of materials science through the synthesis of mesoporous materials. In the present work, we proceeded to the synthesis of two materials: one microporous, very useful for the valorization of small molecules and another mesoporous, for the fractionation of more complex molecules such as sugars and disaccharides.

Resumo

SÍNTESE E CARACTERIZAÇÃO DE MATERIAIS MICRO E MESÓPOLOS PARA PROMOÇÃO DE BIOMASSA CATALÍTICA. Nos últimos anos, a biomassa, especialmente a lignocelulósica, surgiu como uma fonte alternativa de carbono. O fraccionamento do mesmo pode resultar num certo número de plataformas ou compostos químicos que têm muitas aplicações industriais, incluindo o uso como lubrificantes, solventes, aditivos de combustíveis e de produtos de higiene pessoal representa. Industrialmente, o processo de fracionamento utiliza ácidos minerais, altas temperaturas e pressão, o que levou ao surgimento de catalisadores sólidos, como materiais micro e mesoporosos. Estes são separados do meio de reação mais facilmente e são geralmente menos industrialmente agressivos. Por outro lado, para realizar o fraccionamento da biomassa lignocelulósica, são necessários catalisadores que possuam locais ácidos de Brönsted e Lewis. Até agora, para realizar os diferentes passos deste fracionamento, são utilizadas misturas de catalisadores, um que funciona como ácido de Brönsted e outro como ácido de Lewis. O objectivo deste trabalho é a de sintetizar catalisadores bifuncionais que são capazes de realizar reacções de cascatas de recuperação de compostos derivados a partir da biomassa lenhocelulica. Para este fim, foram sintetizados, caracterizados e testados dois catalisadores de zeólito:-p magneticamente recuperável na sua forma ácida e permutados com metais de transição, tais como o irídio, ferro e iões de paládio e dendrimétrica sílica funcionalizado com o ácido sulfónico. Apesar do enorme importância industrial dos zeólitos, as suas aplicações em processos tecnológicos onde os produtos de elevado valor acrescentado são obtidas e que envolvem moléculas grandes estão limitados pelo pequeno tamanho dos seus poros. A necessidade de materiais com um tamanho de poro maior do que um nanômetro impulsionou a pesquisa no campo da ciência dos materiais através da síntese de materiais mesoporosos. Considerando o acima exposto, no presente trabalho procedeu-se à síntese de dois materiais: um microporosas, muito úteis para a recuperação de pequenas moléculas e outras mesoporoso, para o fraccionamento de moléculas complexas, tais como os açúcares e dissacáridos.

Summary

Introduction

1 Introduction

1.1 Biomass upgrading

Biomass is a term used to define all the organic material that comes from plants and animals that are not used as food. This includes all terrestrial and aquatic vegetation as well as organic waste (including those from wastewater plants). In general, it is constituted by carbohydrates that are produced through the photosynthesis of the plants.[1-3]. Four main types of biomass can be defined in general:[2, 4]

- Woody plants,
- Herbs / agriculture plants,
- Aquatic plants,
- Wastes

The lignocellulosic biomass is composed of variable amounts of cellulose, hemicellulose, lignin and a small amount of extractive,[5] the variation in the composition depends on the plant species.[6] Cellulose represents 30-50% of the mass of the lignocellulosic biomass and it is an homopolymer that is formed by β-D-glucopyranose units linked through β-glucosides bonds with an average molecular weight around 100,000. Alpha cellulose is a polysaccharide having $C_6H_{10}O_5$ as general formula (Figure 1.1- a). Hemicellulose accounts for 25-35 wt% of lignocellulosic biomass and it is a complex polysaccharide that exists in association with cellulose in the cell wall (Figure 1.1- b). It is an amorphous polymer consisting of C5 (pentoses) and C6 (hexoses) sugars (mostly) such as glucose, mannose, xylose and arabinose but also methylfluorenyl and galacturonic acids, with an average molecular weight of 30,000. The ratio depends on the type of biomass. The final component, lignin, is an amorphous polymer rich in aromatic monomers (Figure 1.1- c) that accounts for 15–30 wt% of the lignocellulosic biomass. They are often adjacent to cellulose fibers to form a lignocellulosic complex. The structure of lignin depends on many factors and the source of biomass, mainly if it is hardwood or softwood. In general, lignin is composed of three main precursors: 5-*p*-coumaryl, coniferyl, and sinapyl alcohol.[5, 7]

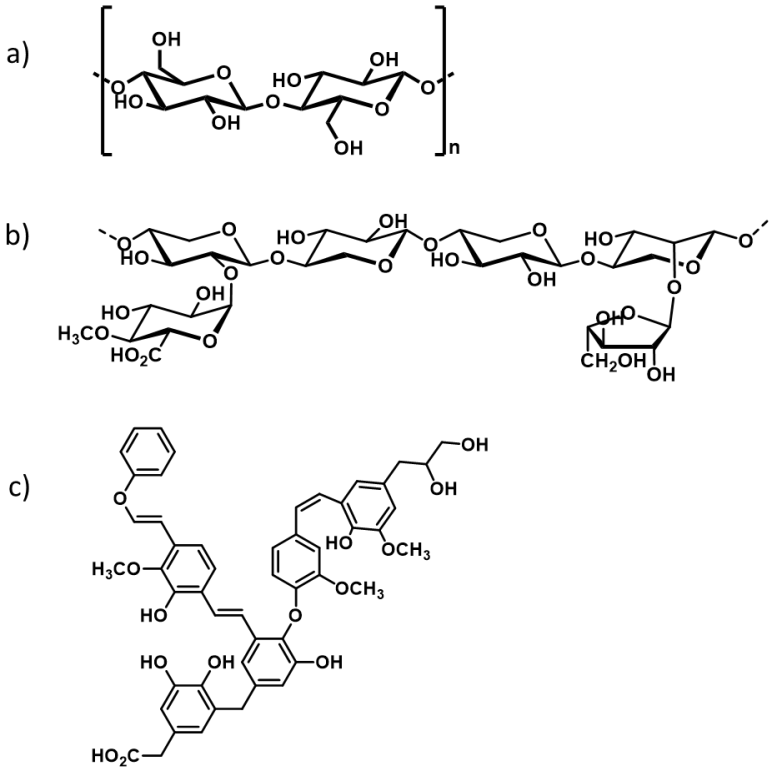

FIGURE 1.1- General structure of a) cellulose, b) hemicellulose and c) lignin.[8]

From the fractionation of lignocellulosic biomass, a series of chemical compounds as well as fuels can be obtained. Cellulose can be used to produce ethanol, chemical platforms, such as levulinic acid (LA) and 5-hydroxymethylfurfural (HMF), and liquid fuels. Hemicellulose is more reactive than cellulose and easier to remove from lignocellulosic biomass, and is typically associated with the production of xylitol, furfural, and furfural derivatives. In the case of lignin, having a complex structure makes it more difficult to process than the other fractions. The Scheme 1.1 shows examples of the different compounds that can be obtained from hemicellulose and cellulose, having interesting chemical properties and the possibility of being converted into products with high added value, Figure 1.2.[7, 9]

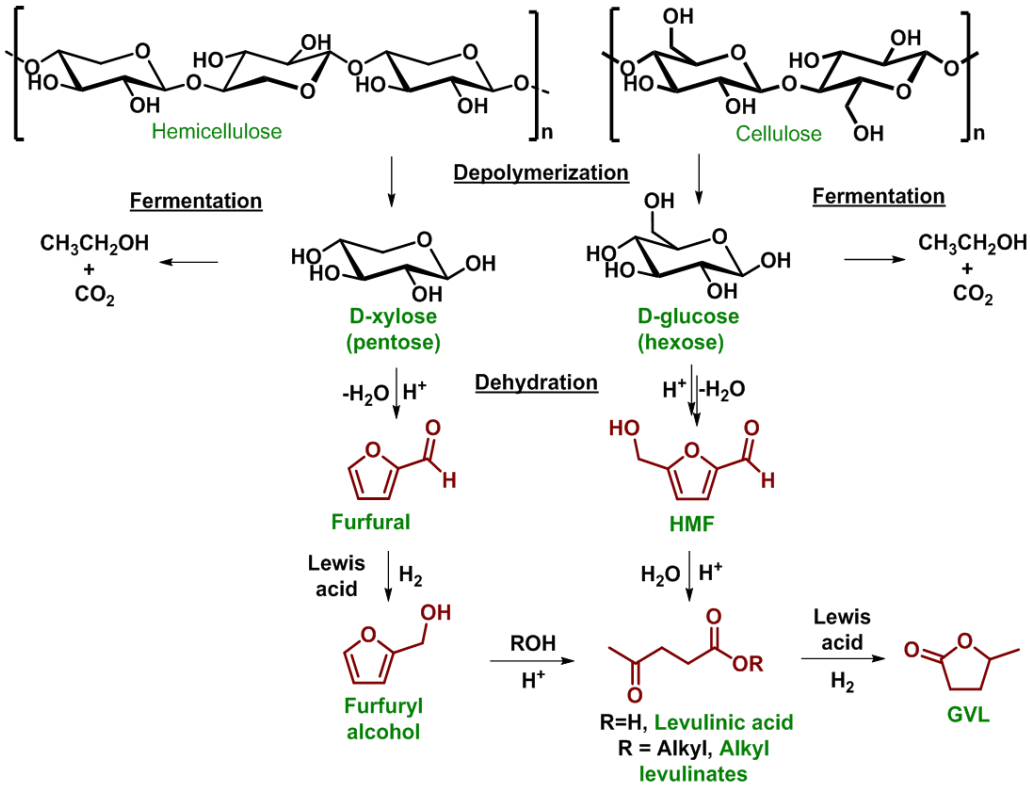

SCHEME 1.1- Fractionation of lignocellulosic biomass.

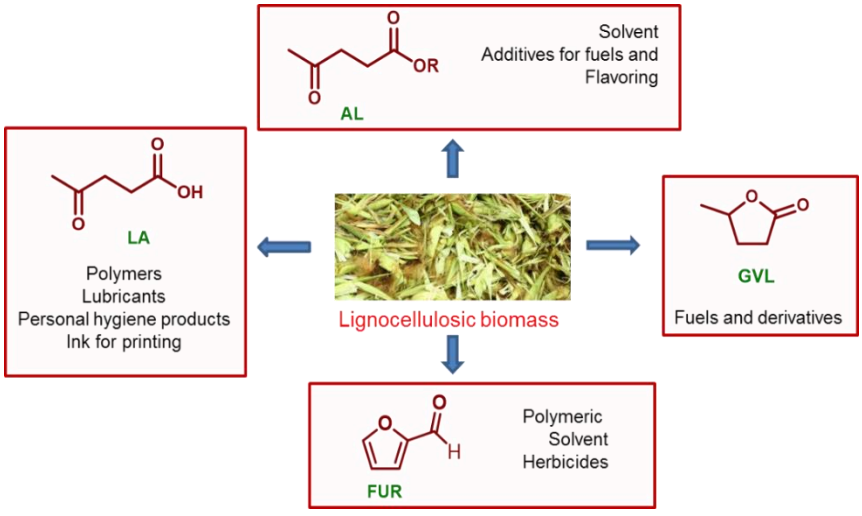

FIGURE 1.2- Chemical platforms derived from lignocellulosic biomass with high added value. AL: alquil levulinate, AL: levulinic acid, GVL: γ-valerolactone, FUR: furfural.

Both cellulose and hemicellulose can be transformed by chemical or enzymatic hydrolysis. If a fermentation process occurs after the hydrolysis, ethanol is obtained. Enzymatic hydrolysis is considered the most attractive way to convert cellulose to glucose. However, this process is very slow for natural cellulose because it is well protected by a matrix of hemicellulose and lignin.[10] Another way to transform cellulose is through chemical hydrolysis, which can be done using acid catalysts such as sulfuric acid (Scholler process),[11] hydrochloric acid (Bergius process),[12] anhydrous HF(Hoechst process).[13, 14] However, the use of these mineral acids has a series of drawbacks among which are its difficult recovery, toxicity, high costs because of the need for corrosion-resistant industrial plants.[15] For this reason, solid catalysts (heterogeneous catalysis) have arisen, which allow a better separation after the reaction, allowing its reuse. In addition, they are usually less aggressive to industrial than minerals acids. On the other hand, multifunctional solid catalysts can be designed to allow the conversion of sugar and/or its dehydration products in tandem reactions.[16]

Also, the sugars D-xylose and D-glucose can also hydrolyze and give furfural and HMF respectively (Scheme 1.1). The hydrolysis of D-glucose starts with an isomerization of glucose to fructose. The mechanism of this aldose-ketose isomerization involves hydrogen transfer from C-2 to C-1 and from O-2 to O-1 of a α-hydroxy aldehyde, to create the related α-hydroxy ketone.[17] This mechanism can occur by an intramolecular hydride shift (Figure 1.2).[18] The dehydration of fructose which starts with the elimination of a water molecule from the anomeric carbon after protonation, followed by the formation of the enol and tautomerization. Finally, another water molecule from carbon 3 and a proton from carbon 4 is eliminated, obtaining the HMF (Scheme1.3 a). Furthermore, the dehydration of xylose starts in its open form with the elimination of a water molecule from carbon 2 after protonation. Next, the removal of two water molecules occurs and furfural is obtained (Scheme 1.3 b).

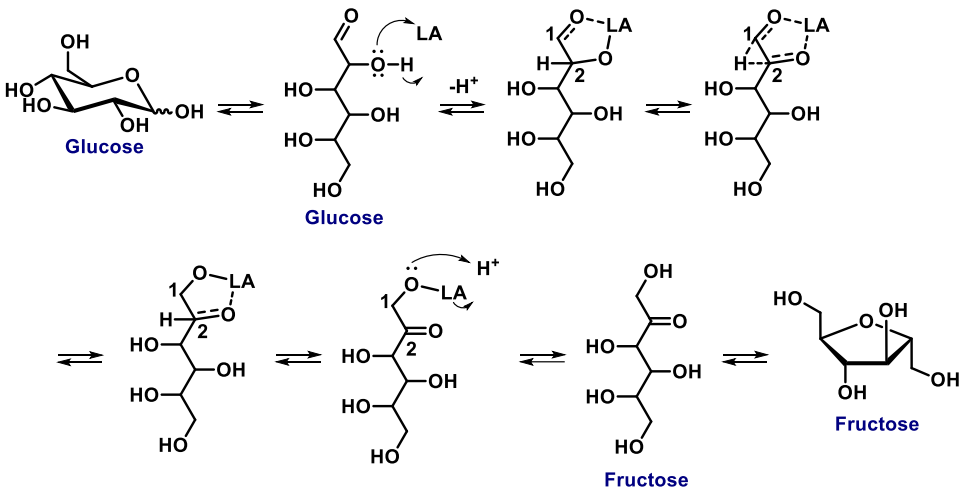

SCHEME 1.2- Mechanism of Isomerization of glucose to fructose by an intramolecular hydride shift.

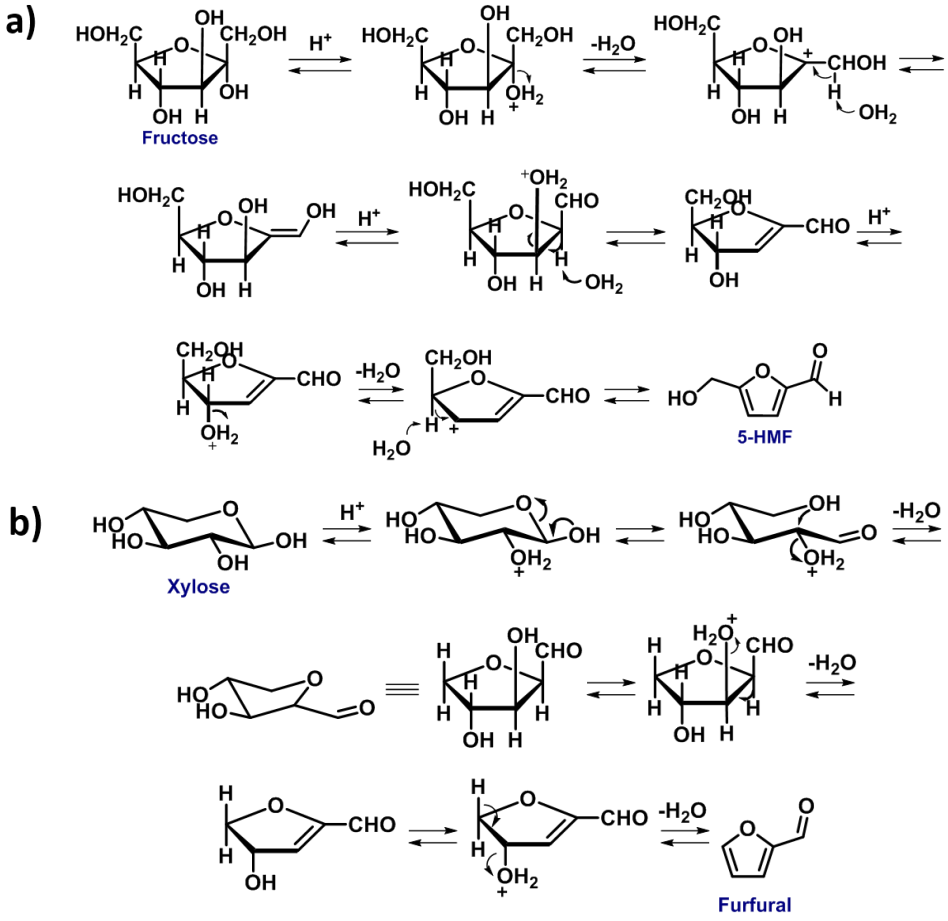

SCHEME 1.3- Dehydration of a) fructose and b) xylose.

The conversion of furfural to other value-added products is a complex cascade process that involves a series of sequential catalytic steps, at times promoted by Lewis acids and sometimes by Brönsted acids (Scheme 1.4). Furfural can be reduced to furfuryl alcohol using Lewis acid catalysts in the presence of a secondary alcohol (e.g. isopropyl alcohol), which acts as both solvent and hydrogen donor in a process known as MPV (Meerwein–Ponndorf–Verley) reduction;[19] the presence of Brönsted acid catalysts in the reaction medium may then lead to the formation of alkyl levulinates via alcoholysis. Since the latter described step proceeds with the elimination of a water molecule, the formed esters are in equilibrium with their acid counterparts. Levulinic acid may also undergo water elimination, forming unsaturated lactones, which can be reduced to γ-valerolactone. An alternative pathway involves the hydrogenation of both levulinic acid and its ester to the correspondent 4-hydroxypentanoates with further cyclization to γ-valerolactone.

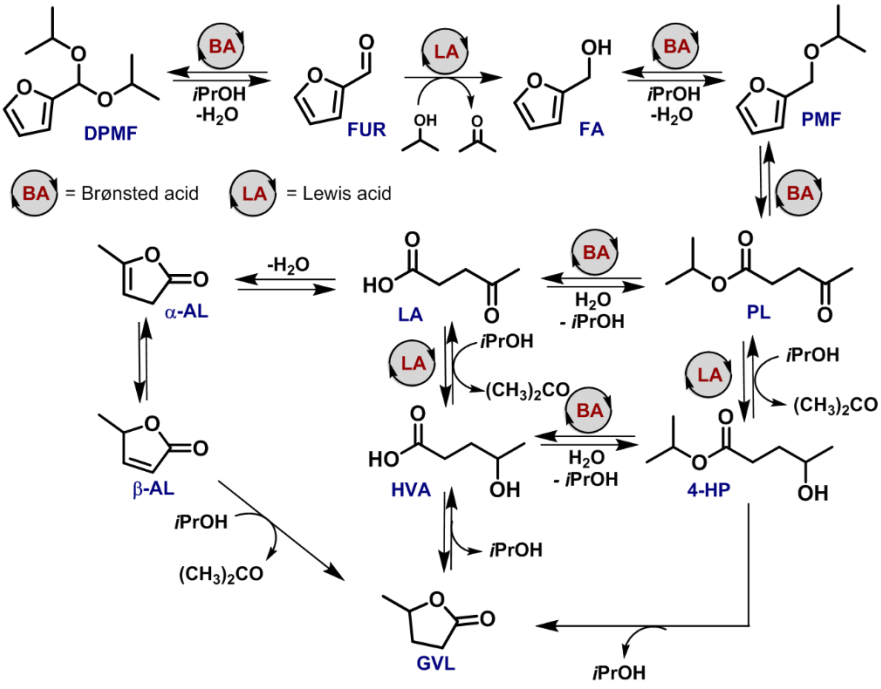

SCHEME 1.4- Conversion of hemicellulose biomass-derived compounds to other value-added chemicals using catalysts with Lewis and Brönsted acid sites in the presence of secondary alcohols. FUR = furfural, FA = furfuryl alcohol, DPMF = 2-(diisopropoxymethyl) furan, PMF = 2-(isopropoxymethyl) furan, α-AL = α-angelica lactone, β-AL = β-angelica lactone, PL = isopropyl levulinate, 4-HP = isopropyl 4-hydroxypentanoate, HVA = γ-hydroxyvaleric acid, GVL = γ-valerolactone. [19]

As previously stated, despite the high added value of all these chemical platforms, their industrial production have disadvantages, hence the use of solid catalysts. For the dehydration of xylose, a series of catalysts have been used such as, modified acidic zirconia catalysts in a toluene-water mixture at 160 ºC with 45% of selectivity and 95% conversion of furfural.[20] Also titanate and niobate catalysts,[21] silica-supported heteropolyacid catalysts[22] and niobium silicate catalysts.[23] In each case, the selectivity to the dehydration was moderate, consistent with the low yield/selectivity normally observed for the conversion of xylose to furfural. However, dehydration using a micro-mesoporous silica functionalized with sulfonic acid groups got 82% of selectivity to furfural and 91% of conversion.[24] In the isomerization of glucose to fructose have been used catalysts such as $AlCl_3$ (homogeneous catalysis) but also Lewis acids such as Sn-BEA[25] (31% conversion, T = 90 ºC and 300 min of reaction time),[26] Y, ZSM-5 and H-USY(55% de conversion, 1 h at 120 ºC, Si/Al = 6).[27] In the case of fructose dehydration to HMF, a range of catalysts have also been used, such as $AlCl_3$/HCl in biphasic system for a 62% of HMF at 170 ºC during 40 min of reaction, [28] ion-exchange resin/activated carbon for a 77% of selectivity to HMF at 90 ºC in 48 h of reaction. [29] Hierarchical ZSM-5(Si/Al=50) for a 60% of conversion and 25% of selectivity to HMF at 130 ºC after 8 h of reaction.[30]

The use of solid catalysts has not only focused on the valorization of carbohydrates but also on the conversion of furans. As an example of this there is the one-pot conversion of furfural into GVL obtaining an 80% using a combination of solid Lewis and Brönsted acids catalyzed (Zr-Beta / Al-MFI-ns) at 120 ºC in 48 h of reaction.[31] Also the hydrogenation of levulinic acid to GVL using a $RuSn_4$/C catalyst reaching maximum conversion at 20 h time-on-stream at 220 ºC.[32] As well as the conversion of furfural to furfuryl alcohol using catalysts of Tin-, zirconium- and hafnium-containing siliceous Beta zeolite.[33]

As it was previously reviewed, numerous efforts have been made in the search for alternative routes to obtain the chemical platforms that are derived from the lignocellulosic biomass. Specifically, these have focused on the synthesis of the catalysts that were used for these purposes, being one of the most concurrent micropores and mesoporous materials.

1.2 Microporous and mesoporous materials

Porous materials have covered many areas of research due to the applications that can be achieved with them. These materials are used as adsorbents, ion exchange systems, for separation of compounds and as catalytic supports or catalysts.[34] One of the most important properties of these materials is the porosity because through the pore systems large surface areas can be created that often result in high activity. According to the IUPAC definition, porous materials are classified into three groups: microporous (pore size <2 nm), mesoporous (2-50 nm), and microporous materials (> 50 nm).[35]

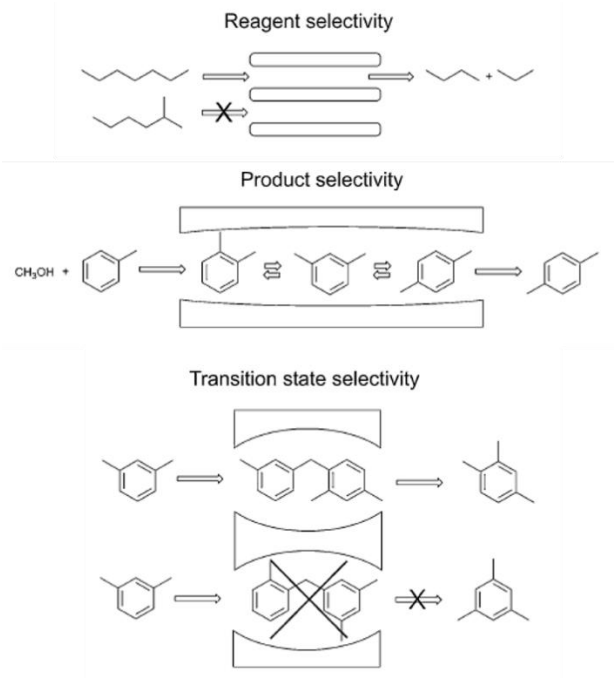

FIGURE 1.3- Shape selectivity in zeolite channels. [36]

In a porous catalytic material, the catalytic sites can be both on the surface of the material and its pores. Generally, the highest concentration of catalytic sites is found inside the pores. This makes possible to control the selectivity of chemical reactions by

selecting the appropriate reagent, product or transition state (Figure 1.3). [36] As can be seen in Figure 1.3 the selectivity of the reagents is the ability of certain molecules to enter the cavities of the porous materials and to undergo a reaction at the catalytic site. The diffusion of molecules that have a large size will be obstructed. In a simplified form it can be said that the selectivity towards the reagents occurs only when one type of reagent molecule can be transported into the pores preferentially. On the other hand, the restricted space within the pore system can prevent the formation of certain unwanted transition states (product requiring more space for their formation than available), thus avoiding the formation of several reaction products (selectivity of the transition state). If several products can be formed only the molecules with the appropriate dimensions can diffuse and thus appear as a reaction product (selectivity of the product). Hence, when parallel or consecutive reactions occur in the pores only that which gives the product of the right size will have the preference to spread.[36]

1.2.1 Microporous materials. Zeolites

Zeolites are microporous crystalline aluminosilicates (pores less than 2 nm in diameter) of natural or synthetic origin. Structurally, zeolites are complex and can be considered as crystalline inorganic polymers based on a three-dimensional network of tetrahedra (T) of SiO_4 and AlO_4 linked together through the oxygen of the vertices. Scheme 1.5 shows the general structure of a zeolite. These networks give rise to a series of channels and cavities of molecular dimensions. In addition, as a consequence of the isomorphic substitution of a proportion of Si^{4+} ions by Al^{3+} ions, a certain negative charge is introduced into the structure that is compensated by protons (Brönsted acids), cations (Lewis acids),[37] water molecules or other types of small molecules.[38]

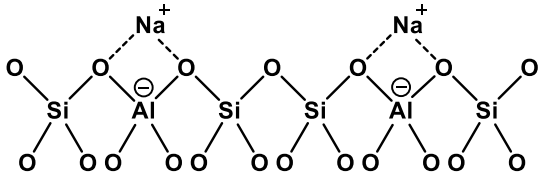

SCHEME 1.5- General structure of the zeolite in its sodic form. [8]

The different ways in which the Si (Al)O_4 tetrahedrons are linked in space give rise to a wide series of channel systems and cages in one, two and three dimensions that will define the structural characteristics of the zeolitic materials. The concrete configuration adopted by the network is specific to each material, although many common elements can be recognized that allow grouping the structures in a few families. The basic unit is a tetrahedron TO_4 ($T = Si^{4+}$, Al^{3+}). The union of a certain number of tetrahedra generates the so-called secondary units (SBU), such as simple rings, double rings or even polyhedral structures. On the other hand, the union of several rings can give rise to important tertiary structures such as the sodalite-type box. The different ways of linking this type of structure in a network originate the different topologies. In addition, due to the different ways in which secondary and tertiary structures are linked, different zeolitic structures can be constructed (Figure 1.4).[38, 39]

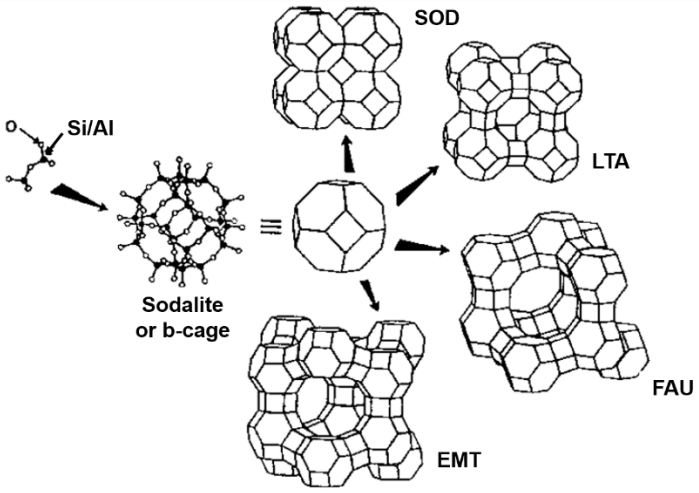

FIGURE 1.4- Structure of a sodalite cage and its derived structures.[38]

The amount of Al within the framework can vary over a wide range, with Si/Al =1 to ∞. Lowenstein proposed that the lower limit of Si/Al =1 of a zeolite framework arises, because the placement of adjacent AlO_4^- tetrahedra is not favored, due to of electrostatic repulsions between the negative charges. As the Si/Al ratio of the framework increases, the

hydrothermal stability and the hydrophobicity increases as well.[38] The Si/Al ratio also influences the type of zeolite that will be obtained (see Figure 1.5).

The most common synthesis of microporous materials such as zeolites is the hydrothermal method. Basically, it consists of two stages: the initial formation of the hydrated aluminosilicate gel and the crystallization thereof. The crystallization process consists of four steps: (1) condensation of polysilicate anions and aluminates; (2) nucleation of zeolites; (3) nucleus growth; and (4) crystalline growth of zeolites.[39]

The preparation of zeolites consists basically on the hydrolysis of Al and Si precursors in basic media in the presence of organic templates. In this process the precursors initially hydrolyze in basic media, forming SiO_2 and Al_2O_3 particles, producing a gel. Next, when submitted to hydrothermal treatment, the gel was converted to small crystalline particles of aluminosilicates that act as seeds embedded in an amorphous aluminosilicate phase that is further solubilized in the medium. In the final step, the aluminosilicates seeds condensate, forming the crystalline zeolitic material. [8] In the Figure 1.6 the general scheme of preparation of the BEA zeolite is shown.

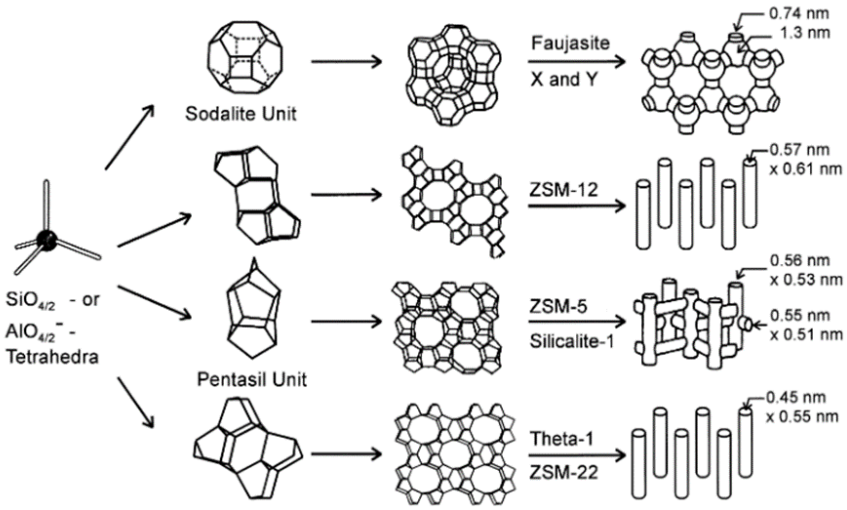

FIGURE 1.5- Structure of different types of zeolites depending on the Si / Al reaction.[40]

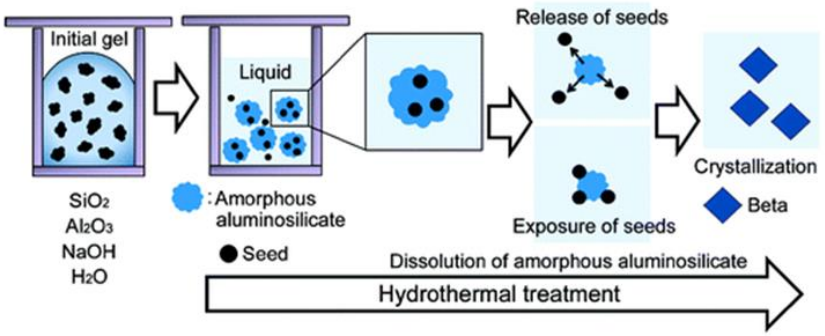

FIGURE 1.6- General scheme of preparation of BEA zeolite.[41]

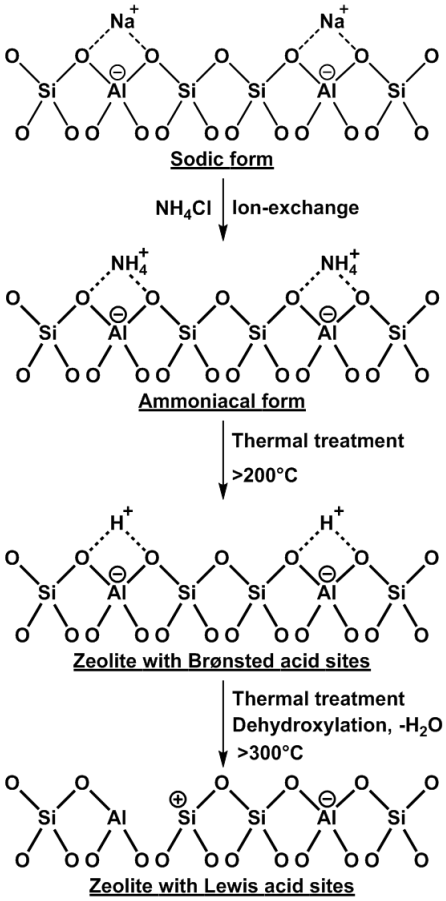

FIGURE 1.7- Generation of acid sites in zeolites through thermal treatment.[8]

These materials are commonly prepared in their sodic form but can be converted to their acid form after an ion exchange stage with ammonia, followed by a heat

treatment above 200 ºC that generates H^+ as charge compensation ion (Brönsted sites). If the thermal treatment is carried out at temperatures above 300 ºC, it causes the dehydroxylation of the structure, generating Lewis acidic sites (see Figure 1.7).[8] The generation of Lewis sites in the structure of the zeolite can be tuned by inserting metal ions into the crystalline lattice of the material or as a charge-compensation ion (see Figure 1.8).

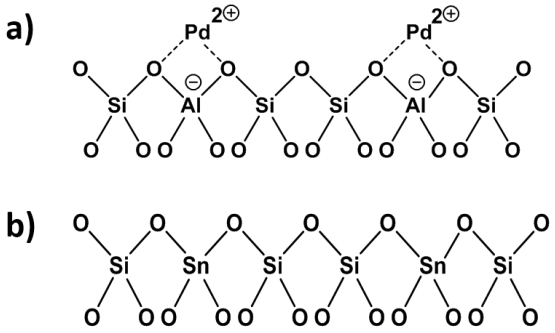

FIGURE 1.8- Generation of Lewis acid sites in the structure of the zeolite: a) Load compensation and b) Crystal lattice.

1.1.1.1 Application of zeolites in biomass valorization

The interesting properties of zeolites, such as their acidity, controllable pore size and the possibility of inserting different metals into their structure, have led to an increasing application of these materials in the conversion of lignocellulosic biomass derivatives to value-added compounds.[42-44] Jayprakash et al. reports, for example, the highly selective conversion of methyl levulinate to GVL using zeolites doped with metals as catalysts or combined with other supported metal catalysts.[45] Likewise, the zeolite HY in which gold nanoparticles were supported has been used in the selective oxidation of 5-hydroxymethyl-2-furfural into 2,5-furandicarboxylic acid (99%).[46] Zeolite of type HZSM-5 with a Si/Al ration of 25 has been used in the esterification of furfuryl alcohol achieving a 58.9% of selectivity of methyl furfuryl ether and a 44.8% of selectivity of ethyl furfuryl ether. [47] It was also used with a Si/Al ratio of 23 in the conversion of furfuryl alcohol to levulinic

acid (70%) in biphasic systems. [48] Supported with nickel on its surface it was used in the hydrogenation of levulinic acid to γ-valerolactone in vapor phase at atmospheric pressure obtaining a 100% of conversion and a 92.2% of selectivity. [49] A recent work by the Paixão group also reported the use of zeolite HZSM-5, but in this case with a considerably lower Si/Al ratio (Si/Al = 12) than the previous ones, in the cascade conversion of furfuryl alcohol to GVL, obtaining a 98% of conversion.[50] In this case the zeolite was supported in a magnetic matrix to facilitate its recovery and reuse.

Another zeolite that has shown an efficient behavior for the valorization of compounds derived from biomass is β-zeolite. Zeolite beta was first described in a U.S. Patent issued to Mobil Oil Corporation in 1967 by the general formula:

$$[xNa\cdot(1\text{-}x)\ TEA]AlO_2\cdot ySiO_2\cdot wH_2O]$$

With $x \leq 1.0$, typically 0.4, $5 < y < 100$, typically 10, $w \leq 4$, and TEA=tetraethylammonium cation. It was the first of the high-silica zeolites to be prepared by using organic additives in its synthesis.[51] Zeolite β (BEA) is a 12-membered-ring large-pore zeolite and has a Si/Al ratio of 5-100.[52] The beta structure is characterized by having rings along the plane (100) of 6.6 x 6.7 A and 5.6 x 5.6 A along the plane (001).[53] This material has a larger pore size than the ZSM-5 zeolite, which suggests an improvement in the strength of the zeolite compared to its deactivation, due to the blocking of the pores and high exposure of aluminum ions as well as charge compensation ions (Na^+, K^+) that facilitates their exchange. The β-zeolite, for instance, has been extensively used in fast pyrolysis of lignocellulosic biomass, mostly in its acidic form.[54] Also this zeolite has been used for the production of platform chemicals in its dealuminated form, that is replacing the aluminum ions of its crystalline network with other metals, as exchanged with ions, the latter being the least common. For example, Sn-containing β-zeolite was used in the isomerization of glucose to fructose in aqueous media[25] and in the production of 5- (hydroxymethyl) furfural (5-HMF) from carbohydrates, with a selectivity over 70% using a "One-pot" biphasic reactor system (water/tetrahydrofuran).[55] On the other hand the Zr-β-zeolite was employed in the preparation of γ-valerolactone (GVL) from furfural obtaining 80% of conversion,[31] and

levulinic acid obtaining a selectivity around 96%.[56] It has also been used in the conversion of glucose to methyl levulinate (~70% conversion).[57] The use of two metals in the same zeolite framework has also been reported, wherein the conversion of 1,3-dihydroxyacetone (DHA) into ethyl lactate (ELA) was achieved with Sn (Lewis acid site) and Al (Brönsted acid site) incorporated in the same framework.[58] Although the use of ion-exchanged β-zeolites has been rather limited, some interesting applications have been noted, e.g. the synthesis of biodiesel from soybean oil and methanol catalyzed by a La-exchanged β-zeolite[59] and the gas-phase dehydration of lactic acid to produce acrylic acid with alkali-ion exchanged β-zeolites as catalysts.[60]

Although zeolites are highly efficient catalysts for the valorization of biomass derivatives, processes that consume time and energy such as centrifugation and filtration are necessary to separate them from the reaction medium. Due to the above, the magnetically recoverable catalysts have emerged as an alternative, since they can be extracted from the reaction medium using an external magnetic field. [61-66]

1.1.1.2 Catalysts with magnetic supports for the valorization of biomass

In recent years, a series of materials have arisen as magnetic supports, among which are metal nanoparticles (Co, Fe), metal mixtures (FePt and CoPt) and oxides (FeO, γ-Fe_2O_3, MFe_2O_4 M = Fe, Co, Mn, Cu, Zn).[63, 64] Within these, the magnetite (Fe_3O_4) has been identified as the ideal and most widely used support in catalysis because of its low cost, easy preparation and availability of various synthesis methodologies.[63, 67, 68]

Magnetite has a cubic inverse spinel structure with a space group of Fd3m. The presence in the crystal structure of non-equivalent cations in two valence states, Fe^{2+} and Fe^{3+}, leads to the formation of a unique magnetic structure. The unit cell also contains $32O^{2-}$ ions which are regular cubic close packed along the [110] direction. Generally, Fe_3O_4 crystals are distributed with octahedral and mixed octahedral/tetrahedral layers along the [111] direction (Figure 1.9).[64]

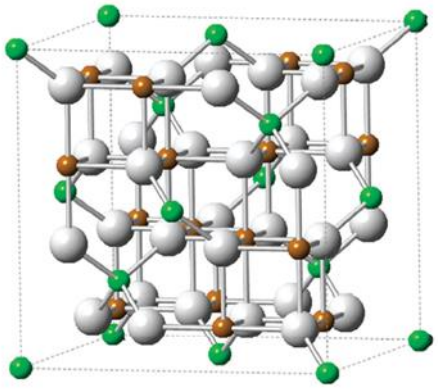

FIGURE 1.9- Crystal structure of Fe_3O_4, green atoms are Fe^{2+}, brown atoms are Fe^{3+}, grey atoms are oxygen. [64]

Among the most used methods for its preparation is coprecipitation, microemulsion, thermal decomposition, pyrolysis, laser and the solvothermal method.[61] The methodology to be chosen will depend on the characteristics of the material you want to obtain, such as its morphology, distribution of size and polarity of the surface. The co-precipitation method, for example, is one of the simplest and most economically operational in which relatively narrow size distribution is formed, with a large distribution of size and a hydrophilic surface. In the case of thermal decomposition, hydrophobic particles are formed with very narrow size distribution and very good shape control; however, it requires high temperatures and the use of toxic reagents. On the other hand the solvothermal method allows to obtain very narrow size distribution and very good shape control, using accessible and low toxicity reagents, it also requires the use of high temperature and pressure.[61, 68]

Magnetic nanoparticles have multiple applications. Among them is its use as a support for the preparation of magnetically recoverable catalysts for the conversion of biomass[69]. Example of the above we have the use of silicon catalysts functionalized with sulfonic acid supported on magnetite nanoparticles or cobalt ferrite for the preparation of 5-HMF from glucose dehydration[70] and also for obtaining furfural from the dehydration of xylose.[71] Another example is the work already mentioned previously of the use of magnetic HZSM-5 zeolite for the conversion of furfuryl alcohol to γ-valerolactone developed by our group.[50]

1.1.1.3 Metals-based catalysts for the valorization of biomass

On the other hand, metal-based catalysts have been used in the upgrading of bio-derived compounds. Among the metals used for these purposes are Fe, Ir and Pd. For example, in the case of the use of Fe-based catalysts in biomass upgrading, the transformation of the gas to C2 through C4 olefins with selectivity up to 60 weight percent has been reported, using catalysts that constitute iron nanoparticles homogeneously dispersed on weakly interactive α-alumina or carbon nanofiber supports. [72] The use of carbon-encapsulated iron nanoparticles (Fe-core/C-shell) to convert synthesis gas (bio-syngas) to liquid hydrocarbons was also reported.[73] Also the use of iron modified zeolites for upgrading the pyrolysis vapors' of pine wood.[74] In the case of Ir-based catalysts it has been used half-sandwich iridium complexes as a catalyst to convert LA into GVL with excellent yields (> 92% conversion. [75] Likewise, iridicycle complexes have been used for the conversion of levulinic acid (LA) into pyrrolidinones via reductive amination using formic acid as the hydrogen source under aqueous conditions.[76] Another example is the use of iridium nanoparticles supported on carbon nanotubes (Ir / CNT) for the conversion of levulinic acid (LA) into γ-valerolactone (GVL) with molecular hydrogen (H_2).[77] Also in Pd-based catalyst it has been used Pd nanoparticles supported on mesoporous N-doped carbon (Pd @ CN0132) for the conversion of vanillin (a typical model of lignin) on 2-methoxy-4-methylphenol (100% of conversion and selectivity). [78] [78] Another example is the use of [γ-Fe_2O_3 @ HAP-Pd (0)] catalyst for the oxidation of 5-hydroxymethylfurfural (HMF) into 2.5-furandicarboxylic acid (FDCA) in water, with 97% HMF conversion and a 92.9% yield of FDCA. [79] As well as Pd/SBA-15 for the conversion of HMF on furfur alcohol with a high yield, up to 96%, in mild conditions.[80]

That has been in this section: the need of Brönsted and Lewis acids for the conversion of products derived from biomass, the use of cooperative catalysis to perform more than one reaction step in the conversion reactions, the benefits of the beta zeolite and the catalysts magnetically recoverable and the use of metals such as Lewis acids, it was decided to prepare magnetically recoverable catalysts exchanged with transition metals that have both Lewis and Brönsted sites in their structure and that are capable of carrying out

cascade reactions for the recovery of compounds derived from lignocellulose biomass. Specifically, it was decided to synthesize a series of new magnetically recoverable catalysts comprising β-zeolites in their acidic form and exchanged with Fe, Ir and Pd. The use of metal-exchanged magnetic β-zeolites as catalysts in the conversion of bio-based entities is unprecedented, to the best of our knowledge.

1.2.2 Mesoporous materials

Despite the enormous industrial importance of zeolites, their application is limited. This is because it has a small pore size that limits its applications in technological processes in which high added value products are obtained and which involve large molecules. The need to dispose materials with a pore size greater than 2 nm boosted research in the field of materials science to the synthesis of mesoporous materials. In this sense, a breakthrough was originated in the early 90's when the synthesis of mesoporous silica materials known as MCM-41, MCM-48 and MCM-50 was reported, with pore sizes between 2 and 10 nm.[81] The term *meso* comes from the Greek prefix meaning -in the middle. Mesoporous materials are described by IUPAC as materials that have pores in dimensions between 2 nm and 50 nm (Section 1.2).[35] These materials have a highly ordered megastructure (highly regular and periodic arrangement of the pores)[82] and a large surface area that allows the diffusion and adsorption of larger molecules.[83]

There is a great variety of materials with mesoporous structures. Some examples are aerogels and clays piled in layers that have disordered pore systems with wide pore size distributions. More ordered pore systems are reported in the literature and are those obtained in mesoporous metal oxide structures.[84, 85] Mesoporous carbon structures have also been extensively studied.[86] Silica is widely used in the production of mesoporous materials. Silicas are polymeric silicon oxides [(SiO_2) n], the general structure is shown in Figure 1.10. These materials have low cost, are thermally stable, have low

toxicity to the environment and are in great abundance in the earth's crust.[83] Silicas are not only mesoporous they cover the entire range from micro to microporous. (Figure 1.11).

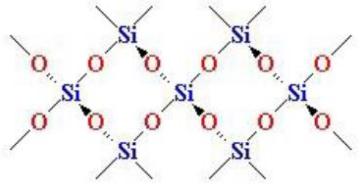

FIGURE 1.10- General structure of silica.

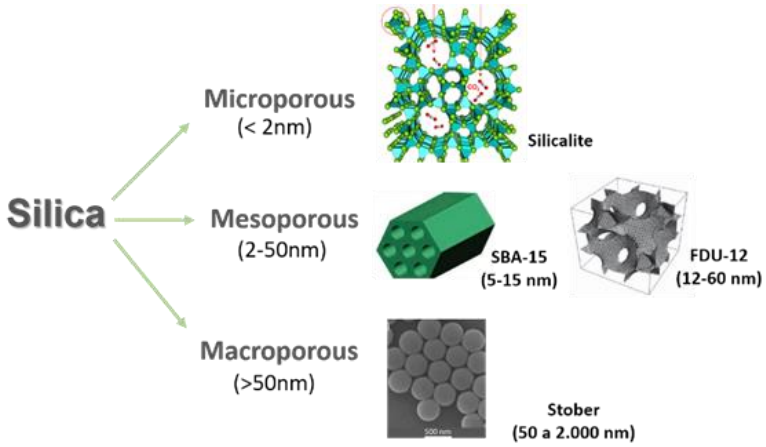

FIGURE 1.11- Classification of porous silica materials according to pore size.

1.2.2.1 Obtaining mesoporous silica

The synthesis of ordered mesoporous materials is carried out through the interaction between an inorganic phase and another micellar phase of organic nature in aqueous solution (Figure 1.12). Surfactants are amphiphilic molecules, with at least one polar group as hydrophilic head and one polar group as hydrophobic tail, both well differentiated.[87] When the concentration of surfactant in the solution reaches a threshold value (critical micelle concentration), its molecules form micelles. The shape of the micelle

is determined by the shape of the amphiphilic molecule that gives rise to it. Subsequently the micelles are grouped to form supremely structures. The phases through which the micelles go is hexagonal, cubic and laminar, in this order as the concentration of surfactant is increased. In mesoporous materials with silica, silicate oligomers condense with each other, around the micelles acting as a "template", by an assembly process. Finally, a solid product is obtained containing a surfactant inside, which is extracted from the solid with suitable solvents by chemical reactions coupled or by calcination in air at elevated temperatures. The selection of one or the other procedure will depend on the chemical nature of the surface of the inorganic skeleton and the physicochemical properties of the material.[82, 88]

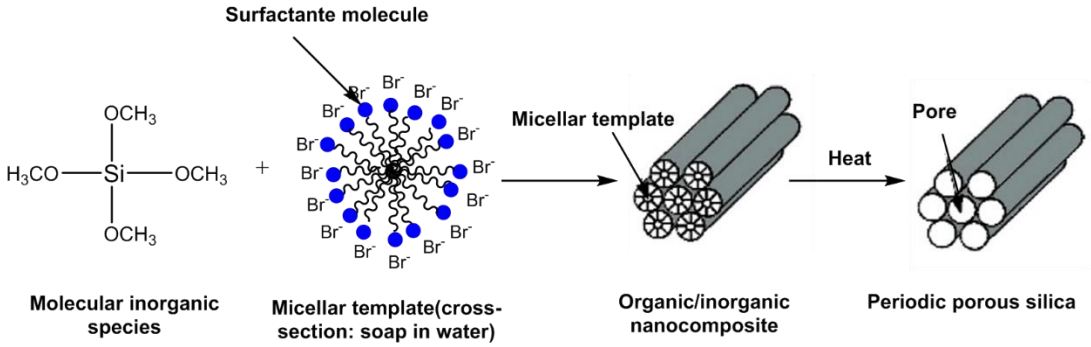

FIGURE 1.12- Diagram of self-assembly of silica-surfactant and formation of mesoporous silica.[82]

Regarding the mechanism of synthesis of ordered mesoporous materials, two processes are postulated. Initially, the liquid crystal model[81, 89] (liquid crystal templating mechanism, LCT) was proposed, in which the structure is defined by the organization of the surfactant molecules in mesostructured liquid crystal phases on is deposited the inorganic phase and that implies concentrations of surfactant higher than the micellar critical concentration (mcc). Later, the cooperative self-assembly mechanism was proposed (cooperative liquid crystal templating, silicate-initiated, CLCT).[90] In this case, it is the interaction between the molecules of the surfactant and the inorganic precursors present in the medium that induces the assembly of the mesophase. This is the commonly accepted

mechanism, although small variations have been suggested.[91] The Figure 1.13 illustrates the formation of mesoporous structures following the two mechanisms described above.[92]

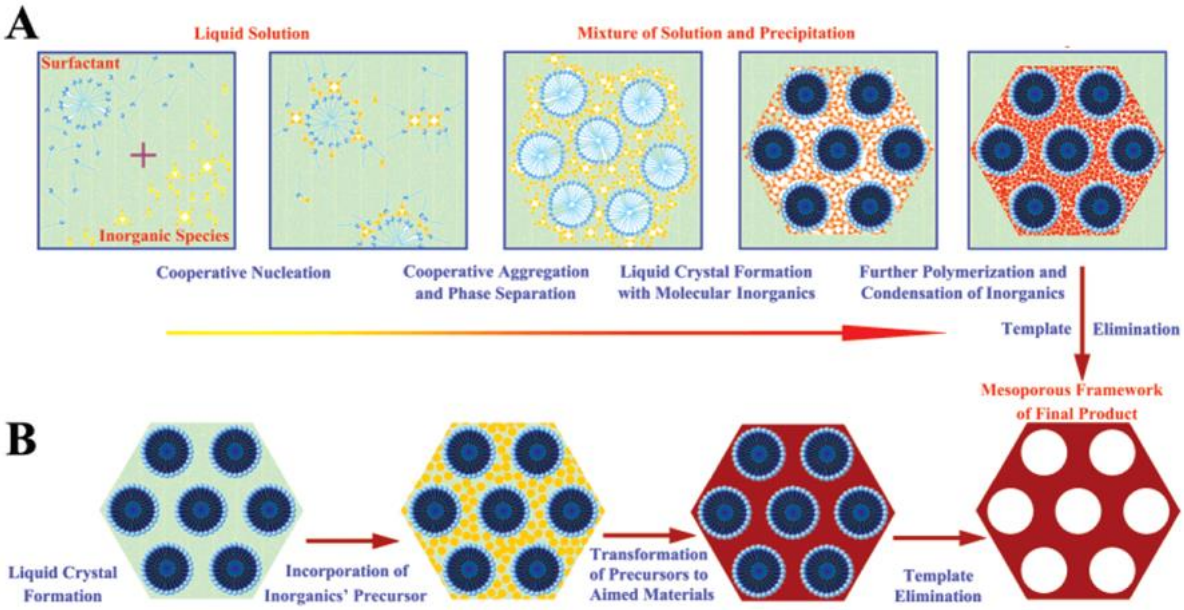

FIGURE 1.13- Two synthetic strategies of mesoporous materials: (A) cooperative self-assembly; (B) liquid-crystal templating process.[92]

In general, the surfactants can be classified as cationic, anionic, neutral and nonionic. The use of one or another surfactant influences the synthesis of mesoporous materials since the nature of the phase obtained is conditioned by the interaction between the inorganic species in the solution and the surfactant, which allow obtaining various structures.[92] The Figure 1.14 shows some examples of mesoporous silica. [8]

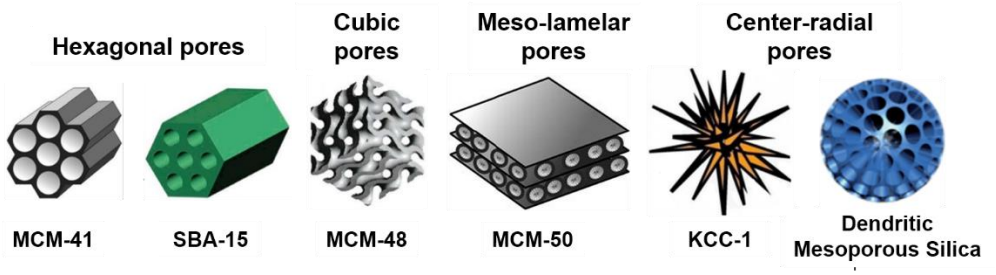

FIGURE 1.14- Different morphology that silicas can present.

1.2.2.2 Dendritic Silica

The dendritic silicas are unique and open 3D superstructures with large pore channels and highly accessible surfaces compared to conventional mesoporous silicas. As can be seen in the Figure 1.15 a, the dendritic silica is composed of fibers or wrinkles of silica that serve as building units and that are arranged along the center-radial ven macromolecules can be moved easily and effectively into or out of the porous matrix through radial open center pore channels (see Figure 1.15 b). This has led to multiple applications in nanomedicine and catalysis.

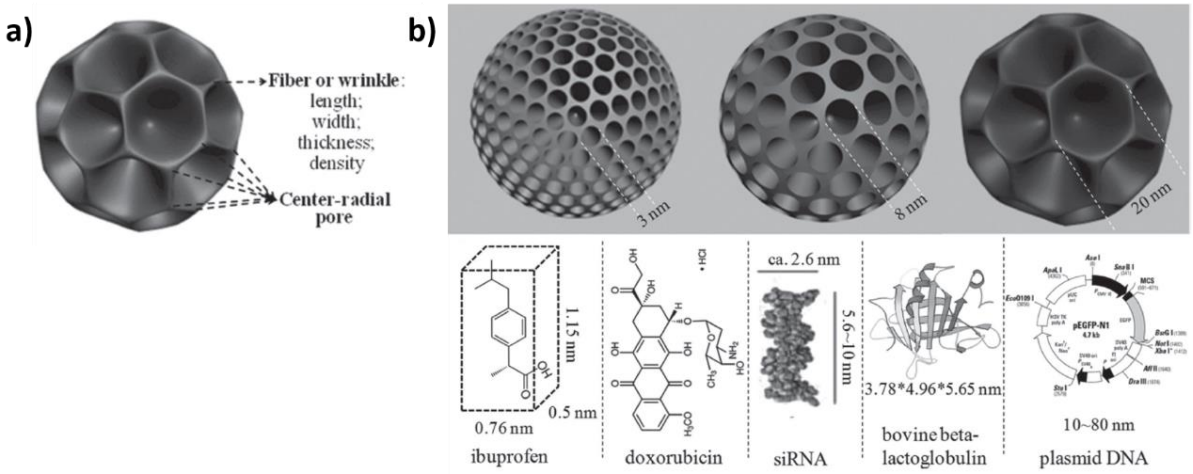

FIGURE 1.15- a) Dendritic spherical silica particles with center-radial pore (fibrous or wrinkle) structures b) Possible molecules that can enter the center-radial particles according to their pore size.[93]

The synthesis of dendritic silica particles with centerradial pore channels can be done by conventional soft or hard template methods as well as biphase layering (or "stratifi cation") of oil-water systems, emulsion systems, surfactant template systems. The conventional soft or hard template methods are not suitable for synthesizing dendritic silica particles with a 3D centerradial pore structure. It seems to be difficult to control the silica growth along the free radial directions or the restricted tangential direction. On the other hand, biphase layering of oil-water systems has been developed to achieve the synthesis of

dendritic silica particles with centerradial pore channels, and even simultaneously with uniform small mesopores (2-5 nm).[93]

In Figure 1.16 we can see the synthesis process of the three-dimensional mesoporous silica nanospheres and Mechanism of Interfacial Growth. The 3D-dendritic mesoporous silica nanospheres can be prepared in a heterogeneous oil-water biphase stratification reaction system. The biphase stratification approach allows the reaction to take place in the interface, and it is convenient to control the assembly on the interface via changing or adding reactants in each phase without disturbing the interface. The upper oil phase is a tetraethyl orthosilicate (TEOS) solution with hydrophobic organic solvent, while the lower aqueous phase is an aqueous solution combined by cationic cetyltrimethylammonium chloride (CTAC) as a template and organic base triethanolamine (TEA) as a catalyst. The dendritic hierarchical mesostructure with several generations can be achieved with a one-pot continuous interfacial growth route, and the pore size can be controlled by changing different hydrophobic solvents. The mechanism passes through several stages as can be seen in Figure 1.16. (a) Nucleation process of the 3D-dendritic mesoporous silica nanospheres; (b) growth process of the first generation of the 3D-dendritic mesoporous silica nanospheres; (c) changing the upper oil phase; (d) growth process of the second generation of the 3D-dendritic mesoporous silica nanospheres; (e-h) the mechanism of one single mesopore-channel growth with swelling.[94]

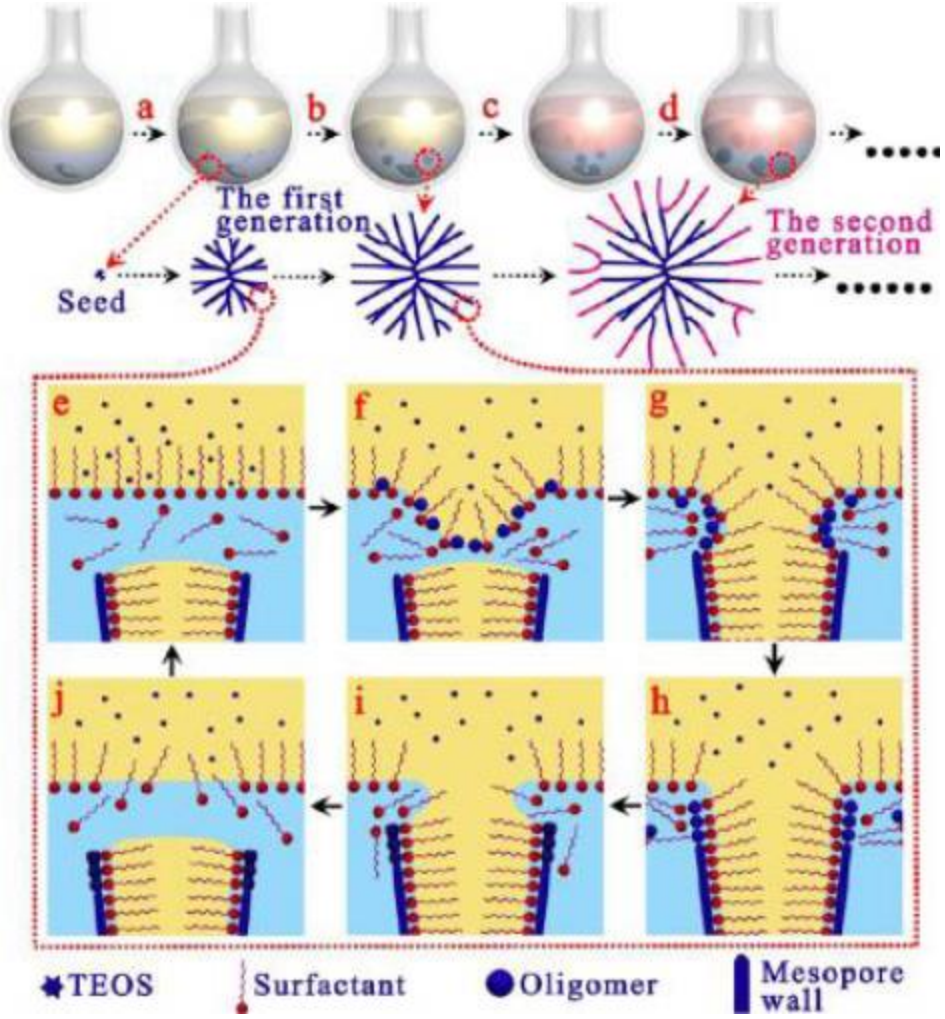

FIGURE 1.16- Synthesis Process of the 3D-Dendritic mesoporous silica nanospheres and mechanism of Interfacial Growth[94]

1.2.2.3 Application of silicas in biomass valorization

Due to the properties mentioned under epigraph 1.2.2 the mesoporous silicas have been widely used as catalytic support in the valorization of bio-derived compounds. Example of this is the report made by Courtright et al., where it was performed the hydrogenation of lactic acid over silica-supported copper (Cu/SiO_2) to 1,2-propanediol with 100% conversion and 88% selectivity.[95] On the other hand Días et al. carried out the

dehydration of xylose to furfural using cesium salts of 12-tungstophosphoric acid supported on MCM-41 obtaining a 91% conversion and 45% selectivity towards furfural. [96] Likewise Shi et al. performed this same dehydration over SO_4^{2-}/ZrO_2/SBA-15 catalysts obtaining 98.7% xylose conversion and 53.4% furfural selectivity.[97] That same year the same author reported this dehydration but using SBA-15 functionalized with sulfonic acid (SBA-15-SO_3H) obtaining ~95% conversion of xylose, with 74% and 70% selectivity and furfural performance respectively.[98] Also Takagaki et al. used silica functionalized with sulfonic acid, but this time in a magnetic support for the pyrolysis of sucrose and cellobiose, obtaining 93% and 88% of glucose respectively (see Scheme 1.6).[99]

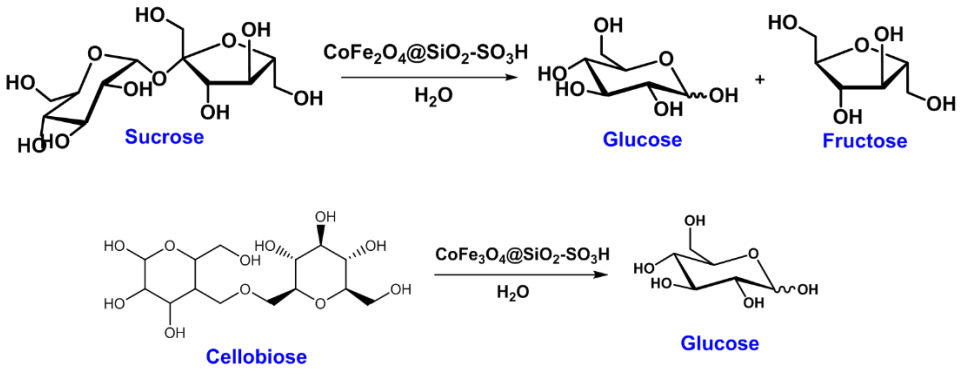

SCHEME 1.6- Hydrolysis of disaccharides using $CoFe_2O_4@SiO_2$-SO_3H.

On the other hand, although there are few reports, center-radial silicas have also been used in the conversion of bio-derived compounds. For example the work done by Chermahini et al. where nanosphere fibrous KCC-1 silica functionalized with propyl sulfonic acid groups are used as a catalyst for the production of 5-hydroxymethylfurfural (HMF) from dehydration of fructose obtaining 67.71% yield and 68.32% selectivity for the HMF and achieving a 99.11% fructose conversion (see Scheme 1.7).[100]

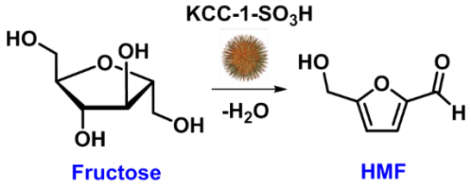

SCHEME 1.7- Dehydration of fructose to HMF whit silica center-radial functionalized with sulfonic acid.

1.2.2.3.1 Functionalization of silicas with sulfonic acid

There are two main strategies to functionalize the surface of porous silica materials: 1) co-condensation or one pot synthesis and 2) post synthesis or grafting technique. In the first, the active phase is added to the reaction mixture, then assembles and condenses into the inorganic framework for the formation of the mesoporous material (see Scheme 1.8 a. In the second, the siliceous support is prepared followed by the modification with active moieties or their precursors (see Scheme 1.8 b). [101, 102]

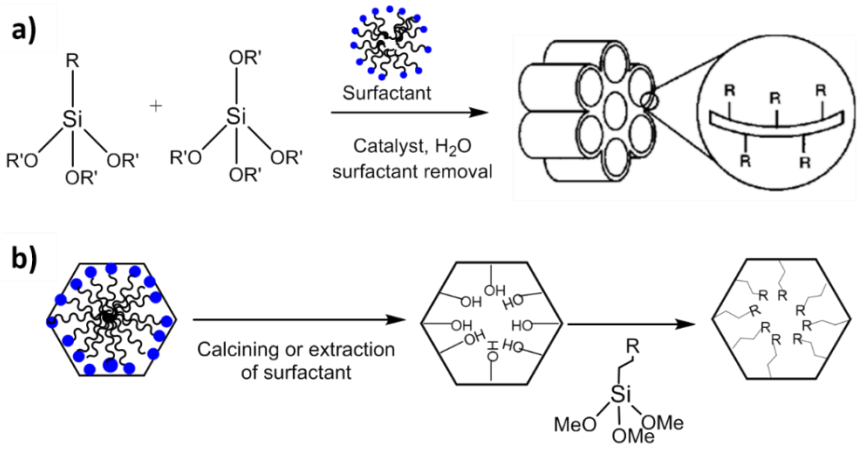

SCHEME 1.8- Preparation of functionalized mesoporous silicates a) by co-condensation and b) by post synthesis. [103]

The methodologies reported for direct synthesis of the sulfonic acid-functionalized mesoporous materials by co-condensation are summarized. Following hydrolysis of the precursors silane (Tetraethyl orthosilicate) is added to the mixture the 3-mercaptopropyltrimethoxysilane (MPTMS) and the aqueous solution of H_2O_2.[101, 104] The MPTMS contains an SH group, a stable propyl spacer and a hydrolysable $Si(OMe)_3$ moiety.[105] In other cases, only the MPTMS is added to the reaction mixture obtaining thiol-functionalized silica and in a second step the thiol group is oxidized.[101, 106-108] On the other

hand, in a typical grafting procedure, MPTMS was added dropwise into the previously dispersed mesoporous silica and in a third step the transformation of -SH to -SO_3H was performed using an oxidizing agent.[104, 109, 110]

Throughout the previous section, it is evident from the examples mentioned that functionalization with sulphuric acid is widely used to obtain catalysts that are subsequently used in the conversion of biomass compounds. Specifically, in the case of functionalized with sulfonic acid has been reduced to the conversion of xylose to furfural and the conversion of fructose to HMF in which only its properties are used as Brönsted acid. Example of the previous conversion are have the works mentioned in the epigraph 1.2.2.2 performed by Shi et al[98] and Chermahini et al.[100] In addition, the work done by Morales et al. performed the conversion of fructose to 5-ethoxymethylfurfural using arene sulfonic acid-modified SBA-15 mesostructured silica (Ar-SO_3H-SBA-15) in ethanol, leading to a maximum EMF yield of 63.4%.[111] Telleria et al. also used the same catalyst but this time to dehydrate xylose to furfural obtaining a 80% yield whit 99% conversion of xylose.[112]This same author performed the same dehydration but in this case he used SBA-15 functionalized with propyl sulfonic, obtaining 96% conversion and 82% selectivity towards furfural.[113] Hua et al. also performed the same dehydration using an anodic aluminum oxide as matrix material, SBA-15 as support and a sulfonic acid group as the active component (AAO / SBA-15-SO_3H) obtaining a conversion of xylose and selectivity of furfural of 90% and 74% respectively.[114] Jackson et al. performed the dehydration of fructose towards HMF obtaining a selectivity of 43.6% using as a catalyst or mesoporous silica functionalized with sulfonic acid.[115]

The use of sulfonic acids as Lewis acid has been little studied and even less used in the conversion of biomass compounds. One of the few reports was carried out by Upare et al., using graphene oxide functionalized with sulfonic acid (GO-SO_3H) for the conversion of glucose to levulinic acid (LA), obtaining approximately around 78% of LA Scheme 1.9.[116] As it is known Brönsted and Lewis acids can play a role in solid catalysts for the chemical conversion of carbohydrates in water and specifically Lewis acid catalysts can successfully isomerize glucose in an aqueous phase.[18, 117] The acidity of Lewis in this material originates in the S=O double bonds of the sulfate complex, due to the electron inductive effect.[118, 119]

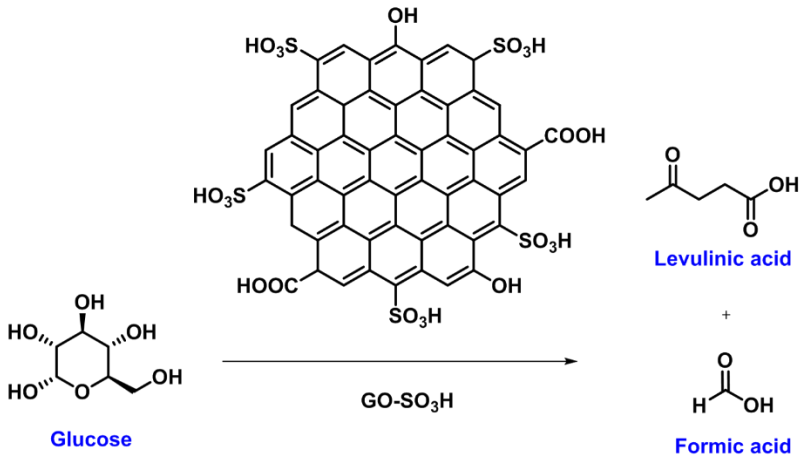

SCHEME 1.9- Chemical conversion of hexose sugars (glucose) to levulinic acid. [116]

In the second part of this work, considering, just like in the case of zeolite, the need of Brönsted and Lewis acids for the conversion of products derived from biomass, the growing applications of materials functionalized with sulfonic acid as catalysts in biomass-derived compounds. Also the unique characteristics of dendritic silica, it was functionalized dendritic mesoporous silica (DMSi) with such groups and explored its catalytic properties. Moreover, the unexplored potential of the sulfonic acids as catalysts in Lewis acid-demanding reactions was evaluated and the results compared with other types of silica.

1.3 Aims-Objectives

As previously mentioned to carry out the fractionation of the lignocellulosic biomass, catalysts are needed that possess acidic Brönsted and Lewis sites. So far, to carry out the different steps of this fractionation are used mixtures of catalysts, one that works as Brönsted acid and another as Lewis acid. The objective of this work is to synthesize bifunctional catalysts that are able to perform cascade reactions for the recovery of compounds derived from lignocellulosic biomass.

As the first part of the Ph.D work, we have designed and development an array of metal-exchanged (Ir, Fe and Pd) and acid magnetically recoverable β-zeolites and their

use in the upgrading furfural and furfuryl alcohol to isopropyl levulinates. Despite the enormous industrial importance of zeolites, their applications in technological processes in which high added value products are obtained and which involve large molecules are limited by the small size of their pores. The need for materials with a pore size greater than a nanometer boosted research in the field of materials science through the synthesis of mesoporous materials. Taking into account as the second part of the Ph.D work, we have designed and developed a sulphonic acid dendritic mesoporous silica (DMSi-SA) and evaluated the unexplored potential of the sulphonic acids as catalysts in Lewis acid demanding reactions in the upgrading of several compounds derived from lignocellulosic biomass. The DMSi-SA was used in the valorization of glucose, fructose, sucrose and cellulose to ethyl levulinate and xylose to furfural. Specific objectives of this work include:

- ✓ The synthesis of catalysts with Brønsted and Lewis acid sites constituted by magnetically recoverable β-zeolite in its acid form and exchanged with Ir, Fe and Pd;
- ✓ The synthesis of a catalyst with Brønsted and Lewis acid sites constituted by sulfonic acid-functionalized dendritic silica nanospheres;
- ✓ The full characterization of the catalysts;
- ✓ The evaluation of the catalytic activity of the magnetically recoverable β-zeolite in the valorization of furfural, furfuryl alcohol and ethyl levulinate;
- ✓ The evaluation of the catalytic activity of the sulfonic acid-functionalized dendritic silica nanospheres in the valuation of glucose, xylose, fructose, sucrose and cellulose;
- ✓ The study of the effect of temperature, catalyst mass, solvent volume, type of solvent, time, use of unconventional sources of heating and time in both types of catalysts, as well as the morphology of silica, in the valorization reactions;
- ✓ The evaluation the influence of recyclability of catalyst;

Results and discussion

2 Results and discussion

2.1 Microporous materials: β-magnetic zeolite exchanged with transition metals

2.1.1 Synthesis

The synthesis of the magnetically recoverable catalysts exchanged with Ir, Fe and Pd was carried out in several stages (Scheme 2.1). The specific methodologies for the realization of each one of these stages were described in the experimental procedure Section (See 3.1.1).

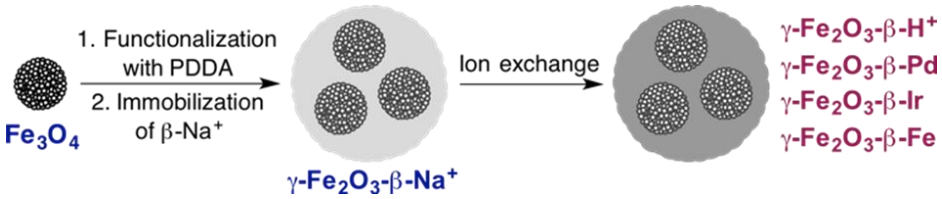

SCHEME 2.1- Preparation of the magnetically recoverable β-zeolite catalysts.

First, the magnetic support, magnetite (Fe_3O_4) microspheres, was prepared via a solvothermal reaction. This reaction consists in the reduction of $FeCl_3.6H_2O$ (iron source) with ethylene glycol, which acts not only as a reducer but also as a solvent, in the presence of sodium acetate as an alkali source and citrate as an electrostatic stabilizer.[120]

Subsequently, the poly diallyldimethylammonium chloride (Figure 2.1), a cationic polymer, was adsorbed on the surface of Fe_3O_4 to form Fe_3O_4/PDDA. Then the immobilization of β-Na^+ occurs, by electrostatic action.[121]

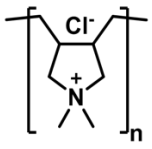

PDDA

FIGURE 2.1- Structure of poly diallyldimethylammonium chloride (PDDA).

The preparation of the zeolite was also carried out by a hydrothermal synthesis. In this procedure, silica gel was the source of silica, sodium hydroxide was the alkali source, tetrapropylammonium hydroxide was the organic template and sodium aluminate was the source of aluminum.[122]

After the immobilization of the zeolite on the magnetite microspheres, an oxidative thermal treatment (temperature up to 550 ºC) was carried out in, the PDDA was eliminated and the Fe_3O_4 was converted to maghemite (γ-Fe_2O_3). This transformation, however, was not an issue, since γ-Fe_2O_3 also presents a high saturation magnetization. Finally, an ion exchange process was carried out and the desired ions (Ir, Fe and Pd) are incorporated to the catalyst.

2.1.2 Characterization

Subsequent the magnetically recoverable catalysts were fully characterized using complementary techniques as: X-ray diffraction (XRD), transmission electron microscopy (TEM), chemical mapping, X-ray photoelectron spectroscopy (XPS), inductive coupled plasma-optical emission spectroscopy (ICP-OES), temperature programmed desorption of ammonia (TPD-NH_3) and Fourier transform infrared spectroscopy of adsorbed pyridine (FTIR-Pyr).

2.1.2.1 Catalyst structure

The crystalline structure of the support and the catalysts was inferred using the XRD technique. The phase analysis of the diffractogram corresponding to the magnetic support (Figure 2.2) revealed that the sample is crystalline and has a diffraction pattern corresponding to a cubic structure of spinel (JCPDS card 19-0629) of Fe_3O_4 or γ-Fe_2O_3. No hematite (α-Fe_2O_3) was found, the peaks corresponding to this phase were not observed. In the diffractograms corresponding to the magnetically recoverable catalysts (γ-Fe_2O_3-β-

H^+, γ-Fe_2O_3-β-Pd, γ-Fe_2O_3-β-Fe, γ-Fe_2O_3-β-Ir), the characteristic diffraction peaks of zeolite β (denoted by B)[123] and also the characteristic peaks of zeolite ZSM-12 (denoted by Z) were observed.[124] The obtention of this other crystalline phase during the synthesis has been reported by other authors.[123, 124] Also the peaks corresponding to the maghemite (JCPDS card 39-1346) denoted as F. Maghemite are specified because during the process of synthesis of the catalysts takes place a calcination process in oxidative atmosphere and it is known that magnetite in these conditions are transformed into maghemite.[50] On the other hand the low intensity of the peaks corresponding to the magnetic support in relation to those of the zeolite indicates the predominance of the zeolitic material in all the catalysts. Also, in the diffractograms, metal oxide peaks such as PdO_2 (JCPDS card 75-584) denoted as P in γ-Fe_2O_3-β-Pd and IrO (JCPDS card 15-870) denoted as I in γ -Fe_2O_3-β- Br were observed.

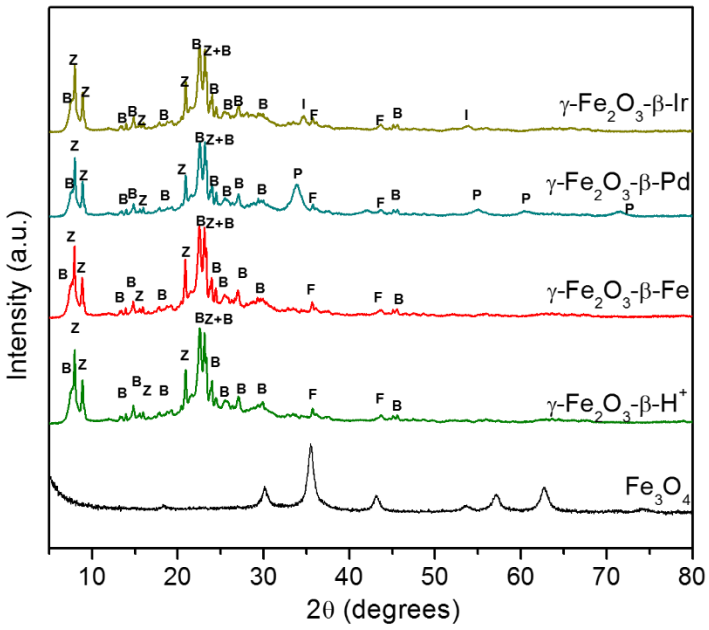

FIGURE 2.2- DRX patterns of Fe_3O_4, the magnetically recoverable catalysts in the acid form (γ-Fe_2O_3-β-H^+) and exchanged with Ir (γ-Fe_2O_3-β-Ir), Pd (γ-Fe_2O_3-β-Pd) and Fe (γ-Fe_2O_3-β-Fe).

To quantify the different crystalline phases in the magnetically recoverable catalysts, the Rietveld procedure was applied to the data obtained for the catalyst in its

sodium form (Figure 2.3). Is important to remember that this material is used later to obtain the different catalysts exchanged with metals. The phase 1 is assigned to the beta zeolite (BEA structure), phase 2 assigned to the ZSM-12 zeolite (MTW structure) and phase 3 is referred to maghemite (γ-Fe_2O_3). It is noteworthy to mention that the values of Rwp, Rp, R(F^2) and χ^2 were 0.0781, 0.0489, 0.0615 and 1.202 respectively, are quite satisfactory to achieve a good refinement. The results showed that in general the catalysts are composed of 5.5% γ-Fe_2O_3, 60.5% zeolite β and 34% zeolite ZSM-12.

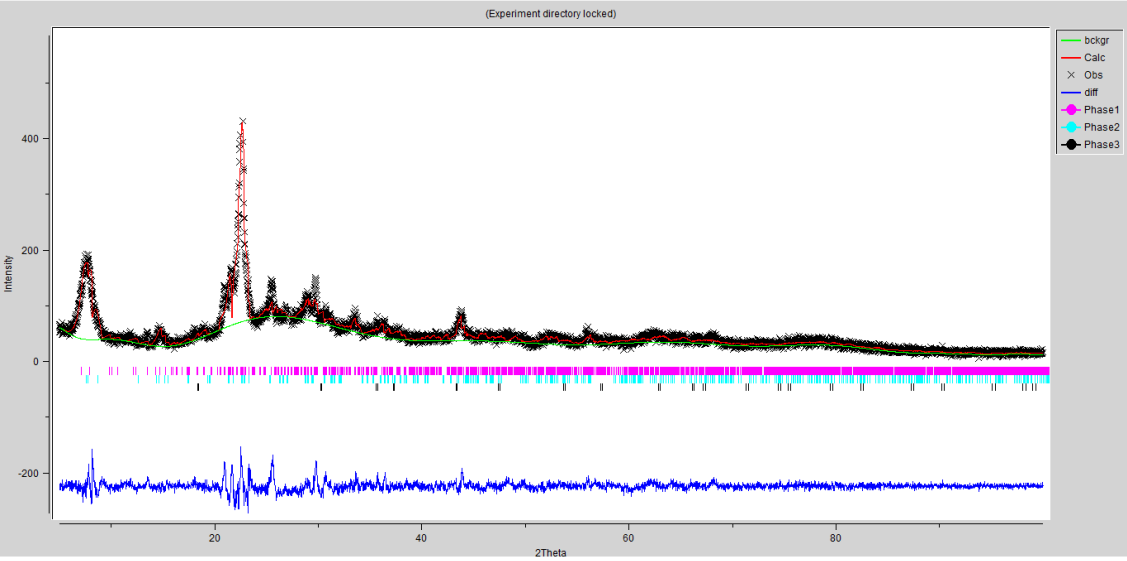

FIGURE 2.3- Rietveld refinement of the magnetic beta zeolite in the sodic form.

The low percentage of magnetic phase in relation to the zeolitic phase obtained by this characterization confirms the relationship of intensities obtained for the magnetic support and zeolite phase in the diffractograms of the catalysts. On the other hand, it can be seen that the β-zeolite phase is in greater proportion than the ZSM-12, although the coexistence of both phases should not affect the catalytic properties of the catalysts because both zeolitic phases present similar characteristics in terms of channel dimensions (Topological: pore opening > 6-ring and maximum diameter of a sphere ≈ 6) [125-131]

To confirm this, the synthesis of both crystalline phases in their pure form (ZSM-12 and βp) and a physical mixture of both phases in the same obtained proportion

were made. The proportion of the physical mixture (320 mg of pure β-zeolite and 180 mg of ZSM-12 zeolite) was carried out based on the results obtained from the Rietveld refinement of the catalyst obtained as a synthetic mixture of the mentioned zeolites. The phase analysis of the obtained diffractograms (Figure 2.4) showed the presence of the characteristic peaks reported for each of these crystalline phases: zeolite βp and zeolite ZSM-12.[123, 124]

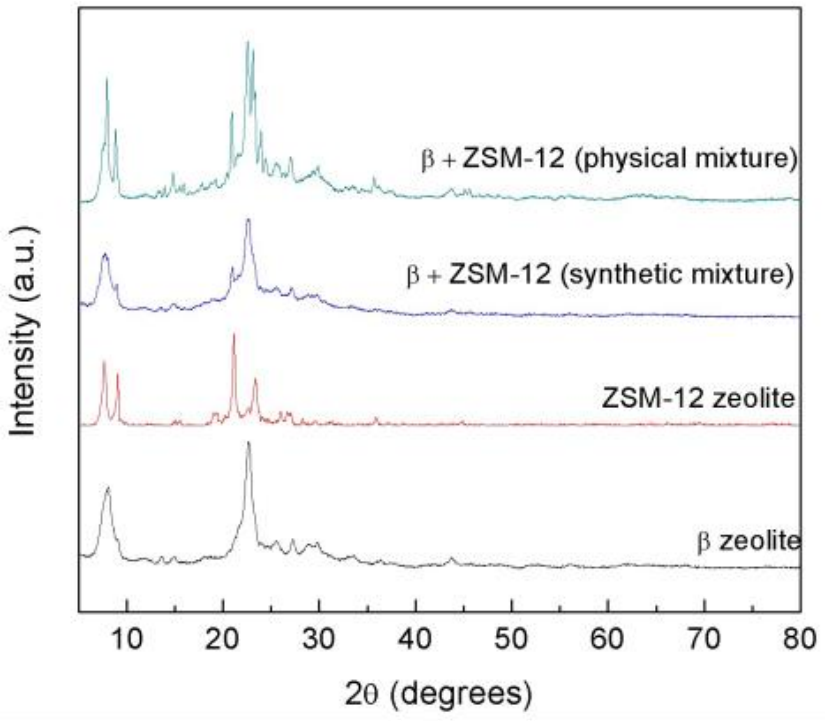

FIGURE 2.4- XRD patterns of β, ZSM-12 pure, physical and synthetic mixture of zeolite in sodic form.

Then, the Si/Al ratio present in each of these zeolites synthesized by X-Ray Fluorescence was determined. The obtained results agree with those theoretically determined (Table 2.1).

TABLE 2.1- Si/Al ratio for the pure zeolites, synthetic mixture and physic mixture determined by X-ray fluorescence.

Zeolites	Si/Al
β	23
ZSM-12	76
β + ZSM-12 (synthetic mixture)	34
β + ZSM-12 (physic mixture)	40

2.1.2.2 Catalyst morphology

The morphology presented by each of the magnetically recoverable catalysts synthesized as well as the morphology of the magnetic support was determined by transmission electron microscopy (TEM). It was observed that the magnetic support (Figure 2.5 a) has a spherical morphology with sizes ranging from 50 nm to 350 nm and an average particle size of 175 nm (Figure 2.6 a). In the case of the magnetically recoverable catalyst in its acid form (γ-Fe_2O_3-β-H^+), it was observed that the magnetic medium is mostly surrounded by zeolite grains (Figure 2.5 b) in some regions the coating was apparently not complete. However, when performing an elemental analysis mapping (Figure 2.7), it was possible to observe that in these areas there is a small layer of aluminosilicates.

The catalyst exchanged with iron (γ-Fe_2O_3-β-Fe) has a similar morphology to the catalyst in its acid form (Figure 2.5 c), however an elemental analysis mapping indicates the presence of iron over the entire catalyst uniformly (Figure 2.8). The palladium-exchanged catalyst (γ-Fe_2O_3-β-Pd) has a similar morphology to the catalyst in its acid form, but additionally presents on its surface well-dispersed palladium nanoparticles (Figure 2.5 d and e), as confirmed by EDX analyses (Figure 2.9), with sizes varying from 2 nm to 12 nm with a size average of 6 nm (Figure 2.6 b). The above indicates that it will be two sources of palladium in the catalyst, one from the substitution of palladium as charge compensation ion and the palladium present as a nanoparticle on its surface. The elemental analysis performed on this catalyst (Figure 2.7) confirms that.

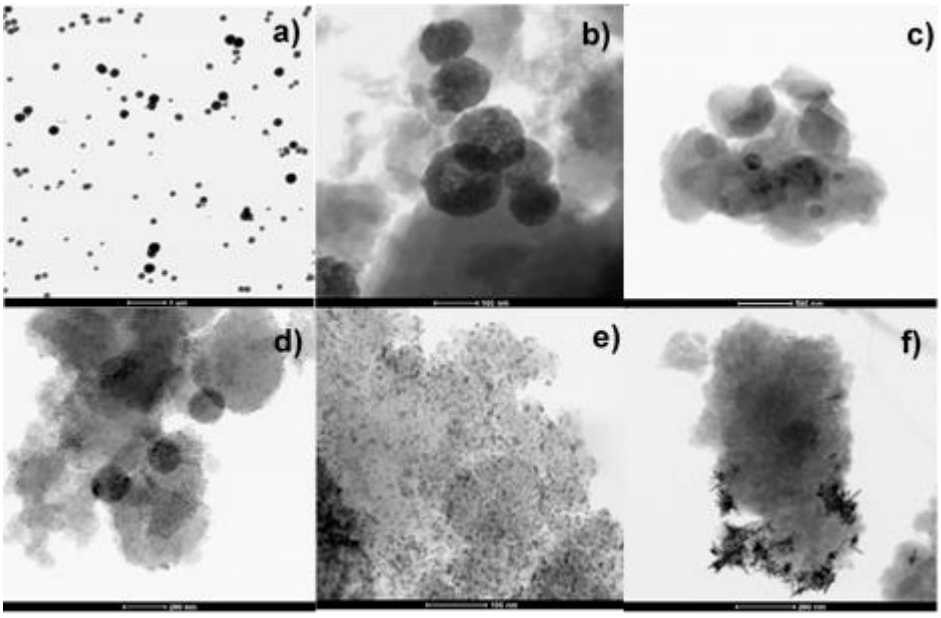

FIGURE 2.5- TEM images of a) Fe_3O_4 microspheres, b) γ-Fe_2O_3-β-H^+, c) γ-Fe_2O_3-β-Fe, d), e) γ-Fe_2O_3-β-Pd and f) γ-Fe_2O_3-β-Ir. Scale bar: a) 1μm, b) 100 nm, c) 500 nm, d) 200 nm, e) 100 nm and f) = 200 nm.

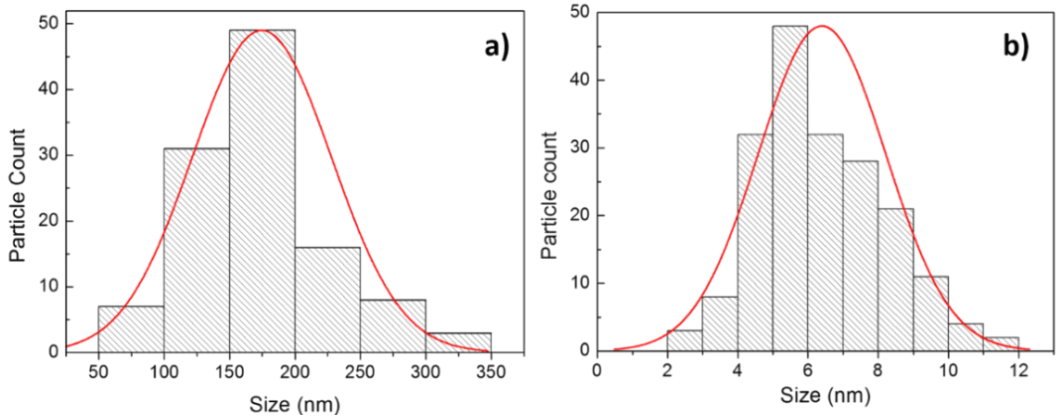

FIGURE 2.6- Histogram showing the particle size distribution constructed from the TEM image depicted in a) Figure 2.5 a and b) Figure 2.5 e.

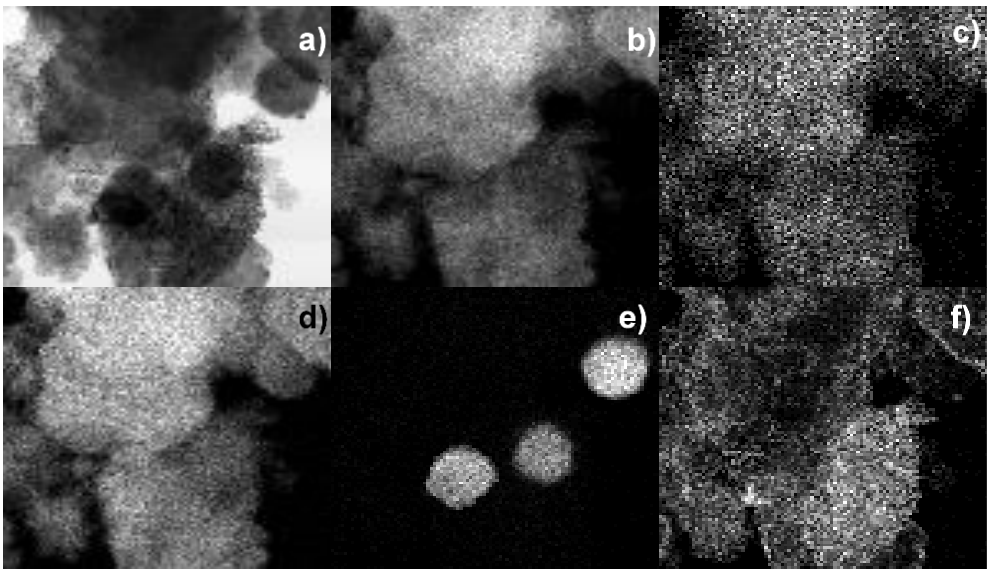

FIGURE 2.7- a) Bright-Field TEM image of the Pd-exchanged catalyst and elemental mapping of b) Si, c) Al, d) O, e) Fe and f) Pd.

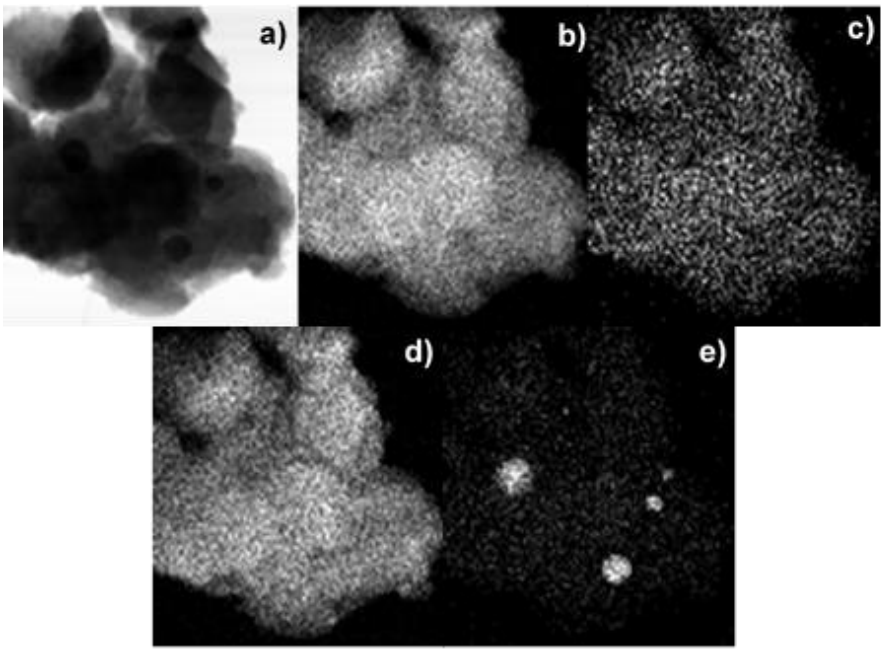

FIGURE 2.8- a) Bright-field TEM image of the Fe-exchanged catalyst and elemental mapping of b) Si, c) Al, d) O and e) Fe.

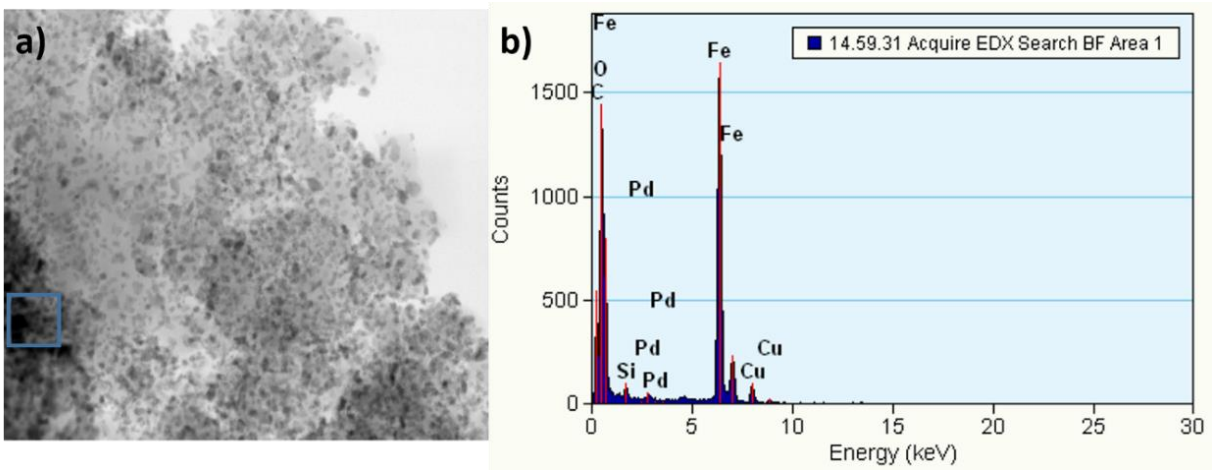

FIGURE 2.9- a) Image of the Pd-exchanged catalyst showing the delimited square area are in which the EDX analysis was performed and b) EDX analysis.

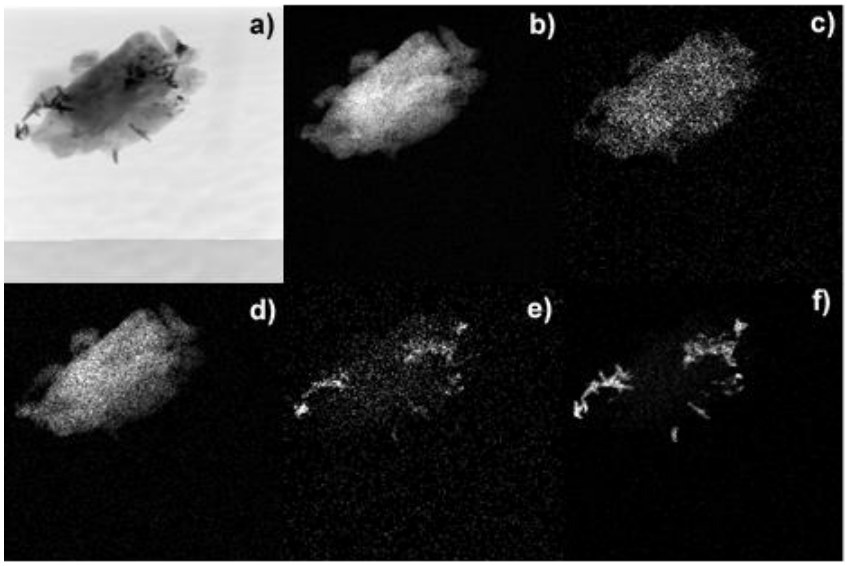

FIGURE 2.10- a) Bright-Field TEM image of the Ir-exchanged catalyst and elemental mapping of b) Si, c) Al, d) O, e) Fe an f) Ir.

On the other hand, the catalyst exchanged with iridium (γ-Fe_2O_3-β-Ir) presents a different morphology (Figure 2.5 f), the zeolite kernels are appreciated, however the particles of the magnetic support are not appreciated, but the original nanoparticles are observed. This indicates that for some reason the particles of the magnetic support collapsed in their nanoparticles. In addition, the presence of iridium oxide needles, which

are somehow associated with the iron oxide particles, is highlighted (Figure 2.10). It is important to note that it was not possible to differentiate the different morphologies corresponding to each of the zeolites present in these catalysts.

On the other hand, it was confirmed that the morphology presented by the catalysts made from the pure zeolites (β and ZSM-12) and their physical mixture (Figure 2.11) have a morphology like that obtained from the synthetic mixture (see Figure 2.5 d).

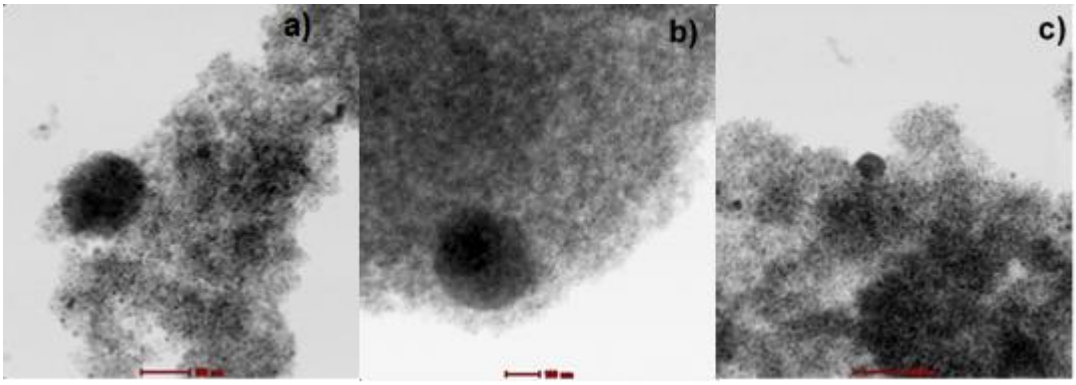

FIGURE 2.11- TEM imagem of a) γ-Fe_2O_3-β(p)-Pd, b) γ-Fe_2O_3-ZSM-12-Pd and c) γ-Fe_2O_3-(β+ZSM-12)-Pd. Scale bar: a), b), c) = 100 nm.

2.1.2.3 Acid properties of the catalyst

To determine the acidic properties present in each of these catalysts we carried out Ammonium Desorption Programmed Temperature studies (NH_3-TPD). The temperature programmed desorption of ammonia is a technique used to evaluate the density and strength of acid sites of a solid. This technique uses the capacity of adsorption until the saturation of a base (in this case NH_3) by the solid (in this case the catalyst). Subsequently with a progressive and controlled increase in temperature the base is desorbed (in a case it was 120 ºC to 600 ºC). During this stage, the amount of base desorbed by the solid, which was dragged by an inert gas (He), was determined. The amount of ammonium adsorbed by the samples was studied as a function of temperature and the integration of the area under

the curve corresponds to the amount of ammonium adsorbed and consequently is equal to all the acid sites in the sample.[132]

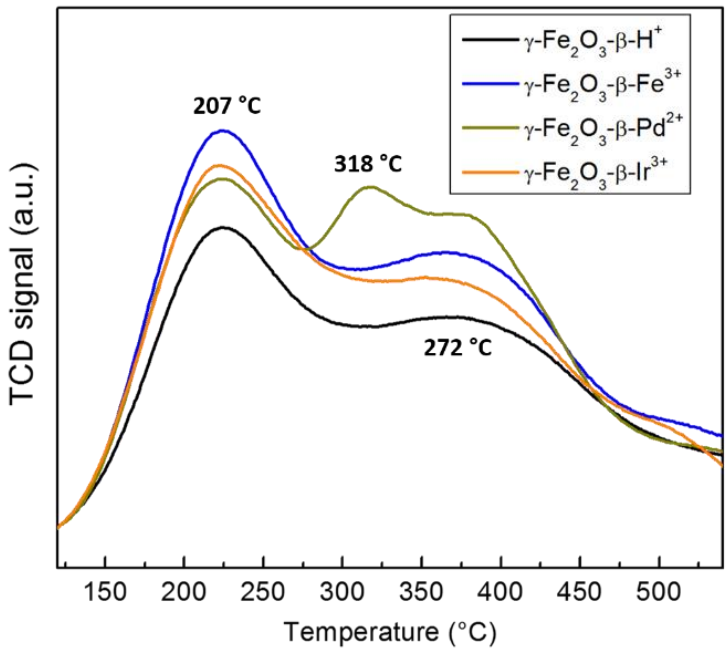

FIGURE 2.12- Temperature programmed desorption of ammonia curves of the magnetically recoverable catalysts

The NH_3-TPD of the catalysts, γ-Fe_2O_3-β-H^+, γ-Fe_2O_3-β-Ir and γ-Fe_2O_3-β-Fe revealed the presence of two different acid sites (Figure 2.12). One corresponding to a weak acid site (peak around 207 ºC) and one with moderate to high strength (peak around 272 ºC). In the case of the palladium-exchanged catalyst, γ-Fe_2O_3-β-Pd, another additional acid site appears in this case of moderate strength (peak around 318 ºC). When determining the total acidity of each of the catalysts, that is computed determining the area under the curve of the graph for the signal fron the TCD vs temperature and then normalizing (in this case was done dividing by the mass of catalyst used to make the analysis that in all cases was 50 mg), was obtained that the catalyst with the highest acidity is the one exchanged with iron (Table 2.2). However, if we analyze more deeply the results obtained in the NH_3-TPD graphs we can see that the greatest numbers of acid sites present in this catalyst are of

weak strength, but this is not the case for the palladium-exchanged catalyst whose highest number of acid sites are of moderate and high strength.

TABLE 2.2- Total acidity of the metal-exchanged catalysts determined by temperature programmed desorption of ammonia NH_3-TPD.

Catalyst	Total Acidity (μmol of NH_3/g of catalyst)
γ-Fe_2O_3-β-H+	1315.5
γ-Fe_2O_3-β-Pd	1807.6
γ-Fe_2O_3-β-Ir	1685.9
γ-Fe_2O_3-β-Fe	1919.5

Once the number of acid sites was quantified, the percentage of metals present in each of the catalysts was determined by Inductively Coupled Plasma Optical Emission Spectrometry (ICP-OES) analysis. ICP-OES is one of the branches of analytical spectrometry where analytical information is obtained as well as an atomic spectrum in the region of the ultraviolet (UV) and visible (VIS) electromagnetic spectrum, with a wavelength range of 165 nm at 403 nm for UV and from 404 nm to 782 nm for VIS. It allows to obtain qualitative information of the sample and in a general way, it is based on the vaporization, dissociation, ionization and excitation of the different chemical elements that make up the sample inside a plasma, exciting them to a level where they emit light of a characteristic wavelength. Subsequently, a detector measures the intensity of the emitted light and calculates the concentration of that element, in particular, in the sample.[133] The total amount of metals in the catalysts was determined and the values were: 1.1% for Pd in the Pd-exchanged catalyst, 0.5% for Ir in the Ir-exchanged catalyst and 1.8% for Fe in The Fe-exchanged catalyst (for the determination of Fe in its Fe-exchanged catalyst, the amount of Fe in the catalyst in its sodic form was determined in triplicate and subtracted from that in the Fe-exchanged catalyst).

Then, in order to verify the acidic properties of the catalysts synthesized from the pure zeolites(γ-Fe_2O_3-βp-Pd, γ-Fe_2O_3-ZSM-12- Pd) as well as their physical mixture(γ-Fe_2O_3-(β+ZSM-12)-Pd), the total acidity of the catalysts was determined by NH_3-TPD and

the percentage of metals, specifically palladium, was determined for each one of these catalysts by ICP-OES (Table 2.3). As expected, the total acidity of the catalyst made with the physical mixture of both pure zeolites, has acidity very similar to that shown by the catalyst with the same proportion of zeolites but obtained in a synthetic form (γ-Fe_2O_3-β-Pd). The γ-Fe_2O_3-βp-Pd catalyst, which was prepared from the pure β zeolite, was the one with the highest acidity, and that may be reasonable considering its lower Si/Al ratio (Table 2.1) and its higher Pd content; a similar inference can be made for the γ-Fe_2O_3-ZSM-12-Pd catalyst, which has the lowest acidity and Pd content, a direct consequence of its Si/Al ratio (Table 2.1). As for the catalysts with the zeolite mixture, both the synthetic and physical mixtures had similar acidity and Pd content.

TABLE 2.3- Total acidity of the metal-exchanged catalysts determined by temperature programmed desorption of ammonia NH_3-TPD and percent of palladium determinate by ICP-OES.

Catalyst	**Total Acidity (μmol of NH_3/g of catalyst)**	**Pd% (%wt)**
γ-Fe_2O_3-β(p)-Pd	1887	2.6
γ-Fe_2O_3-ZSM-12-Pd	1199	0.8
γ-Fe_2O_3-(β+ZSM-12)-Pd	1830	1.2
γ-Fe_2O_3-β-Pd	1808	1.1

Once the acid sites were quantified, their nature was determined by FT-IR with pyridine. Spectroscopic measurements of adsorbed base molecules offer the convenient way for distinguishing Brönsted-type and Lewis acid sites.[134] When a molecule gets in contact with a solid surface, the formation of adsorption complexes will cause some specific bands to shift, affording various types of information. Among these molecules is pyridine, which is widely used to determine the nature of the acidic sites of a solid because the ring vibration modes are very sensitive to the environment, which allows the differentiation of Brönsted and Lewis acid sites.

When pyridine is absorbed on an acid solid surface, it may interact with it in three different ways: (1) if the acid site is of Lewis type, a coordination complex will be formed, while if the site is of Brönsted type, (2) the pyridinium ion is formed through the

protonation of pyridine by strong acid sites, or (3) pyridine interacts with weak acid sites through hydrogen bonding (Scheme 2.2).[8] The pyridine reacts with acidic OH groups to form pyridinium ion. This interaction are characterized by band at 1540–1550 cm^{-1} and at the same time, the band due to acidic OH groups disappears. Pyridine also reacts with Lewis acid sites to show the bands at 1440–1445 cm^{-1}. [134]

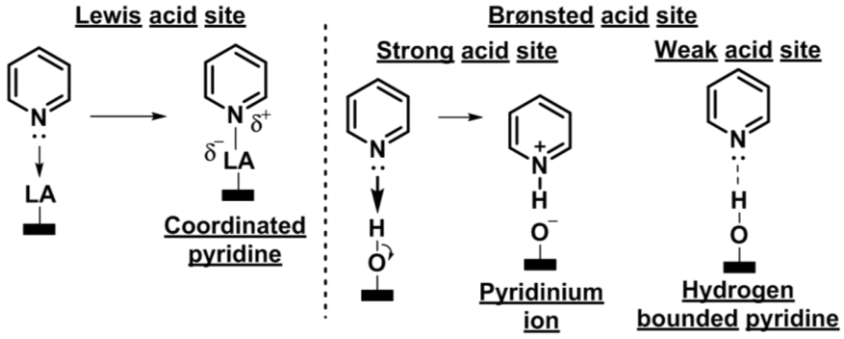

SCHEME 2.2- Interaction of pyridine with different acid sites on a solid acid catalyst.

In figure 2.13-a can see that all magnetically recoverable catalysts exchanged with the different transition metals as well as its acid form have a similar spectrum, presenting in all cases both Lewis and Brönsted acid sites. The band at 1455 cm^{-1} is ascribed to pyridine strongly bound to Lewis acid sites, and the one at 1497 cm^{-1} corresponds to both Lewis and Brönsted acid sites; the ones at 1553 and 1656 cm^{-1} are related to the pyridinium ion, which implies the presence of Brönsted acid sites, while the band at 1603 cm^{-1} is attributed to H-bonded pyridine.[135-137] On the other hand in figure 2.13-b can see that the catalysts synthesized from the pure zeolites exchanged with palladium, as well as the physical mixture exchanged with palladium also present both acid sites. The catalyst γ-Fe_2O_3-ZSM-12-Pd showed a considerably higher amount of weak Brönsted acid sites, this is a consequence of its high silicon content combined with the relatively low Pd amount.

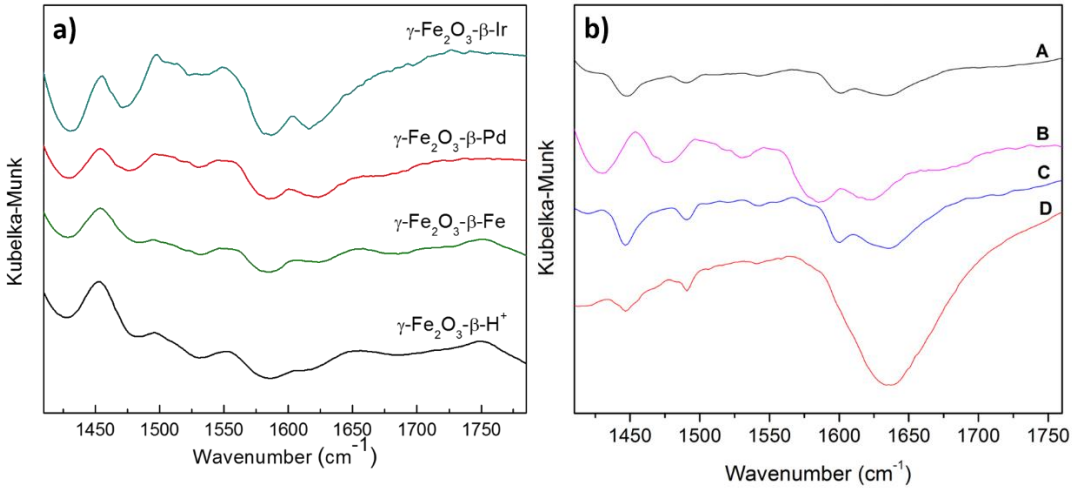

FIGURE 2.13- Fourier transform infrared spectroscopy of adsorbed pyridine spectra of the magnetically recoverable catalysts. a) γ-Fe_2O_3-β-H^+, γ-Fe_2O_3-β-Fe, γ-Fe_2O_3-β-Ir and γ-Fe_2O_3-β-Pd and b) A = γ-Fe_2O_3-(β+ZSM-12)-Pd, B = γ-Fe_2O_3-β-Pd, C = γ-Fe_2O_3-βp-Pd and D = γ-Fe_2O_3-ZSM-12-Pd.

2.1.2.4 Identification and quantification of the metals present in the catalyst

By X-ray photoelectron spectroscopy (Xps) analysis, it was possible to determine the different species of metal ions present in each of the magnetically exchanged catalysts. XPS is the most widely used surface characterization method for the qualitative and quantitative determination of all elements present at the surface in the sample except for H_2 and He. Specifically, it gives information about the atomic composition of the sample, as well as the structure and degree of oxidation of the compounds examined. The theoretical basis of the technique is based on the photoelectric effect, according to which, when a sample is irradiated with photons of a higher energy than the bonding of the electrons of the atoms, the electrons leave the sample with a kinetic energy equal to the excess energy of the photon with respect to the binding energy. Each element gives rise to a single spectrum, so that the spectral peaks of a mixture correspond approximately to the sum of the individual peaks of each of the components.[138]

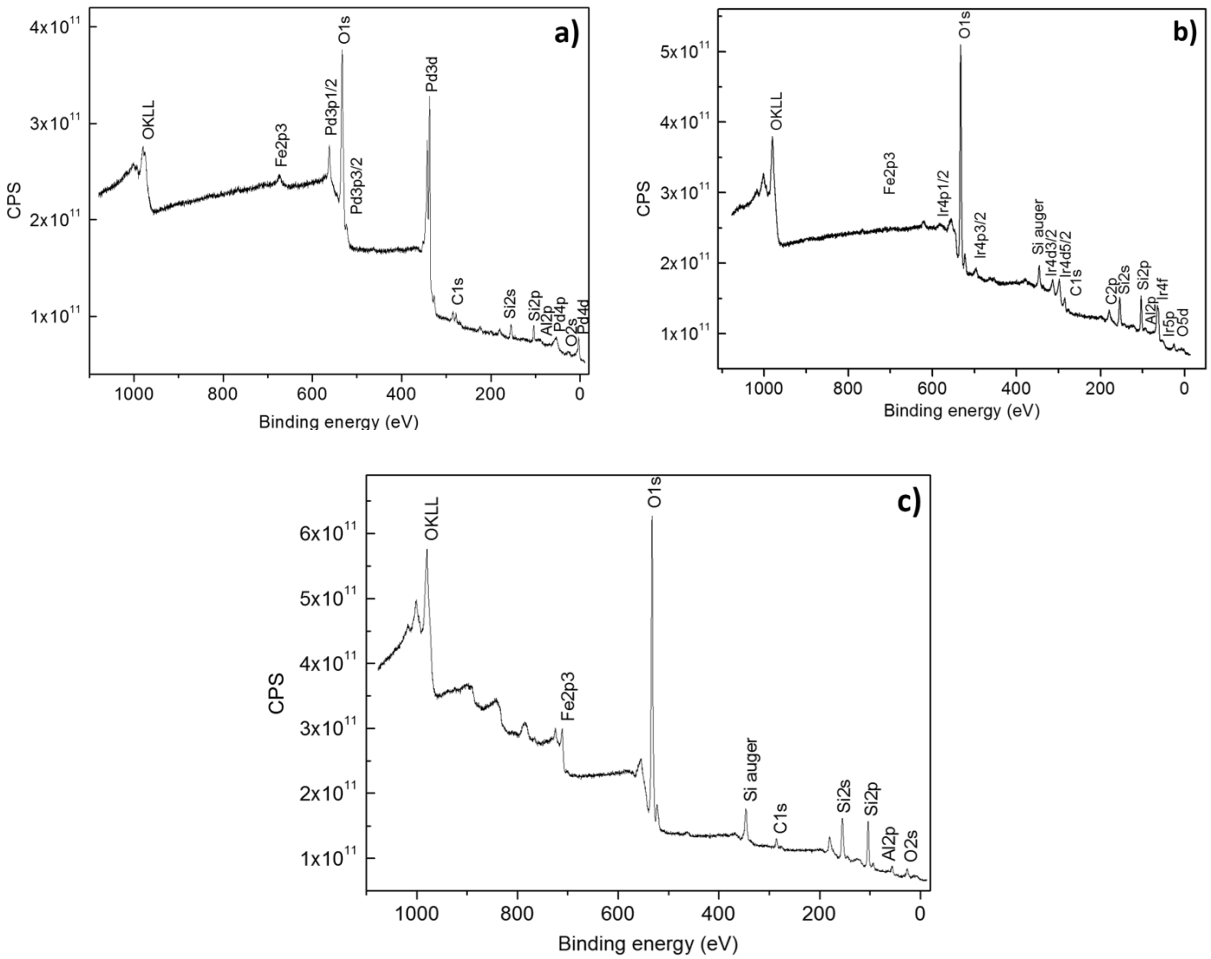

FIGURE 2.14- XPS scan for: a) Pd-exchanged catalyst, b) Ir-exchanged catalyst and c) Fe-exchanged catalyst.

In the case of the catalyst exchanged with palladium it was evident that the palladium ion is mainly in the form of PdO and PdO_2 as confirmed by a closer look at the Pd3d core level (Figure 2.14 a, 2.15 a and Table 2.4). However, the presence of Pd^{2+} ions exchanged into the zeolite was also detected in a considerable amount. Intermediate Pd species like Pd^{+} and Pd^{3+} were also present, but in a very low concentration.[139] As for the Ir-exchanged catalyst, it was possible to observe the presence of IrO_2, Ir^{3+} and Ir^{4+} exchanged into the zeolite, as confirmed by the analysis of the Ir4f core level (Figure 2.14 b, 2.15 b and Table 2.4). [140, 141] Finally, the further study of the Fe2p core level of the Fe-exchanged catalyst (Figure 2.14c, 2.15c and Table 2.4) showed the presence of a small

amount of Fe^{2+} attributed to the magnetite structure, thus inferring that the conversion of Fe_3O_4 to γ-Fe_2O_3 was not complete,[50] Fe^{3+} from the γ-Fe_2O_3 structure, and Fe^{3+} exchanged into the zeolite.[142, 143]

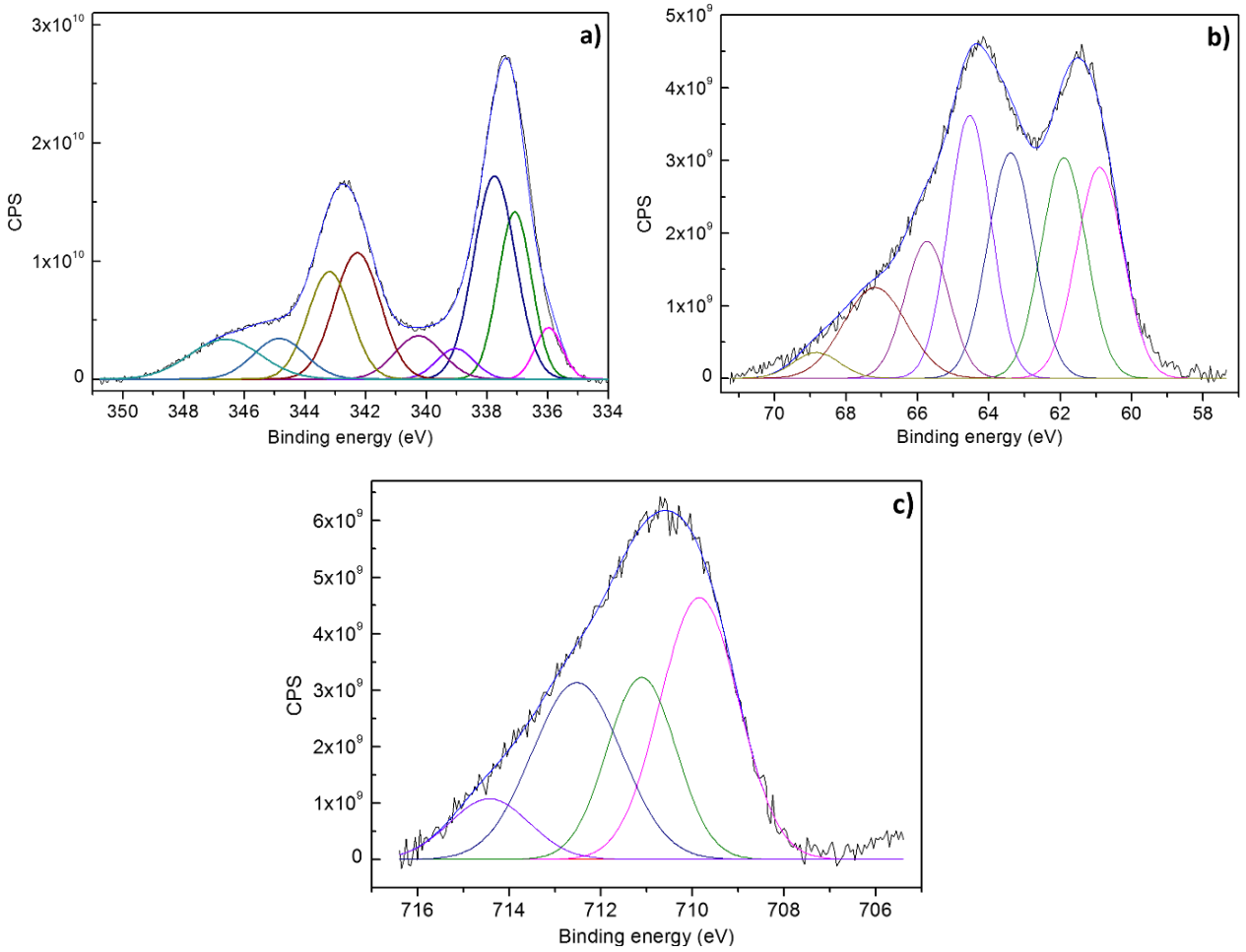

FIGURE 2.15- a) Pd3d core level XPS spectrum for the Pd-exchanged catalyst, b) Ir4f core level XPS spectrum for the Ir-exchanged catalyst and c) Fe2p core level XPS spectrum for the Fe-exchanged catalyst.

TABLE 2.4- Relative quantitative amount of each Pd, Ir and Fe species in the surface of the Pd, Fe and Ir exchanged zeolite.

Core level	Binding Energy (eV)	Species	Area (%)
Pd3d	335.96	Pd^{2+}	8.6
	337.08	Pd^{+}, PdO	33.6
	337.75	PdO_2	50.9
	339.04	Pd^{3+}	6.9
Ir4f	61.90	Ir^{3+}	32.8
	63.39	Ir^{4+}	35.6
	64.53	IrO_2	31.6
Fe2p	709.85	Fe^{2+} (Fe_3O_4)	41.9
	711.11	Fe^{3+} (γ-Fe_2O_3)	25.7
	712.52	Fe^{3+}	32.4

TABLE 2.5- Specific surface area and micropore volume of zeolite in the sodic form and of metal-exchanged catalysts.

Sample	Specific Surface Area (m^2/g)	Micropore Volume (cm^3/g)
γ-Fe_2O_3-β-Na	398	0.190
γ-Fe_2O_3-β-H^{+}	358	0.138
γ-Fe_2O_3-β-Fe	296	0.142
γ-Fe_2O_3-β-Ir	283	0.136
γ-Fe_2O_3-β-Pd	285	0.137

Subsequently, the surface area of the catalyst in its sodic form was determined with respect to the catalyst exchanged with metals by means of nitrogen adsorption isotherm analysis. The results show (Table 2.5) that the exchange with metals did not markedly affect the surface area or the micropore volume of the materials.

Magnetization curves were obtained for the magnetic support as well as for the catalyst exchanged with palladium to know its magnetic behavior. The measurements

were made at room temperature via SQUID. As can be seen in the Figure 2.16 a) and b), the maghemite microspheres presented a high saturation magnetization (64.2 emu·g^{-1}) on the contrary for the Pd exchanged catalyst that presented 6 emu·g^{-1}. It is known that the value of saturation magnetization is a volumetric measurement that depends on the mass, so when measuring the sample, there is part of it that does not manifest magnetic response (the zeolite, a diamagnetic material) and its value is underestimated. It is know that the amount of zeolitic material in relation to the magnetic support is high. To recalculate the saturation magnetization value obtained for the catalyst exchanged with Pd the amount of γ-Fe_2O_3 was determined in the same using the iron concentration as discerned by ICP-OES, which was 2.3%. Interestingly, though, when only the saturation magnetization of γ-Fe_2O_3 in the catalyst was considered, it was increased with respect to the support, which may be termed magnetostriction effects,[144, 145] an occurrence that is currently being scrutinized and will be reported in due time. However, as can be seen in Figure 2.16 c) and 2.16 d), it is possible to separate the catalyst from the reaction medium easily with the aid of a magnet.

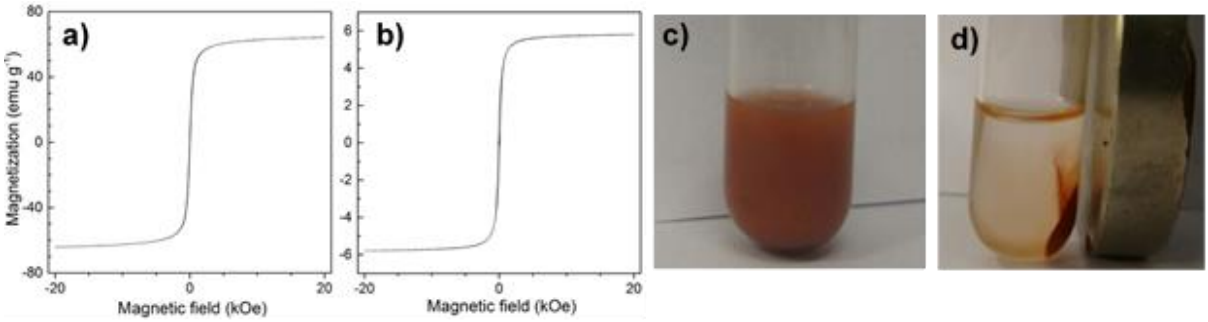

FIGURE 2.16- SQUID magnetization curves of a) the magnetite microspheres used as support and b) the Pd-exchanged catalyst, and images depicting c) the catalyst in the reaction right after stirring and d) the separation of the catalyst with a magnet after 10 s.

Finally, to confirm the identity of the iron phases in the sample, room temperature Mössbauer spectroscopy experiments were performed to Pd-exchanged catalyst. This technique is based on the recoilless emission and the recoilless resonant absorption of photons by the nucleus. The most widely used in the characterization of materials is the Mössbauer spectroscopy of the ^{57}Fe isotope. The Hyperfine interactions isomer shift (δ), quadrupole splitting (ΔE_Q), linewidth (Γ), hyperfine magnetic field (B_{hf}) and

relative area of the individual spectral components (RA) are characteristic parameters of this technique. Through this technique, it is possible to identify the different types of iron oxides;[146, 147] hence, we can differentiate between magnetite and maghemite. The ^{57}Fe Mössbauer spectrum is showed in Figure 2.17 and the values of the Mössbauer hyperfine parameters, derived upon spectrum fitting, are listed in Table 2.6. The ^{57}Fe Mössbauer spectrum showed the presence of two spectral components: one sextet (line S1) and one doublet (line S2). The sextet component was the major one, 89% relative area (see Table 2.6), and its isomer shift value is consistent with that expected for Fe^{3+} ions with a high-spin state (S =5/2) in both tetrahedral and octahedral coordination. The presence of this component with such a high relative area corroborates the SQUID results and confirmed our initial belief that iron oxides are present in the catalyst predominantly as maghemite. [148] As for the other component, it consisted of a doublet with a wide line width which could be assigned to ionic Fe^{3+} and/or small nanoparticles within the superparamagnetic domain (characteristic of particles with sizes below 15 nm).

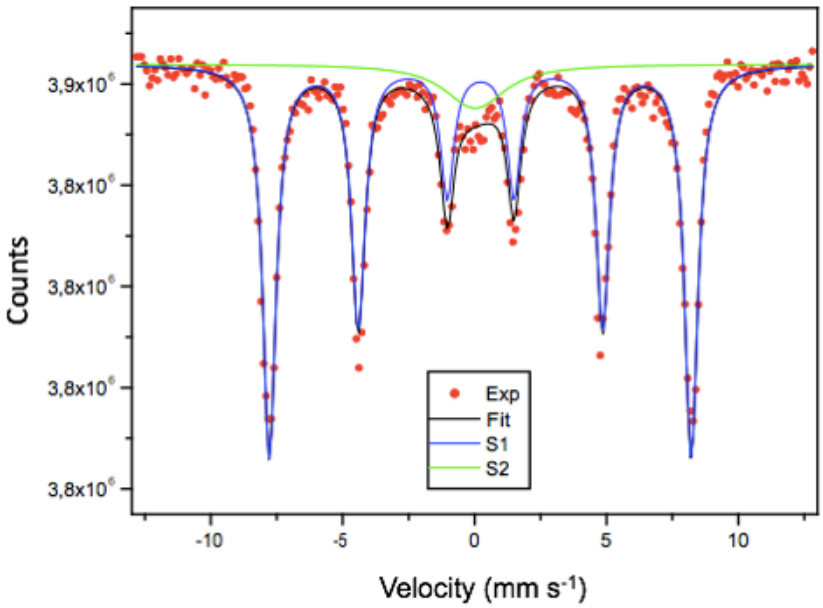

FIGURE 2.17- ^{57}Fe Mössbauer spectrum of the Pd-exchanged catalyst measured at room temperature.

TABLE 2.6- Data extracted from the least-squares fitting of the room temperature ^{57}Fe Mössbauer spectrum of the Pd-exchanged catalyst.

Component	δ (mm s^{-1})	ΔE_Q (mm s^{-1})	Γ (mm s^{-1})	B_{hf} (T)	RA (%)
Sextet	0.33	-	0.61	49.7	89
Doublet	0.13	0.53	2.61	-	11

2.1.3 Catalytic applications

2.1.3.1 Evaluations of magnetically recoverable catalysts in the conversion of furfural, furfuryl alcohol and ethyl levulinate

Once the magnetically recoverable catalysts were synthesized and characterized (γ-Fe_2O_3-β-Pd, γ-Fe_2O_3-β-Fe, γ-Fe_2O_3-β-Ir, γ-Fe_2O_3-β-H^+) were used in the valorization of lignocellulosic biomass-derives. The above was performed to evaluate the effect can have the different metals exchanged into the zeolite core in these reactions. To start the study, three chemical platforms were selected: furfural (FUR), furfuryl alcohol (AF) and ethyl levulinate (EL). In all cases, was employed 0.3 mmol of each starting material, 750 µL of isopropanol as the solvent and source of hydrogen, 75 mg of each catalyst, the working temperature was 130 ^oC and the reaction time was 24 hours.

When the study was carried out using furfural as the starting platform (Figure 2.18 a), it was observed that the major product obtained for all the catalysts was isopropyl levulinate (PL), which shows the efficiency of all the catalysts in promoting two reaction steps in the valorization of furfural according to Scheme 2.3. The first step consists in the hydrogenation of the furfural in the presence of a Lewis acid to produce the furfuryl alcohol which goes through an alcoholysis process (second step) in the presence of a Brönsted acid and generates isopropyl levulinate. The proposed mechanism for the conversion of furfural to isopropyl levulinate can be seen in Scheme 2.4.

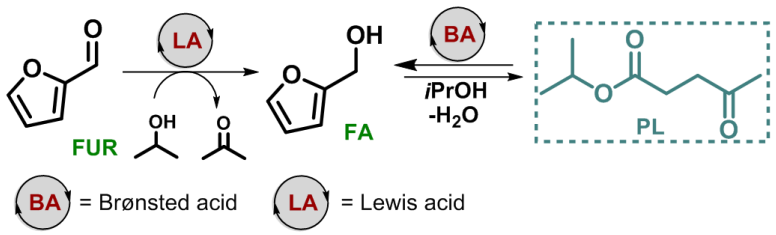

SCHEME 2.3-Conversion of furfural (FUR) to propyl levulinate (PL)

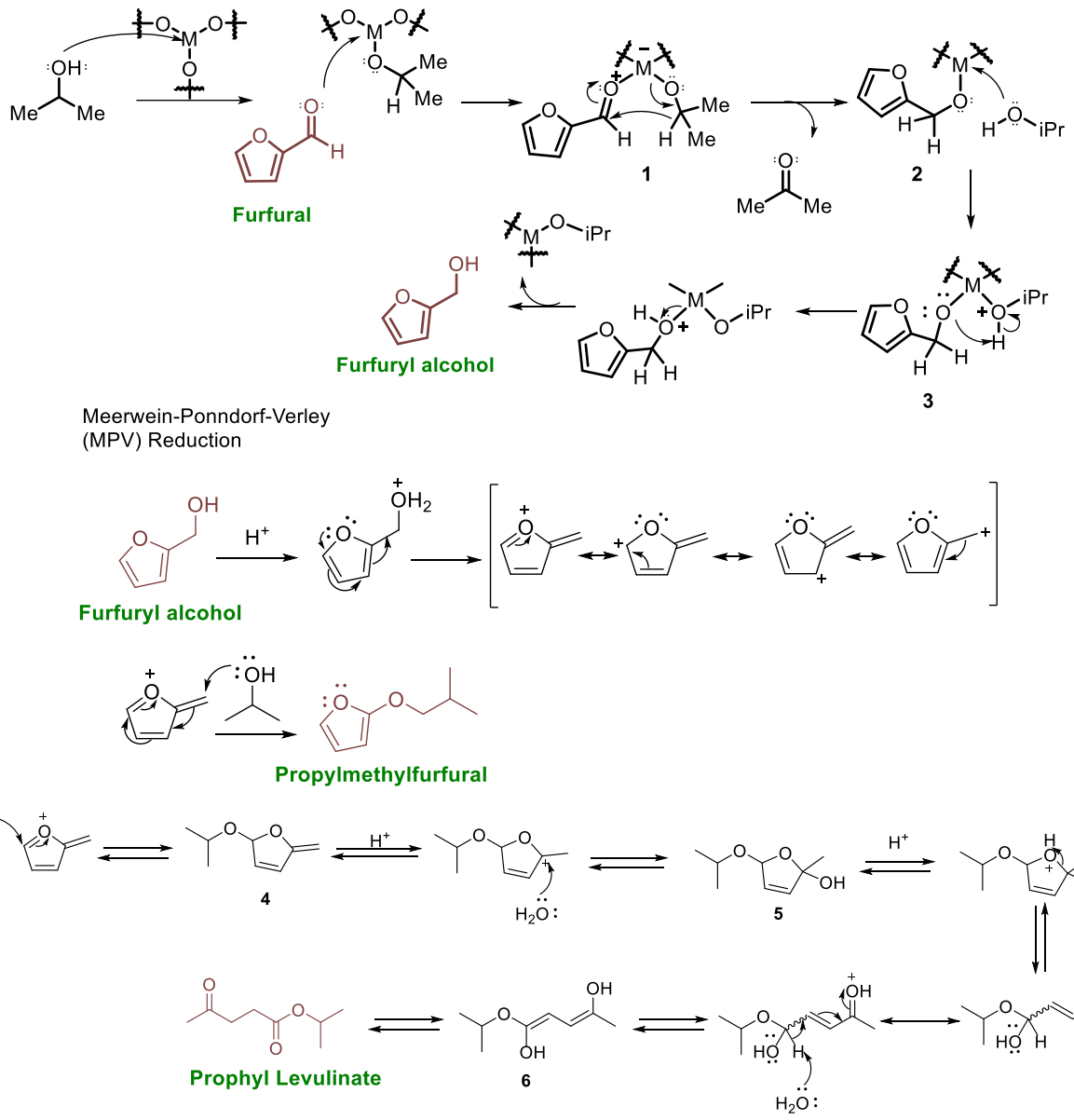

SCHEME 2.4- Proposal of mechanism for the conversion of furfural to propyl levulinate. M = metal

First the isopropyl alcohol is coordinated to a Lewis acid site of the catalyst, then the oxygen of the carbonyl group of furfural is coordinated to the same acidic site forming the intermediate 1. Subsequently there is a transfer of hydrogen from isopropyl alcohol to furfural releasing a molecule of propanone and intermediate 2 is formed. Next, another molecule of isopropyl alcohol is again coordinated to the Lewis site forming intermediary 3. Oxygen outside the furan ring takes a proton of isopropyl alcohol, producing furfuryl alcohol and regenerating the catalyst again.

Subsequently, the furfuryl alcohol in the presence of a Brönsted acid is protonated releasing a molecule of water and leaving a carbocation stabilized by resonance. If the isopropyl alcohol attack the double bond that is outside the ring of resonant structure, propylmethylfurfural will be obtained. On the other hand, if the attack is on the C4 of the furan ring, then intermediate 4 is produced, which in the presence of Brönsted acid undergoes a protonation of the exocyclic double bond forming a tertiary carbocation which suffers a nucleophile attack from water producing the intermediate 5. This intermediary undergoes the protonation of the oxygen of the ring producing the rupture of the cycle and forming an acyclic carbocation. Subsequently, a nucleophile attack of a water molecule and an electron rearrangement occurs that gives rise to the intermediate 6 which, through a keto-enol balance, produces the isopropyl levulinate.

In general, the conversion of furfural carried out by all the tested catalysts was about 60% except the palladium one which provided a 100 % conversion. Regarding to the selectivity of this process, the catalyst in the acidic form (γ-Fe_2O_3-β-H^+) provides the higher selectivity to the ester product (~88%) and the Fe and Ir exchanged catalysts giving moderate selectivity (76% and 67% respectively) and generates a more complex mixture of products. The lower conversions in the presence of these catalysts may be due to the lower amount of strong acidic sites; higher catalyst loadings would therefore be required in reactions with these materials. On the other hand, the only catalyst that gave 100% selectivity towards the ester was γ-Fe_2O_3-β-Pd. This result is comparable or superior when compared with other known catalysts.[149-151] This may be due to the presence of different active Pd^{2+} species on the surface of the catalyst (PdO and PdO_2) that facilitate the hydrogenation step. In addition to the large number of acid sites of moderate and high

strength compared to the other catalysts, this was evidenced in the results obtained by NH_3-TPD.

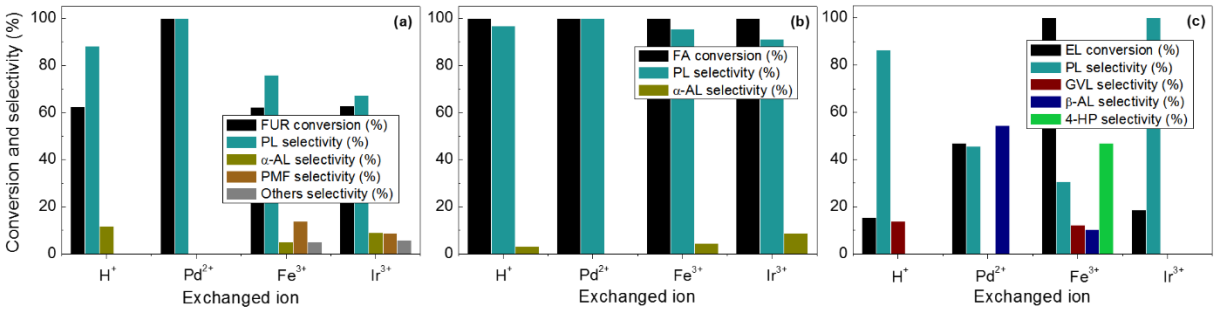

FIGURE 2.18- Magnetically recoverable β zeolite-promoted valorization of a) furfural, b) furfuryl alcohol and c) ethyl levulinate. FUR = furfural, FA = furfuryl alcohol, EL = ethyl levulinate PMF = 2-(isopropoxymethyl) furan, α-AL = α-angelica lactone, β-AL = β-angelica lactone, PL = isopropyl levulinate, 4-HP = isopropyl 4-hydroxypentanoate, GVL = γ-valerolactone.

On the other hand, when furfuryl alcohol is used as the starting material (Figure 18 b) all the catalysts produce 100% conversion for that chemical platform with a selectivity in all cases greater than 90% towards propyl levulinate. Also, the palladium catalyst gave 100% selectivity to the ester. Moreover, in all cases the only observed by-product was α-angelica lactone. The results obtained for this chemical platform are due to the fact, that all that is needed to promote the conversion of furfuryl alcohol to isopropyl levulinate, are Brönsted acid sites and according to the results obtained in the FT-IR with pyridine, all the catalysts present many of this acid site.

When the ethyl levulinate (Figure 2.18 c) was evaluated as the sharing platform the γ-Fe_2O_3-β-H^+, γ-Fe_2O_3-β-Pd, γ-Fe_2O_3-β-Ir catalysts afforded conversions below 50%, while the Fe-exchanged catalyst achieved a full conversion of the starting material. Unfortunately, a mixture of products was obtained for all catalysts. In all cases, one product was isopropyl levulinate. This does not correspond to a conversion process of this chemical platform; it was a transesterification of ethyl levulinate in the presence of isopropyl alcohol towards the isopropyl levulinate according to Scheme 2.5.

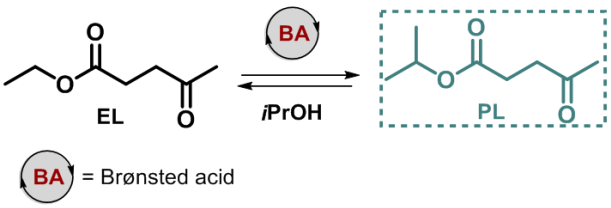

SCHEME 2.5-Transesterification of ethyl levulinate (EL) to propyl levulinate (PL).

As can be noticed, in the case of Fe-exchanged catalyst the mayor product was isopropyl 4-hydroxypentanoate, a product of the reduction of isopropyl levulinate. Aiming to induce the cyclization of the 4-HP intermediate to GVL combining the Fe-exchanged catalyst with the one in the acidic form (γ-Fe_2O_3-β-H^+) was tried. However, even after extensive studies, it was not possible to achieve the optimal conditions for this transformation via a cooperative catalysis mediated by the designed catalysts. Consequently, low conversions and selectivity in the processes were observed (Figure 2.19) using this starting material. These results led to the discontinuity of this path.

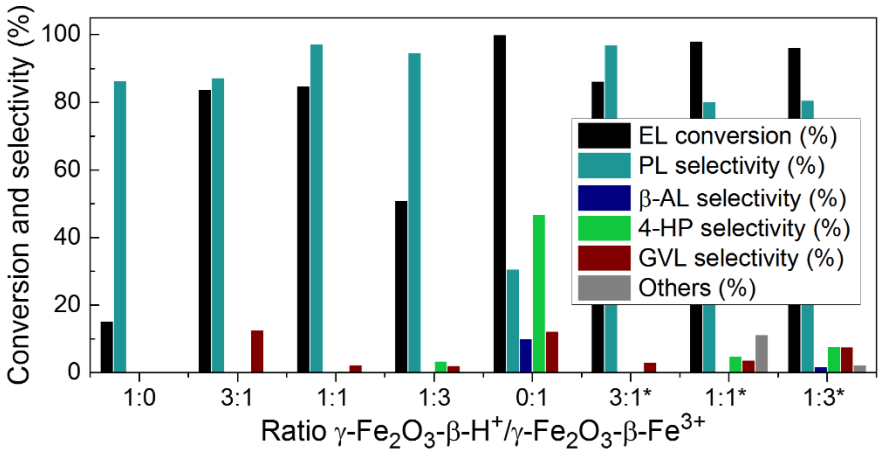

FIGURE 2.19- Upgrading of ethyl levulinate in the presence of different ratios of the catalyst γ-Fe_2O_3-β-H^+/γβ-H_2O_3-β -Fe^{3+}. *Reactions performed at 150°C. EL =ethyl levulinate, PL =isopropyl levulinate, β-AL =β-angelica lactone, 4-HP =isopropyl 4-hydroxypentanoate, GVL =γ-valerolactone. Reaction conditions: 0.3 mmol of ethyl levulinate, 750 µL of isopropyl alcohol and different amounts of catalyst at 130°C for 24h.

2.1.3.2 γ-Fe_2O_3-β-Pd studies of the reaction parameters in the conversion of furfural and furfuryl alcohol to isopropyl levulinate using as catalyst.

As can be seen in the tests carried out previously, the magnetically recoverable catalyst exchanged with palladium was the one with best activity. It presented 100% of conversion and selectivity towards isopropyl levulinate when used furfural and furfuryl alcohol as chemical starting platforms. Because of that, for both reactions was studied the influence of different experimental parameters such as temperature, mass of catalyst and concentration of starting material in the conversion and selectivity.

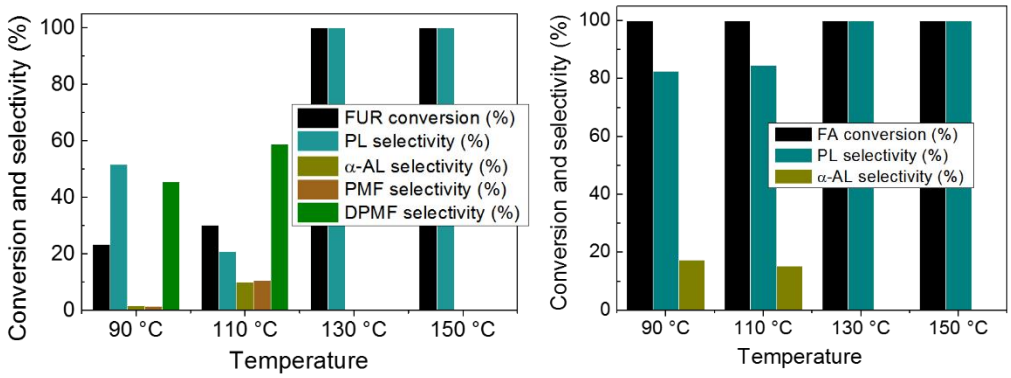

FIGURE 2.20- Evaluation of the temperature in the valorization of (a) furfural and (b) furfuryl alcohol using a magnetically recoverable Pd-exchanged β zeolite catalyst. FUR = furfural, FA = Furfuryl Alcohol, PMF = 2-(isopropoxymethyl) furan, α-AL = α-angelica lactone, PL = isopropyl levulinate, DPMF = 2-(diisopropoxymethyl)furan.

The first parameter to be evaluated was the temperature, the tests were carried out using 0.3 mmol of starting material, 750 µl of isopropanol, 75 mg of γ-Fe_2O_3-β-Pd and 24 h of reaction at different temperatures in an oil bath. In the case of the tests carried out using furfural as starting material (Figure 2.20 a), 23.4% the conversion and 30% the selectivity, were obtained at 90 ºC and 110 ºC respectively; with a mixture of products present at the end of the reaction. However, at a temperature of 130 ºC and 150 ºC a 100%

conversion and selectivity was obtained. As at 150 ºC there were no different results, it was selected 130 ºC as the working temperature. On the other hand, when using as starting material furfuryl alcohol (Figure 20 b) even at low temperatures 100% conversion and moderate selectivity values to propyl levulinate (> 80%) are produced. As in the test carried out with furfural, 100% selectivity was achieved at temperatures of 130 ºC and 150 ºC. In this case, it was also chosen 130 ºC as a working temperature.

Having defined for both cases 130 ºC as working temperature, the influence of the catalyst loading for both reactions was evaluated. The reactions were set up using 0.3 mmol of furfural or furfuryl alcohol, 750 µL of isopropyl alcohol and different amounts of the γ-Fe_2O_3-β-Pd catalyst at 130 ºC for 24 h. When furfural is used as the starting material (Figure 2.21 a) it was found that this parameter has an influence significant on both, the conversion and selectivity of the reaction. When a small amount of catalyst was employed (5 mg), a conversion around 6.5% was observed, and only α-AL and the DPMF ether were present as products. When the catalyst loading was increased to 15 mg, the conversion was slightly higher (7.6%), but traces of the ester product started to emerge among the products, and with 25 mg the conversion was still low, but PL was then the major reaction product. A further increase of the catalyst loading to 50 mg resulted in a large increase in both conversion (76%) and selectivity to PL (around 91%). Finally, with 75 mg of catalyst, the conversion of furfural was achieved with a total selectivity to PL. On the other hand, when furfuryl alcohol is used as the starting material (Figure 2.21 b), it can be stated that it does not have a dramatic effect on the conversion, but it dictates the selectivity. This is explained on the basis that the etherification product, PMF, can be readily formed even when small amounts of catalyst are present in the reaction medium, but its full conversion to isopropyl levulinate requires a minimum catalyst loading, in this case, 75 mg.

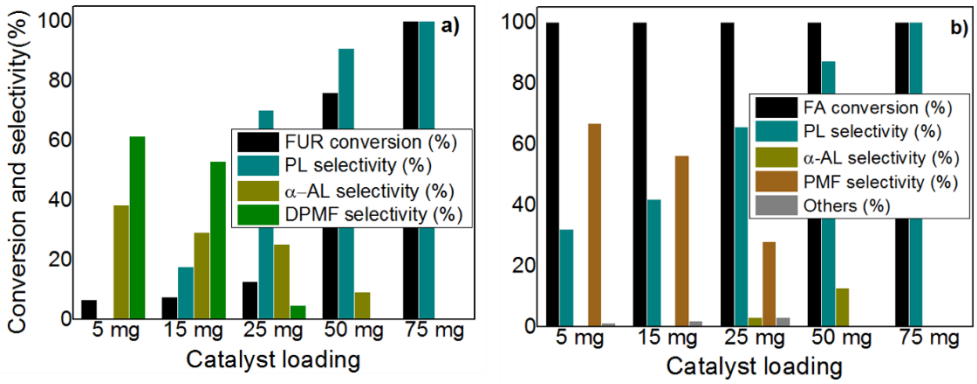

FIGURE 2.21- Evaluation of catalyst loading in the valorization of a) furfural and b) furfuryl alcohol using a magnetically recoverable Pd-exchanged β zeolite catalyst. FUR = furfural, FA = Furfuryl Alcohol, PMF = 2-(isopropoxymethyl) furan, α-AL = α-angelica lactone, PL = isopropyl levulinate, DPMF = 2-(diisopropoxymethyl)furan.

Having already set the temperature and the mass of catalyst, the concentration of the reaction medium was evaluated. The reactions were conducted with 0.3 mmol of furfural or furfuryl alcohol, variable amounts of isopropyl alcohol (iPrOH), and 75 mg of the γ-Fe_2O_3-β-Pd catalyst at 130 ºC for 24 h. When furfural is used as a starting material (Figure 2.22 a), the use of a relatively concentrated reaction medium (molar ratio FUR: iPrOH 1:10, when using 230 µL of isopropyl alcohol) led to a full conversion of furfural, but also to the formation of non-identified by-products, and consequently, to a diminished selectivity to PL (approximately 89%). A decrease in the molar ratio FUR: iPrOH to 1:20 and 1:30 (with the corresponding isopropyl alcohol amounts of 460 µL and 750 µL, respectively) caused the conversion to remain the same, but a full selectivity to PL was obtained in both cases. A further decrease in the molar ratio led to a significant drop in the conversion to approximately 62%, although the selectivity was unaltered. Due to this, molar ratio FUR: iPrOH 1:20 was selected. In the case of using furfuryl alcohol as the starting material (FIGURE 22 b), the evaluation of the molar ratio AF: iPrOH shows that for values in the range of 1:10 - 1:30, the conversion and selectivity were not affected to a great extent, but the further dilution of the reaction medium (molar ratio 1:40, when using 920 µL of isopropyl alcohol) caused a marked decrease in both the conversion and selectivity to isopropyl levulinate. Hence the optimal molar ratio FUR: iPrOH is 1:10.

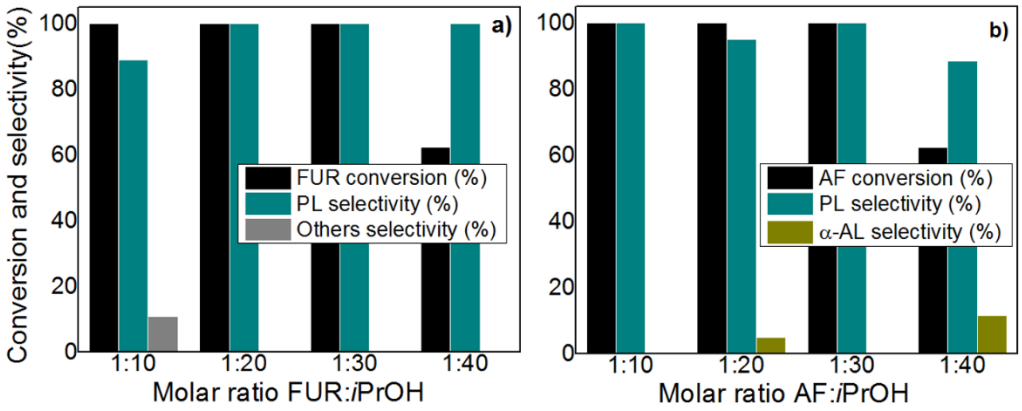

FIGURE 2.22- Evaluation of molar ration FUR or AF: iPrOH in the valorization of a) furfural and b) furfuryl alcohol using a magnetically recoverable Pd-exchanged β zeolite catalyst. FUR = furfural, FA = Furfuryl Alcohol, α-AL = α-angelica lactone, PL or iPrOH = isopropyl levulinate.

Aiming of understand how the reaction conversion and composition changed over time, we next conducted experiments under the identified optimal conditions by varying the reaction time. Starting from furfural as starting material (Figure 2.23 a) at time (3 h), a very low conversion of furfural was observed (approximately 13%), with the formation of PL with a 75% selectivity and α-angelica lactone being the only other reaction product. The conversion of furfural increases progressively with the increase of the reaction time, with the rise of the selectivity to the ester product being less pronounced over time. The conversion attains its maximum within 18 h, but only at 24 h the selectivity to PL reaches its maximum (100%). When furfuryl alcohol was used as starting material (Figure 2.23 b) at the initial evaluated time (15 min) the conversion was already complete, with a selectivity around 70% to isopropyl levulinate; the selectivity then slowly increases from this point until it reaches its maximum after 21 h.

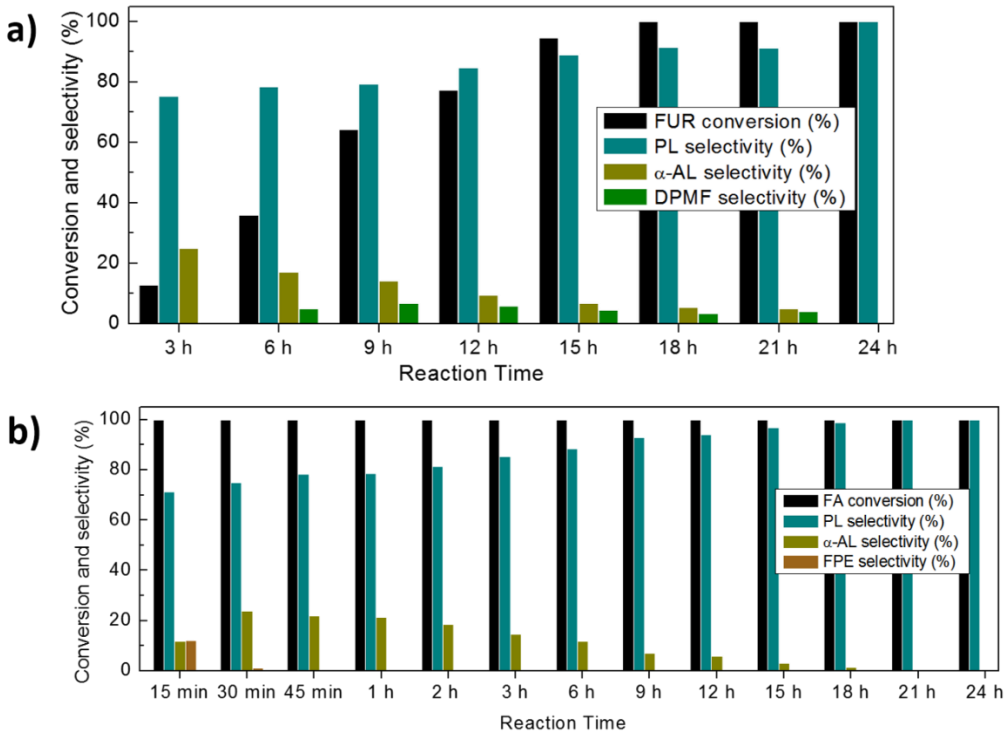

FIGURE 2.23- Evaluation of the reaction time in conversion and selectivity in the valorization of a) furfural and b) furfuryl alcohol over time using a magnetically recoverable Pd-exchanged β zeolite catalyst. FUR = furfural, FA = Furfuryl Alcohol, α-AL = α-angelica lactone, PL = isopropyl levulinate.

To confirm that the presence of the ZSM-12 zeolitic phase in the synthesized catalysts did not affect the catalytic activity a catalytic evaluation was made. For this it was used the magnetically recovered catalysts recovered with palladium synthesized from pure zeolites (γ-Fe_2O_3-βp-Pd, γ-Fe_2O_3-ZSM-12-Pd, γ-Fe_2O_3- (ZSM-12 + βp) -Pd). For the above, optimal conditions already established for both furfural and furfuryl alcohol were selected. The reactions were conducted with 0.3 mmol of furfural or furfuryl alcohol, 750 µL of isopropyl alcohol for the reaction with furfural or 230 µL for the reaction with furfuryl alcohol, 75 mg of the catalysts at 130 ºC for 24 h. All catalysts afforded full conversion of both furfural and furfuryl alcohol, with complete selectivity to isopropyl levulinate. The high activity of the γ-Fe_2O_3-ZSM-12-Pd even with a lower Pd content and acidity can be rationalized considering its high micropore sizes, combined with the great amount of Brönsted acid sites

in its structure. Those observations confirm our initial suppositions, the presence of ZSM-12 in the catalysts does not have a deleterious effect in their catalytic activity, quite the contrary.

Considering the great improvements that microwave-induced reactions have represented in the valorization of bio-derived compounds in recent years,[152] it was decided to evaluate this alternative heating source in addition to the conventional one. For this, optimal conditions already established for both furfural and furfuryl alcohol were selected only the time was variable. When was used furfural as starting material (Figure2.24 a) full conversion was obtained with 96% selectivity to PL in only 45 minutes and a complete selectivity within 1 h of reaction. In the case of furfuryl alcohol (Figure 2.24 b) were achieved the same levels of conversion and selectivity obtained using conventional heating,100% of conversion and selectivity to PL, in this case only in 30 min of reaction.

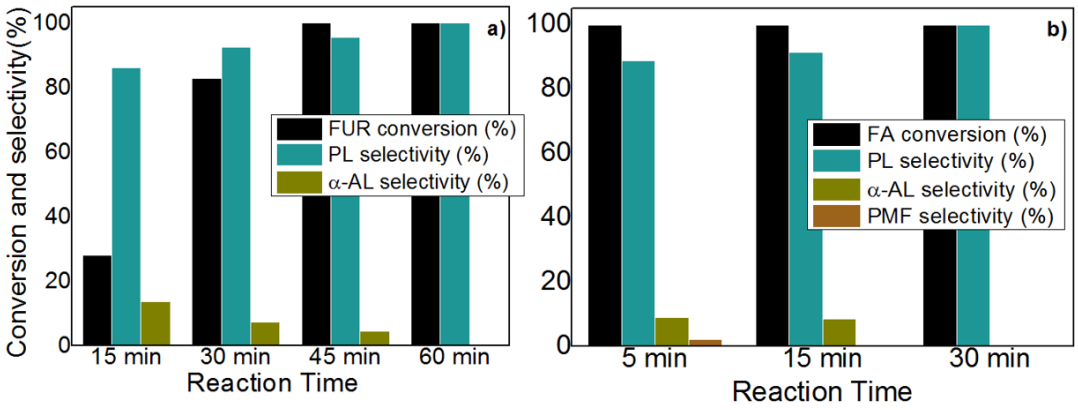

FIGURE 2.24- Evaluation of the reaction time in conversion and selectivity in the valorization of a) furfural and b) furfuryl alcohol over time using a magnetically recoverable Pd-exchanged β zeolite catalyst under microwave irradiation. FUR = furfural, FA = Furfuryl Alcohol, α-AL = α-angelica lactone, PL = isopropyl levulinate.

On the other hand, it was decided to take advantage of another interesting feature of the developed Pd catalyst, the presence of well-dispersed PdO nanoparticles on its surface.[153-156] The use of alternative hydrogen sources for the Lewis acid-promoted reduction steps and the possibility of conducting the reaction in water. It is well-known that water is a deactivation agent for zeolites,[42] however, was expected that the presence of the PdO nanoparticles in the surface of the catalyst would prevent its complete deactivation.

To confirm this hypothesis, we set up a reaction protocol by using furfural as the starting material in the presence of the Pd-exchanged catalyst in water at 60 ºC using sodium formate as hydrogen source. This salt was chosen because it is readily available, reacts neatly in water and at relatively low temperatures.[157-160] Fortunately, after an evaluation of the sodium formate amount and the reaction concentration (Table 2.7) was could attain a reaction condition obtaining a 76% conversion to exclusively furfuryl alcohol from furfural (Table 2.7, entry 2). Additionally, formic acid was evaluated as hydrogen source, but no furfural conversion was observed. Once again, very similar results in terms of conversion and selectivity could be attained using microwave irradiation in a considerably shorter time (1 h, Table 2.7, entry 6).

TABLE 2.7- Evaluation of the hydrogenation of furfural using the Pd-exchanged catalyst and sodic formate as hydrogen source.

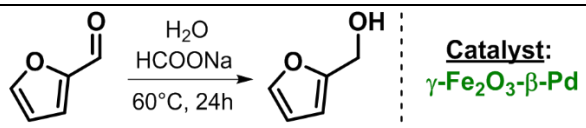

Entry[a]	Molar ratio FUR:HCOONa	Solvent amount (ml)	Conversion[b] (%)
1	1:40	1	41.6
2	1:20	1	76.2
3	1:20	0.5	61.9
4	1:10	0.5	29.8
5[c]	1:20	1	0
6[d]	1:20	1	77.6

[a]Unless stated otherwise, the reactions were set up in a sealed vial using 0.15 mmol of furfural, 3 mmol of sodic formats, 1ml of water and 32.5 mg of catalyst for 24 h; [b]The conversion of furfural was determined by GCMS; [c]Reaction performed with 18.75 mg of catalyst; [d]Reaction performed under microwave irradiation for 1h.

2.1.3.3 Recyclability of the catalyst γ-Fe_2O_3-β-Pd in the conversion of furfural and furfuryl alcohol to propyl levulinate.

To study the possible morphological changes that the catalyst could have undergone, once it was used in the conversion reaction of furfural and furfuryl alcohol, a series of characterizations of the material were carried out. The catalysts were characterized using TEM to discern possible morphological changes, and ICP-OES, to rule out eventual metal leaching issues. For both reactions no significant changes in the morphology of the materials were observed in the TEM (Figure 2.25) images, and the amount of Pd remained virtually unchanged.

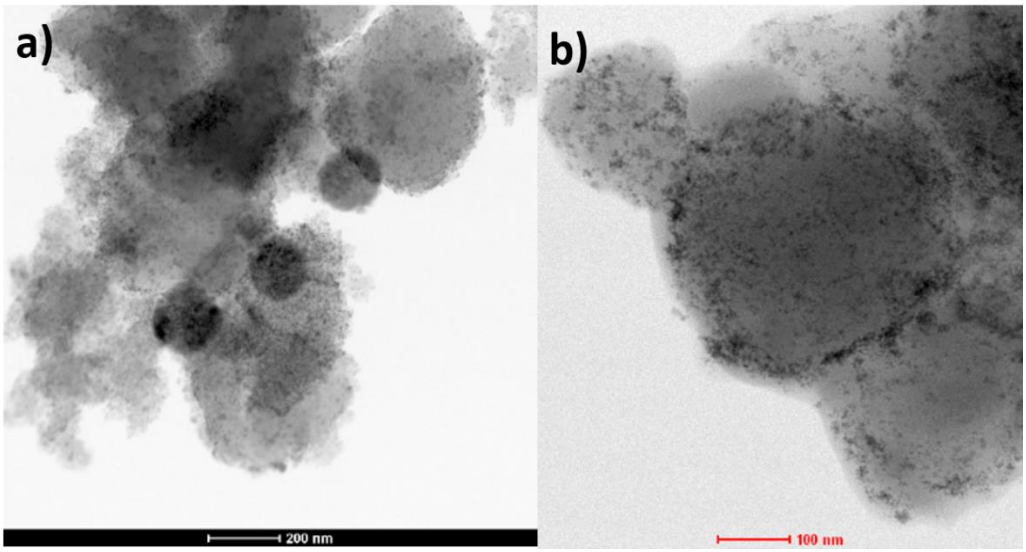

FIGURE 2.25- TEM image of the Pd-exchanged catalyst a) before the reaction an b) after the reaction. Scale bar: a) 200 nm and b) 100 nm.

Finally, we evaluated the recyclability of the Pd-exchanged catalyst in the conversion of furfural and furfuryl alcohol to isopropyl levulinate under the optimized conditions (Figure 2.26 a and 2.26 b). When furfural was used as starting material, the catalyst could be recycled by tree additional reaction cycles maintaining conversions above 60% and selectivity over 80% to isopropyl levulinate; at the 4^{th} reaction cycle, however, the

conversion was significantly reduced. In the case of furfuryl alcohol, no substantial reduction was noticed in the conversion, but the selectivity to isopropyl alcohol was highly affected, being 40% in the 3rd reaction cycle. In the case of the reaction with furfural, the conversion decreased after each reaction cycle probably due to the formation of hemins in the medium, which possibly blocked the Lewis acid sites needed to promote the first step of the reaction, the reduction of furfural to furfuryl alcohol. In the case of FA, however, the conversion remains high even after a series of reaction cycles. These results can be reasoned on the basis that even a small amount of Brönsted acids could promote the conversion of the alcohol to the intermediate ether (PMF); the evaluation of the composition of the reaction medium over time had already shown that the conversion of FA to PMF occurred very quickly (see Figure 2.23 b). However, when the selectivity to PL was examined in detail, similar trends were observed for the reactions with FUR and FA.

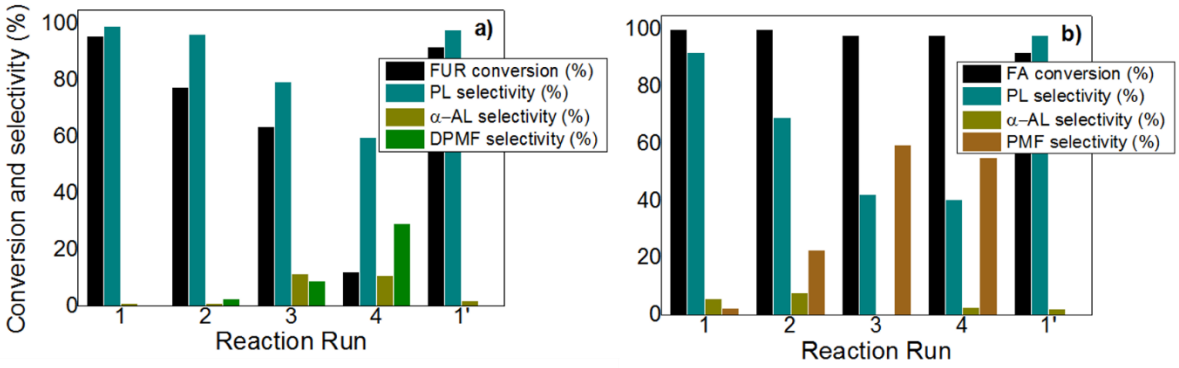

FIGURE 2.26- Evaluation of the recyclability of the Pd-exchanged catalyst in the upgrading of a) furfural and b) furfuryl alcohol to isopropyl levulinates. FA = Furfuryl Alcohol, DPMF = 2-(diisopropoxymethyl)furan, PMF = 2-(isopropoxymethyl)furan, α-AL = α-angelica lactone, PL = isopropyl levulinate.

Aiming to confirm that the hemins formed in the surface and pores of the catalyst were indeed responsible for its deactivation, was performed recalcination after the fourth reaction cycle (at 500 ºC for 5 h) and reexamined the upgrading of FUR and FA. The catalytic activity of this material was fully restored in both processes (reaction run denoted by 1' in Figures 2.26-a and 2.26-b), with conversions and selectivity to PL like the ones achieved when the fresh catalyst was used.

2.2 Mesoporous materials: sulfonic acid- functionalized dendritic silica

2.2.1 Synthesis

Due to the previously mentioned characteristics (epigraph 1.2.2 and 1.2.2.2) the dendritic mesoporous silica (DMSi) was selected as catalytic support and the sulfuric acid as active phase. The synthesis of the sulfonic acid- functionalized dendritic silica was carried out in several stages (Scheme 2.6). The specific methodologies for the realization of each one of these stages were described in the experimental procedure section (See 3.2.1).

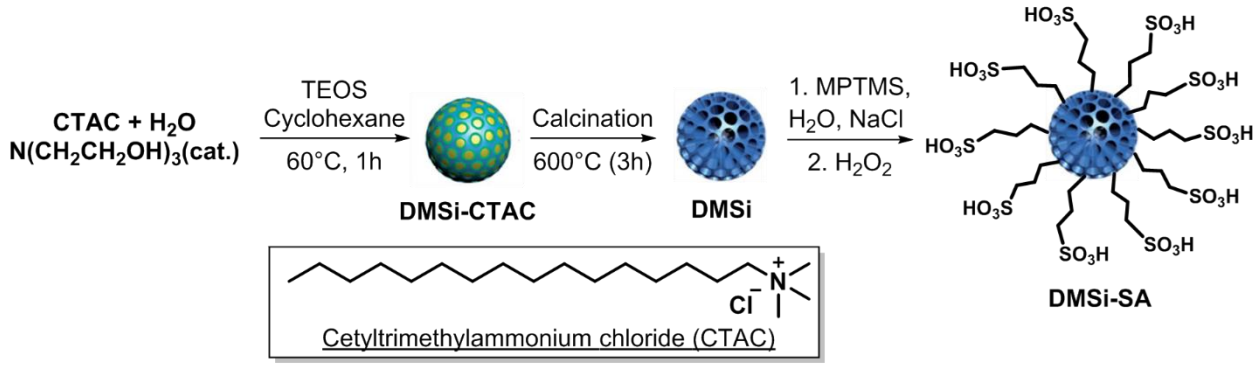

SCHEME 2.6- Preparation of sulfonic acid-functionalized dendritic mesoporous silica.[8]

First, the catalytic support, three-dimensional dendritic mesoporous silica nanospheres (DMSi), was prepared using a heterogeneous oil−water biphasic stratification reaction system developed by Yang and co-workers. The reaction takes place in the interface. The upper oil phase is a tetraethyl orthosilicate (TEOS) as the silicon source with hydrophobic organic solvent (cyclohexane), while the lower aqueous phase is an aqueous solution combined by cationic cetyltrimethylammonium chloride (CTAC) as pore template and organic base triethanolamine (TEA) as catalyst. The formation of DMSi requires a series of complex dynamic processes and the process of obtaining these particles involved four stages: nucleation process of the DMSi, growth process of the first generation of the DMSi,

changing the upper oil phase and growth process of the second generation of the DMSi.[94] The support was then functionalized with thiol groups using mercaptopropyl trimethoxy silane (MPTMS) using hydrothermal saline promoted grafting method. In this method the NaCl is used to increase the grafting efficiency of MPTMS, which is limited by the concentration of active Si-OH, particularly on calcined silicas. Finally the thiol groups are transformed into sulfonic acid by mild oxidation protocol using hydrogen peroxide as oxidizer.[161]

2.2.2 Characterization

Subsequent the silica catalysts were fully characterized using complementary techniques such as: high-resolution transmission electron microscopy (HRTEM), chemical mapping, X-ray photoelectron spectroscopy (XPS), nitrogen sorption measurements, inductive coupled plasma-optical emission spectroscopy (ICP-OES), X-ray fluorescence (XRF) and Fourier transform infrared spectroscopy of adsorbed pyridine (FTIR-Pyr).

2.2.2.2 Morphology and structure

The morphology presented by the synthesized catalyst (DMSi-SA) was determined by HRTEM. The determination of its chemistry composition in a qualitative way was done by elemental analysis mapping as well as Energy-dispersive X-ray spectroscopy (EDS). The characterization of the support material(DMSi) was not performed because it's well known and its functionalization with sulfonic acid does not produces significant changes in the material morphology.[8]

Figure 2.27 a, b, d and e shows HRTEM images of sulfonic-modified DMSi (DMSi-SA) material. In Figure 2.27 a and b can be observed that the particles of DMSi-SA are highly uniform nanospheres, forming agglomerates, with a narrow mean particle size of ~71 nm (Figure 2.27 c). The materials present the architecture of the dendritic particles

(Figure 2.27 d y e) with center-radial mesopore channels of 7.4 nm (Figure 2.27 f). To know the chemical elements of the synthesized catalyst an EDS was made.

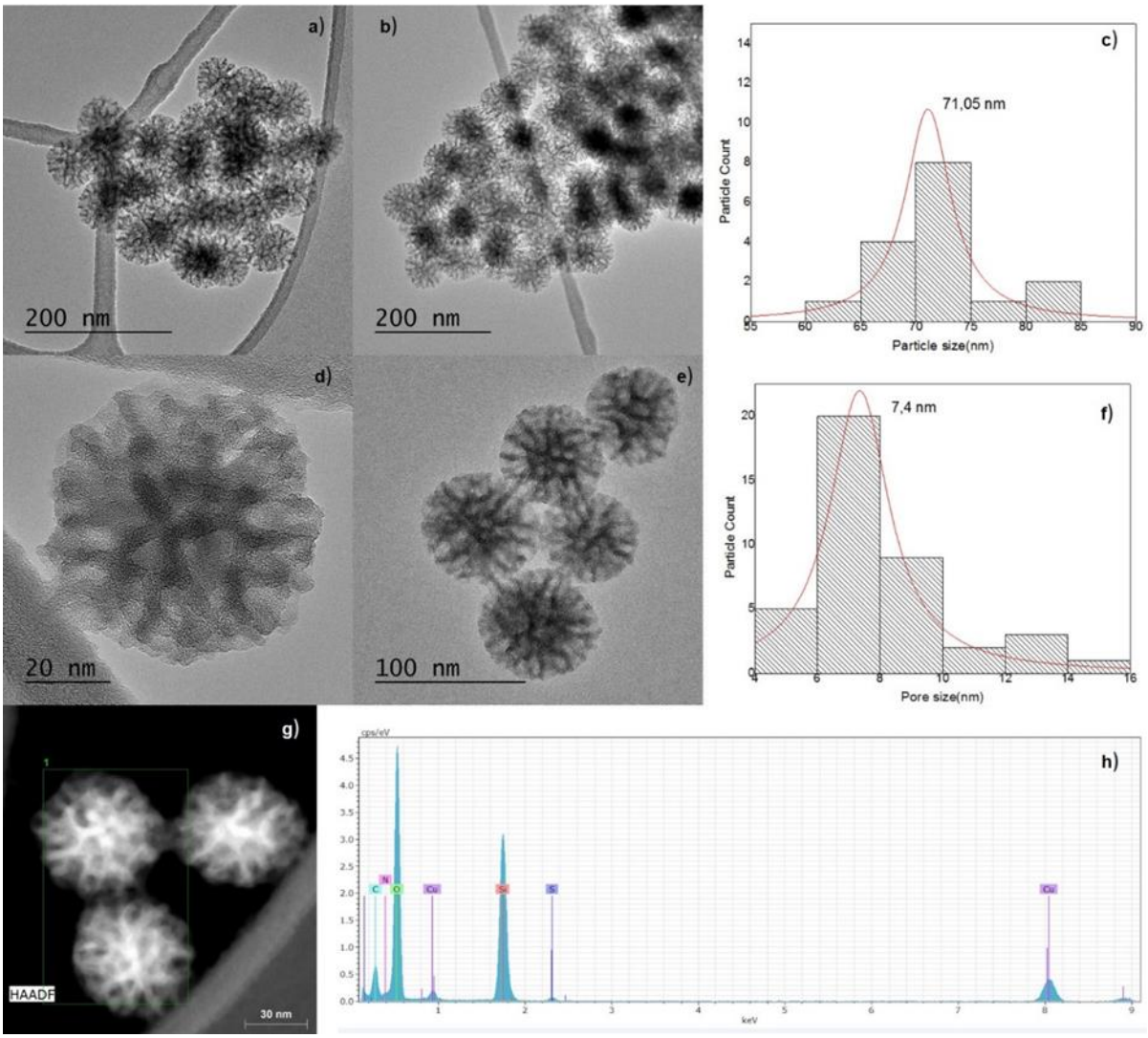

FIGURE 2.27- a), b), d), e), g) HR-TEM images of DMSi-SA, c) particle size distribution analysis from particle of Figure b, f) pore size distribution analysis of particle of Figure- e h) EDS spectrum of DMSi-SA. Scale bar: a), b) 200 nm, d) 20 nm, e) 100 nm and g) 30nm.

Energy dispersive X-ray spectroscopy (EDS) is a standard method for identifying elemental compositions in a very small sample of material (even a few cubic micrometers). In a properly equipped SEM, atoms on the surface are excited by the electron

beam, emitting specific wavelengths of X-rays that are characteristic of the atomic structure of the elements. A dispersive energy detector (a solid-state device that discriminates between the X-ray energies) can analyze these X-ray emissions. The appropriate elements are assigned, resulting in the composition of the atoms on the surface of the specimen. An EDS spectrum is made up of peaks that correspond to the energy levels for which most of the X-rays have been received. Each of the peaks is unique to an atom and therefore corresponds to a single element. The position of the lines gives the information about the qualitative composition of the sample.[162] Figure 2.27h shows the EDS obtained for the DMSi-SA confirming the presence of silicon, oxygen and sulfur atoms on this material.

Subsequently, the textural characterization of the pure DMSi nanospheres as well as the final catalyst (DMSi-SA) were conducted by nitrogen physisorption. The physisorption technique of gases is the most usual in the determination of surface areas and distribution of pore sizes of solids. This technique is based on the adsorption of nitrogen at 77 K. The obtained isotherms (representation of the volume of nitrogen in the solid compared to the relative pressure of nitrogen) correspond to the process of adsorption and desorption of the gas in the solid, producing hysteresis when the adsorption isotherm does not coincide with the desorption isotherm. The solids can be classified according to the type of isotherms they present. The adsorption isotherms, for the most part, can be grouped into five different types (I, II, III, IV, V). The presence of hysteresis between adsorption and desorption is characteristic of type IV and V isotherms, and there are five types of hysteresis according to De Boer. Each type of hysteresis is related to a particular form of pore.[163, 164]

The nitrogen adsorption and desorption isotherms of DMSi (silica support) and DMSi-SA (catalyst) are shown in Figure 2.28 a. Both isotherms could be classified as type IV, it is characteristic of mesoporous materials with pore condensation (Figure 2.28 b). Pore condensation is the phenomenon whereby a gas condenses to a liquid-like phase in a pore at a pressure p less than the saturation pressure p_0 of the bulk liquid. The hysteresis loop was type H3. Materials that give rise to H3 hysteresis have slit-shaped pores (the isotherms revealing type H3 do not show any limiting adsorption at high P/Po, which is observed with non-rigid aggregates of plate-like particles).[165] In Figure 2.28 b it was confirmed that the material is mesoporous and the existence of three scattering peaks in the DMSi and DMSi-

SA indicates that we are in the presence of a dendritic silica of three generations (third-generation shells). These particles are full of craters on the surface, also revealing an opening state of the mesopore channels on the third-generation shells. The three scattering peaks at ~3.6 nm, 6.3 nm (5.9 nm in DMSi-SA) and 25.9 nm (25.2 nm in DMSi-SA), indicating uniform mesostructure with three different cell parameters and pore sizes. It further suggests a hierarchically mesoporous structure.[94] The Figure 2.28 b also shows a large particle dispersion for both materials, decreasing a little the dispersion of the particles in the DMSi-SA.

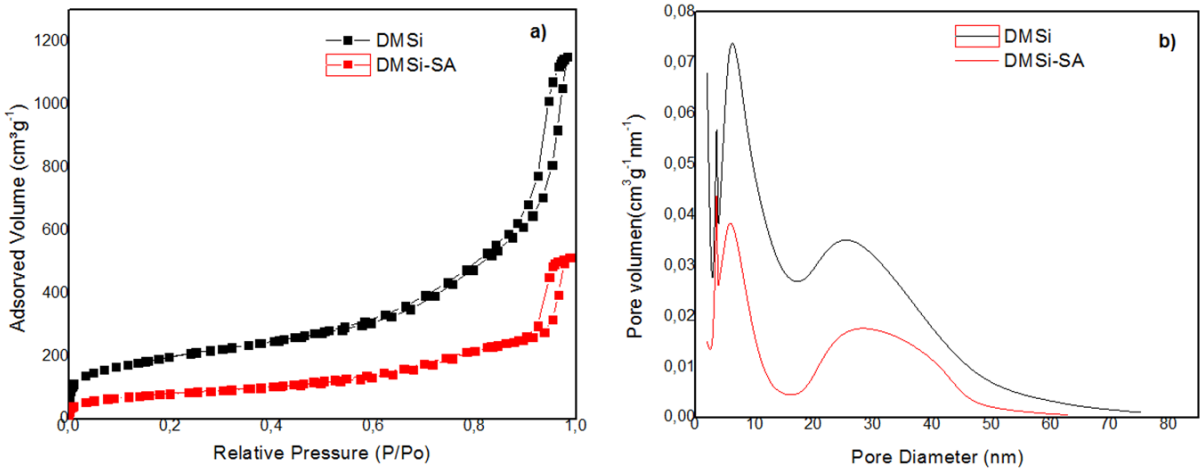

FIGURE 2.28- Textural characterization of silica support (black line) and silicas functionalized with sulfuric acid (red line) (a) isotherms of adsorption / desorption of N_2 and (b) pore distribution.

The Brunauer-Emmett-Teller (BET) surface area, external and micropore area, Barrett-Joyner-Halenda, (BJH) by volume (mesoporous and micropore) and pore size for DMSi were determined by N_2 adsorption / desorption isotherms and compared with its corresponding silica support (see Table 2.8). The DMSi has a high surface area. It is in correspondence with the values reported for this silica by other authors.[93, 94] Although there was a significant decrease in the surface area of the sample and the pore volume of the DMSi-SA when compared to the DMSi, there was no reduction in the pore size. This indicates that the functionalization in this case did not cause blockage of the pores.

Comparing the pore size reported in Table 2.28 with that obtained by the pore size distribution chart (Figure 2.28 b) and with the pore size obtained by HRTEM (Figure 2.27 f), they do not coincide. This is because the morphology of these particles which are very difficult to determine the pore size by HRTEM. The pore size determined by B.J.H is an average value of the three pore sizes present in the structure.

TABLE 2.8- Values to the textural characterization of silica supports, and silica functionalized with sulfuric acid.

Silica	**$S_{B.E.T}$ ($m^2 \cdot g^{-1}$)**	**$A_{micropore}$ ($m^2 \cdot g^{-1}$)[a]**	**$V_{micropore}$ ($cm^3 \cdot g^{-1}$)[a]**	**Total pore volume ($cm^3 \cdot g^{-1}$)[b]**	**Pore diameter (nm)[b]**
DMSi	704.7	50.8	0.0199	1.711	11.4
DMSi-SA	286.2	20.3	0.00765	0.768	11.5

[a] Calculated using t-plot method; [b] Calculated using B.J.H. method

With the purpose of studying the dispersion of the sulfonic groups in the DMSi nanospheres, chemical mapping analyses were performed (Figure 2.29). The chemical maps of O, S and Si show a very homogeneous distribution throughout the DMSi-SA structure. The mapping corresponding to the sulfur atom indicates the sulfur atom of sulfuric group is attached to the entire surface of the material, however, its highest concentration is seen in the mesoporous channels.

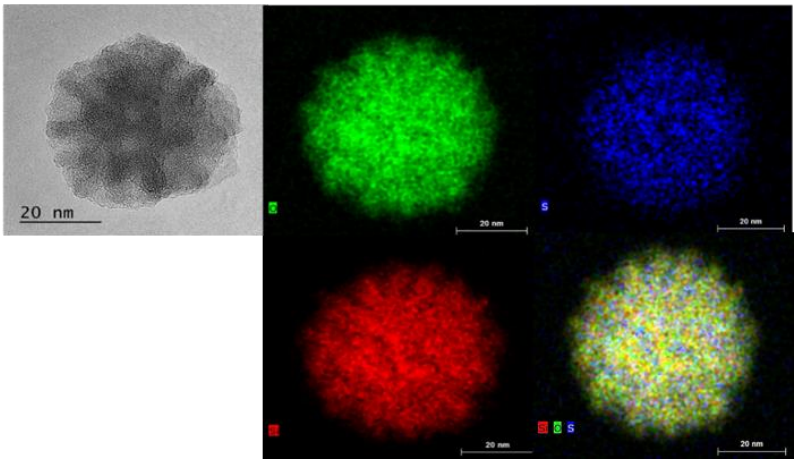

FIGURE 2.29 Chemical mapping of the DMSi-SA catalyst.

2.2.2.2 Composition

To evaluate the number of exchangeable protons, the acid capacity (Brönsted) of the sulfonic-modified materials, previously oxidized, an aqueous titration was performed. The aqueous titration of the catalyst was conducted using methyl thymol blue as indicator. The sample was previously subjected to an ionic exchange with KCl and the resulting HCl was titrated with a NaOH solution, previously standardized using potassium hydrogen phthalate ($KHC_8H_4O_4$). All analysis were performed in triplicates and in different batches of the catalysts. The obtained value was 0.69 $mmol \cdot g^{-1}$. Subsequently with the purpose of quantize the amount of total sulfur in the catalyst it was characterized by ICP-OES obtaining a value of 0.98 $mmol \cdot g^{-1}$; indicating that a little more than half of the thiol groups were converted to sulfonic acid.

To determine the way in which the sulfur element is found in the sample (thiol, sulphonic acid or both) and to know if the oxidation was complete or did not proceed an X-ray photoelectron spectroscopy (XPS) was made. The XPS technique allows the quantitative and qualitative analysis of all elements, except hydrogen. It is a superficial technique (the beam only travels 0.5 nm to 3.0 nm) that allows the investigation of chemical and structural changes of the elements present in the surface of the material studied. It basically consists in the excitation by means of an X-ray beam of the innermost levels of the atoms, causing the emission of photoelectrons that provides information about the energy of each level and, therefore, about the nature of each emitting atom. It involves the measurement of the spectra of the photoelectrons induced by X-ray photons. The binding energy of the peaks associated with the emission of photoelectrons is very well defined, allowing the identification of the oxidation state of cations and anions. Thus, non-equivalent atoms of the same element (difference in the oxidation state, in the molecules that surround it or in the position in the network).[166, 167]

The spectra of the S 2p core-level is shown in Figure 2.30, it shows two types of sulfur species, one at low binding energy (~164 eV), corresponding to a -SH groups, and another at higher binding energy (~169 eV), associated with $-SO_3H$ groups.[110] The

deconvolution of both peaks allows to appreciate that they are formed by doublets one at 168.6 eV, 169.7 eV and the other at 163.9 eV, 165.1 eV. From the graph it was possible to determine the percentage of -SH and -SO_3H in the sample being 45.2 % and 54.8% respectively. This indicates that approximately a little more than half of the sulfur content in the sample is in the form of -SO_3H.The above corroborates the results obtained by titration and ICP-OES.

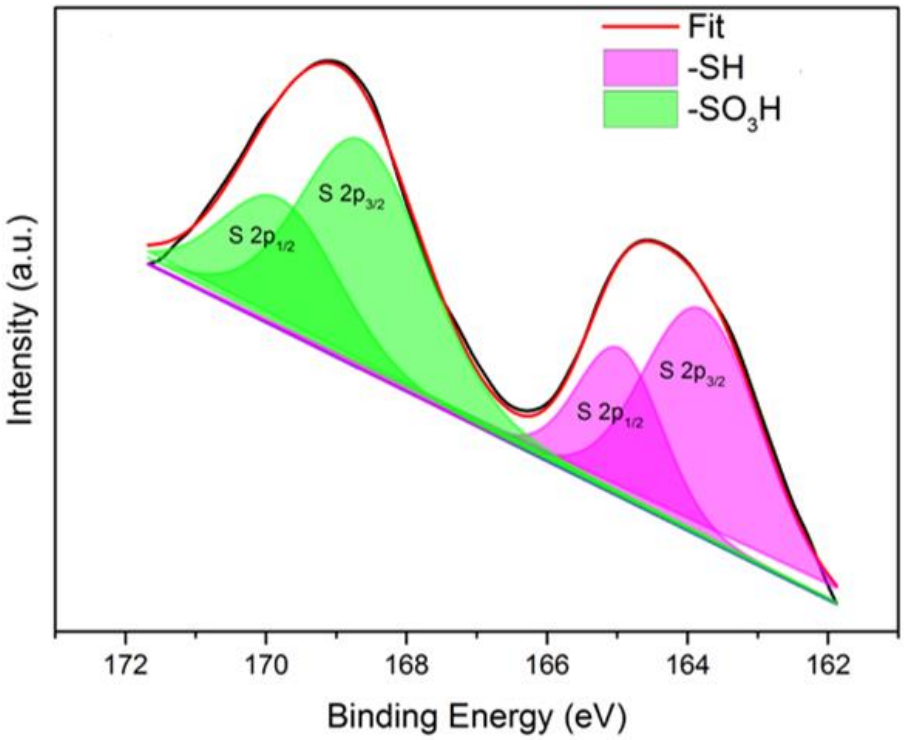

FIGURE 2.30- S 2p core level XPS spectrum for the DMSi-SA catalyst.

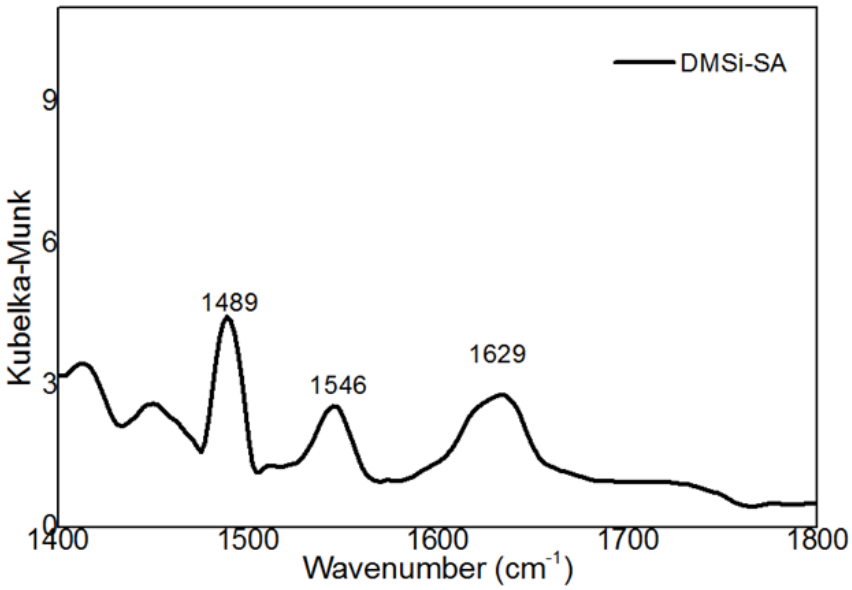

FIGURE 2.31- Infrared of adsorbed pyridine of the DMSi-SA catalyst.

As already mentioned before, the pyridine is used as a probe to provide more detailed information on the site's types, strength, and amount.[118] The Figure 2.31 shows the FT- IR spectra of adsorbed pyridine of DMSi -SA in the range of pyridine ring-stretching modes after desorption. The band at 1489 cm^{-1} is characteristic of both Brönsted and Lewis acid site. The bands at 1546 cm^{-1} and 1629 cm^{-1} are attributed to the vibration of the Pyridium ion formed by protonation of pyridine ring, and used as evidence of the presence of Brönsted acid sites.[168]

2.2.3 Catalytic applications

2.2.3.1 Evaluations of the DMSi-SA in the conversion of fructose and xylose

Once the catalyst was synthesized and characterized, it was used in the valorization of lignocellulosic biomass derivatives. To start the study, two sugars were selected: fructose and xylose. In all cases, it was used ethanol as solvent and source of

hydrogen, the working temperature was 130 ºC and the reaction time 24 h. To determine the different compounds, both qualitatively and quantitatively, that were obtained from the catalytic reactions, gas chromatography coupled to mass analysis was used. For the quantitative determination of the different compounds, the multiple point internal standard method was used. Para-nitrophenol, which is soluble in ethanol (solvent in which the reactions develop), does not react with the reaction medium and has a retention time that does not interfere with any of possible products, for these reasons he was selected as internal standard (See Appendix). Calibration curves were made for furfural, furfuryl alcohol, ethyl levulinate, hydroxymethyl furfural and the ether of hydroxymethyl furfural from 0.01 $mol \cdot L^{-1}$ (0.02 mmol) to 0.7 $mol \cdot L^{-1}$ (1.4 mmol) it was added the same amount of internal standard 0.7$mol \cdot L^{-1}$ (1.4 mmol) (See Appendix).

When the study was carried out using fructose as the starting platform, two reaction products were observed: 47% of ethyl levulinate (EL) and 41% of 5- (ethoxymethyl) furan-2-carbaldehyde (EHMF), the remaining 12% can be attributed either to fructose that remained unreacted or to the polymerization of 5-HMF in acid medium. In any case, the main product obtained was ethyl levulinate, a product with multiple applications in the industry, among others: the polymer industry, lubricants and articles for personal hygiene. Obtaining the EL demonstrates the efficiency of the catalyst in terms of promoting three reaction steps in the valorization of fructose according to Scheme 2.7.

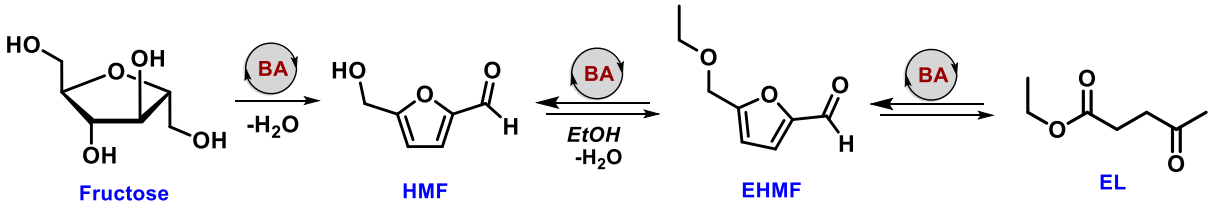

SCHEME 2.7- Conversion of fructose to ethyl levulinate. HMF= ethyl levulinate, EHMF= 5- (ethoxymethyl) furan-2-carbaldehyde, EL = ethyl levulinate

The first step involves the dehydration of fructose, in the presence of a Brönsted acid to 5-hydroxymethylfurfural (HMF), which undergoes a condensation with

ethanol in the presence of Brönsted acid (second step) to EHMF, which finally undergoes a ring opening by a decarboxylation step that releases formic acid and ethyl levulinate (third step).

On the other hand, when xylose was used as starting material, only one reaction product was observed, 14% of furfural (FUR) according to Scheme 2.8. As known, furfural is another product with wide industrial applications, among others it is used as a solvent, in the production of furfuryl alcohol as well as in the production of herbicides.

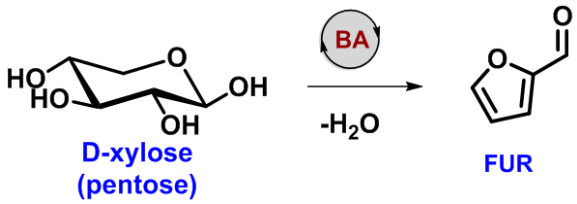

SCHEME 2.8- Conversion of xylose to furfural (FU)

2.2.3.2 Studies of the reaction parameters, in the conversion of fructose and xylose to ethyl levulinate and furfural respectively, using the DMSi-SA as catalysts

For both reactions, the influence of different experimental parameters such as temperature, mass of catalyst and concentration of starting material, in the conversion of both chemical reactions towards the products of interest, were studied.

The first parameter evaluated was the temperature; the tests were carried out using 1 mmol of starting material, 2 ml of ethanol and 72.5 mg of DMSi-SA and 24 h of reaction at different temperatures in an oil bath. For the tests carried out using fructose as starting material (Figure 2.32 a), at a temperature of 110 ºC, the conversion was 100%, obtaining 24% of EL and 76% of EHMF. On the other hand, as the temperature increases, the selectivity of the reaction towards EL was greater. In addition, it is noticed that there is a direct relationship between the increase in temperature and the conversion of EHMF to

EL, obtaining at 170 ºC, 62% of EL and only 1% EHMF, so it was taken 170 ºC as work temperature. On the other hand, when xylose is used as starting material (Figure 2.32 b), at lower temperatures such as 100 ºC the conversion of the reaction is zero; however, as the temperature increases the concentration of furfural increases, obtaining 0.42 mmol at 170 ºC, so it was chosen also 170 ºC as working temperature. The conversion of fructose to ethyl levulinate and from xylose to furfural, confirm once again, the presence of sulphuric acid on the surface of the material.

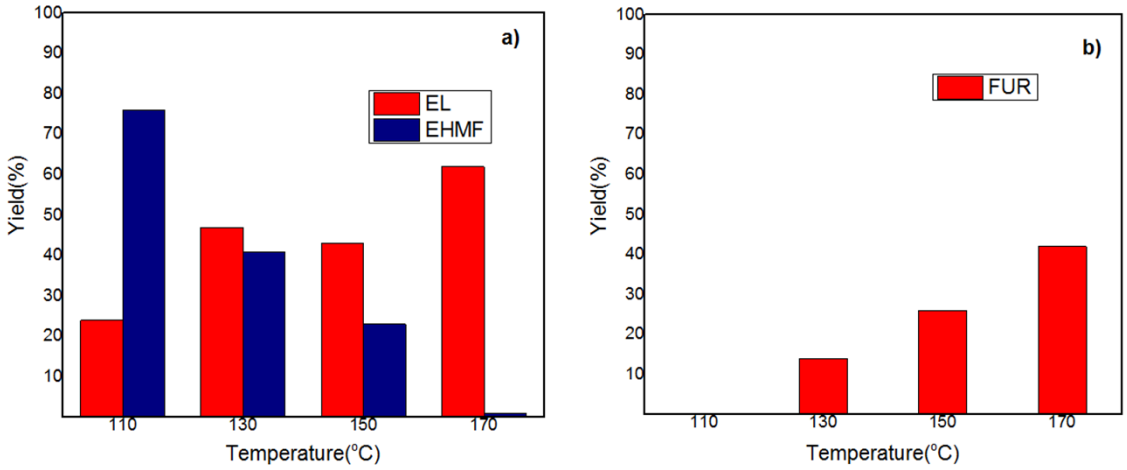

FIGURE 2.32- Evaluation of the temperature in the valorization of fructose and xylose using DMSi-SA catalyst. EL= ethyl levulinate, EHMF=5-(ethoxy methyl)furan-2-carbaldehyde, FUR= furfural.

Having defined for both cases 170 ºC as working temperature, we proceeded to study the influence of the catalyst mass used for both reactions. When fructose is used as starting material (Figure 2.33 a), with low catalyst mass 14.5 mg (1 mol% of -SO_3H) and 43.5 mg (3 mol% of -SO_3H) the conversion of fructose is total, however, a mixture of two products is obtained, the ethyl levulinate (product of interest) and the EHMF, being the last one the predominant material (EHMF).

On the other hand, when higher catalysts mass: 145 mg (10 mol% -SO_3H), 217 mg (15 mol% -SO_3H) and 290 mg (20 mol% -SO_3H) are used, the presence of the EHMF is not appreciated and a greater amount of EL is obtained, but among them with the increase in the mass of the catalyst used the amount of EL decreases. The foregoing may

be due, to a greater amount of polymeric material formation during the reaction, induced by the increase of Brönsted acid sites caused by the increase in catalyst mass. The highest concentration of ethyl levulinate (66%) was obtained using 72.5 mg (5 mol% -SO_3H) hence, 72.5 mg was chosen as the working catalyst mass. In addition, when the xylose is used as starting material (Figure 2.33 b), the behavior is very similar to that experienced in the case of fructose.

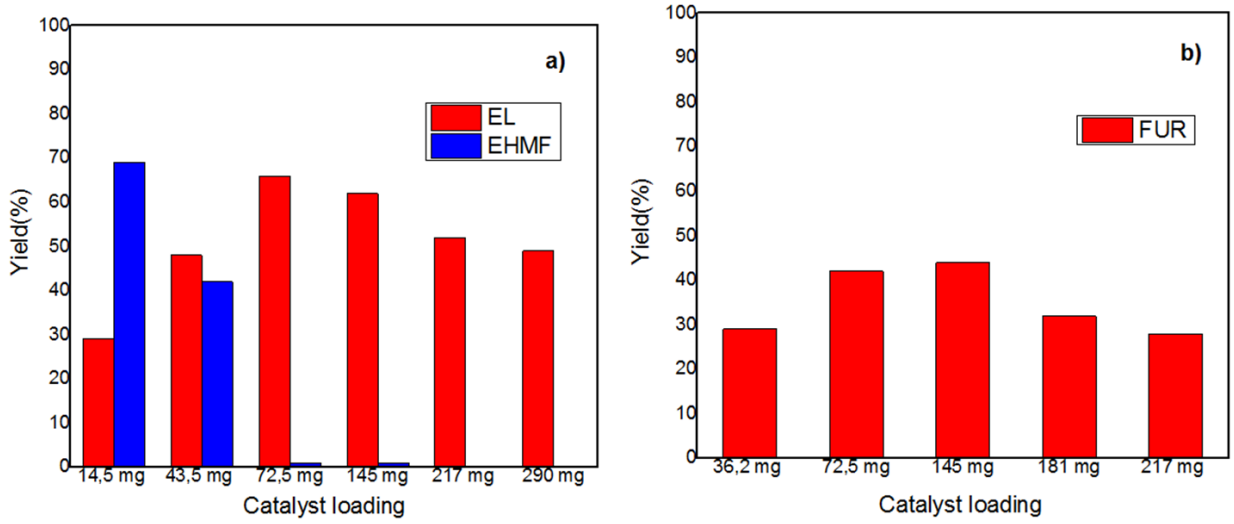

FIGURE 2.33- Evaluation of catalyst loading in the valorization of fructose and xylose using DMSi-SA catalyst. EL=ethyl levulinate, EHMF=5-(ethoxy methyl) furan-2-carbaldehyde, FUR= furfural.

At low catalyst mass 36.2 mg (2.5 mol% -SO_3H), the molar concentration obtained from furfural is low: 29%. When using a greater catalyst mass, the concentration of furfural obtained is greater, but also decreases with a further increase of the catalyst mass, possibly for the same reason exposed previously, in this case the polymer is formed from the furfural, it is known that polymerizes just like HMF in acid medium. It should be noted that the highest concentration of furfural was obtained using 145 mg (10% -SO_3H) of catalyst mass, obtaining 44% of FUR, however, 72.5 mg (5.5 mol % -SO_3H) was also chosen as the working catalyst mass and 42% of FUR is obtained. It is because, as can be seen, there are no significant differences between the amounts of FUR obtained for both catalyst mass.

Having already set the temperature (170 ºC) and the catalyst mass (72.5 mg), the concentration of the reaction medium was evaluated. When fructose is used as starting material (Figure 2.34 a), as the volume of ethanol increases, the concentration of EL increases until it reaches a point (3.5 ml of ethanol), where the system is very dilute and the molar concentration of EL begins to decrease. Due to this, it was taken 3 ml of ethanol as work volume and 83% of ethyl levulinate and only 12% of EHMF were obtained. When xylose is used as the starting material (Figure 2.34 b), the same behavior experienced by fructose is observed, it was also chosen 3 ml as working volume of ethanol and the total conversion to furfural (1mmol) is obtained.

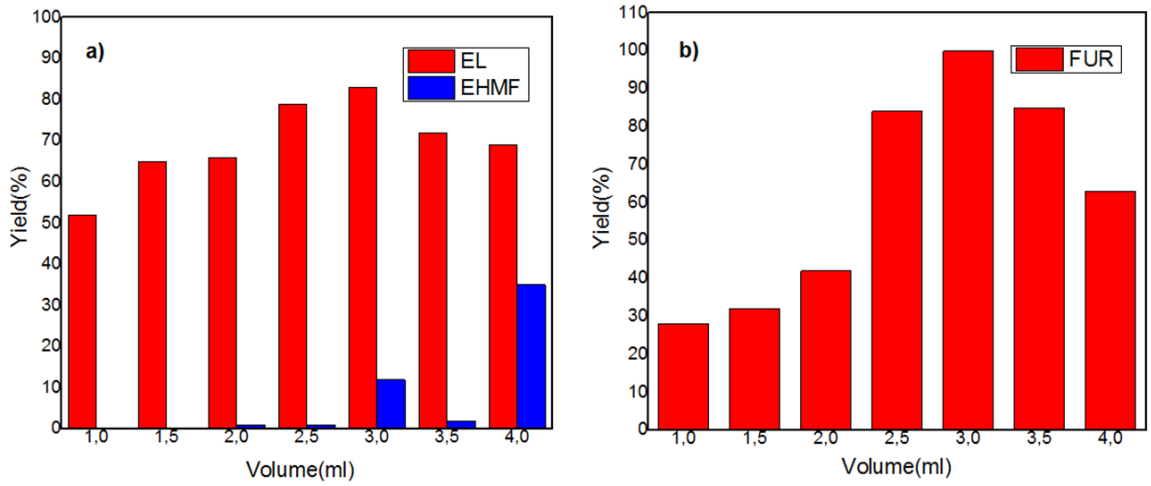

FIGURE 2.34- Evaluation of volume of ethanol in the valorization of fructose and xylose using DMSi-SA catalyst. EL=ethyl levulinate, EHMF=5-(ethoxy methyl) furan-2-carbaldehyde, FUR= furfural.

With the aim of understand how the reaction conversion and composition changed over time, we next conducted experiments under the identified optimal conditions varying the reaction time. With fructose as starting material (Figure 2.35 a) at 3 h, a 100% of conversion was accomplished, being EHMF (91%) the main product and EL (9%) the smaller product. With higher reaction times, the EHMF quantity decreases and the EL increases, until reaching the higher reported values previously, at 24 h. This suggest that EHMF is an intermediary product of the conversion reaction from fructose to EL. Also indicates that the fructose during the first reaction hours, in the presence of a Brönsted acid,

produces EHMF and them EL. When xylose is used as starting material (Figure 2.35 b) at the initial evaluated time, 3 h, there is only one reaction product, furfural (0.18 mmol). As time increases, the conversion from xylose to furfural also increases, until a total conversion is reached at 24 h of reaction.

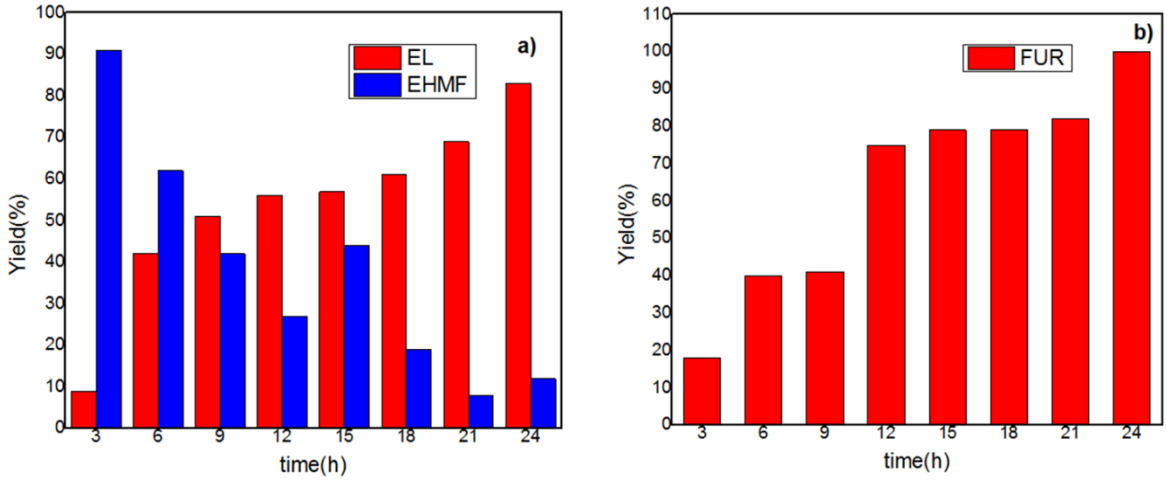

FIGURE 2.35- Evaluation of reaction time in the valorization of fructose and xylose using DMSi-SA catalyst. EL=ethyl levulinate, EHMF=5-(ethoxy methyl) furan-2-carbaldehyde, FUR= furfural.

2.2.3.3 Evaluations of DMSi-SA catalysts in the conversion of glucose

In the previous section, it was demonstrated the catalytic activity of DMSi-SA as a Brönsted acid, because for the conversion of fructose to EL and xylose to furfural is needed a Brönsted acid. To test the catalytic activity of catalyst as a Lewis acid, glucose was used as starting material.

It was used ethanol (3 ml) as solvent and source of hydrogen, the working temperature was 170 ºC, the mass of catalyst 72.5 mg and the reaction time 24 h. When the study was carried out two reaction products were observed: 5% of ethyl levulinate (EL) and 2% of 5- (ethoxy methyl) furan-2-carbaldehyde (EHMF), the remaining 93% can be attributed either to glucose that remained unreacted, to the polymerization of 5-HMF in acid medium or the mixture of both. In any case, it was obtained EL but in a small amount. The presence of EL in the products, demonstrates the existence of Lewis acid sites in this

catalyst and the efficiency of the catalyst in terms of promoting domino reaction, in the valorization of glucose according to Scheme 2.9.

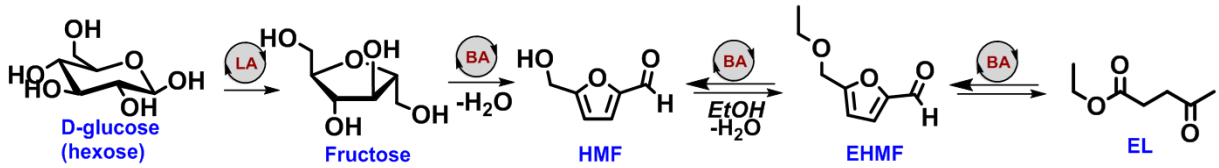

SCHEME 2.9- Conversion of D-glucose to ethyl levulinate. HMF= ethyl levulinate, EHMF= 5- (ethoxy methyl) furan-2-carbaldehyde, EL = ethyl levulinate

The first step involves the isomerization of glucose to fructose in the presence of Lewis acid, followed by the steps mentioned previously (section Evaluations of the DMSi-SA in the conversion of fructose and xylose) for valorization of fructose to ethyl levulinate.

With the aim of increasing the quantity of EL, we proceed to vary the catalyst mass and after this, the concentration of the reaction medium in the reaction. When the catalyst mass is changed (Figure 2.36 a) to 145 mg (10 mol% de-SO_3H) the quantity of EL increases to 62%, but when using 217mg (15 mol% de-SO_3H) the quantity decreases slightly to 60%.

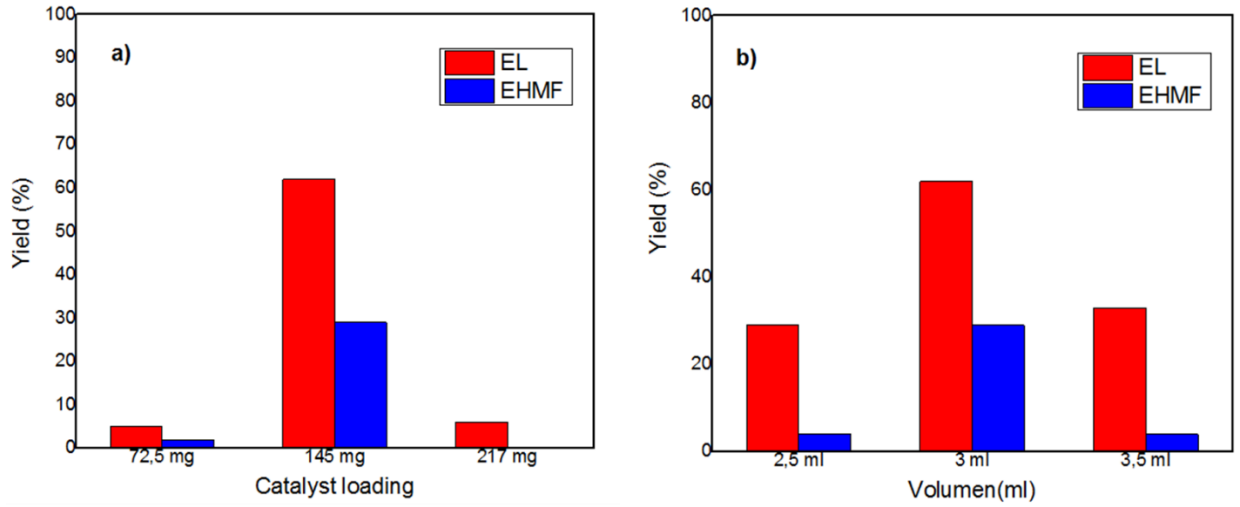

FIGURE 2.36 - Evaluation of catalyst loading (a) and volume of ethanol (b) in the valorization of glucose using DMSi-SA catalyst. EL=ethyl levulinate, EHMF=5-(ethoxy methyl) furan-2-carbaldehyde, FUR= furfural.

The decrease of EL, with the increase of the catalyst mass from certain value on, may be due to the formation of polymer during the reaction, this was mentioned previously. Then, it was chosen in this case also 145 mg, as catalyst mass. Having already set the catalyst mass (145 mg), the concentration of the reaction medium was evaluated (Figure 2.36 b). When the ethanol volume was 2.5 ml and then 3.5 ml, the quantity of EL drops to 29% and 33% respectively. In the first case, the decrease may be due to the formation of polymeric material; in the second, the system is very dilute and the molar concentration of EL begins to decrease. Hence, the best result was obtained using 3 ml of ethanol, obtaining 62% of EL and 4% of EHMF.

2.2.3.4 Evaluations of DMSi-SA catalysts in the conversion of sucrose and cellulose

In view of results obtained in the previous section it was tested the catalytic potential of DMSi-SA for convention sucrose and cellulose. As known, the sucrose is a disaccharide made of fructose and glucose units; cellulose is a polymer constituted by monomeric units of D-glucose.

It was used ethanol (3 ml) as solvent and source of hydrogen, the working temperature was 170 ºC, the mass of catalyst 72.5 mg and the reaction time 24 h. When the study was carried out using sucrose as the starting platform, two reaction products were observed: 33% of ethyl levulinate (EL) and 9% of 5- (ethoxy methyl) furan-2-carbaldehyde (EHMF), the remaining 58% can be attributed either to sucrose that remained unreacted or to the polymerization of 5-HMF in acid medium. In any case, the main product obtained was ethyl levulinate. Obtaining EL demonstrates the efficiency of the catalyst in terms of promoting domino reaction in the valorization of sucrose according to scheme 2.10.

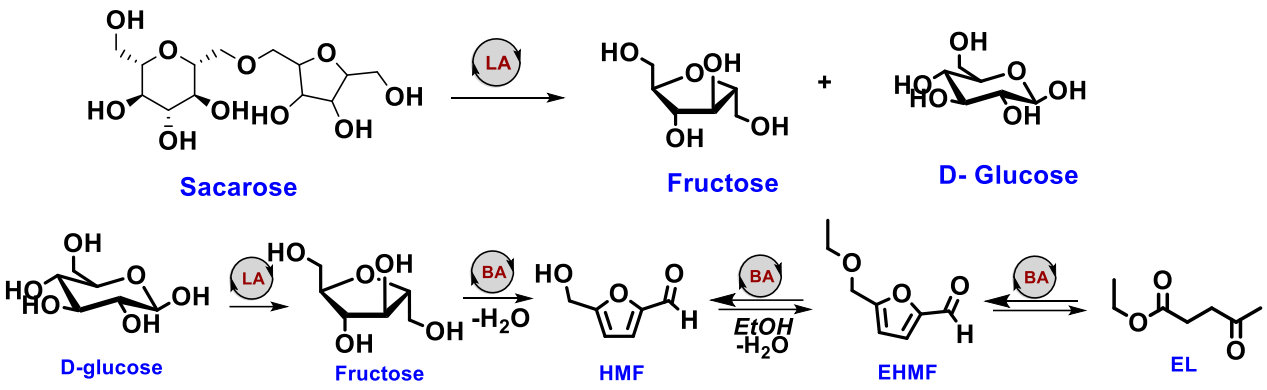

SCHEME 2.10-Conversion of saccharose to ethyl levulinate. HMF= ethyl levulinate, EHMF= 5- (ethoxy methyl) furan-2-carbaldehyde, EL = ethyl levulinate

The first step involves the rupture of sucrose in fructose and glucose. The glucose can isomerize to fructose in the presence of a Lewis acid, and the process continues with the same steps previously mentioned (section Evaluations of the DMSi-SA in the conversion of fructose and xylose) for valorization of fructose to ethyl levulinate.

On the other hand, when cellulose was used as starting material, non-reaction product was observed.

For both reactions, with the aim of increasing the quantity of EL (for sucrose) and to obtain EL (for cellulose), it was varied the catalyst mass used in the reaction. When using sucrose as starting material (Figure 2.37 a), it was evidenced that, with the increase of the catalyst mass to 145 mg (10 mol% de -SO_3H) increases the quantity of the EL to 89%, but, further increasing in the catalyst mass to 181 mg (12.5 mol% de -SO_3H) and 217 mg (15 mol% de -SO_3H) causes that the quantity of EL decreases until 58%. The decrease of EL with the increase of the catalyst mass may be due to the formation of polymeric material during the reaction, mentioned before. Then, the optimal mass of catalyst founded in the experimental conditions for sucrose was 145 mg because it allows to obtain 0.89 mmol of EL. On another hand in the case of the tests carried out using cellulose as starting material (Figure 2.37 b), when increased the catalyst mass to 145 mg it resulted in a small amount of EL (4%). Further increase in the catalyst mass result in the increase of the quantity of EL, the maximum quantity of EL obtained was 27% for a catalyst mass of 435 mg (35 mol% of -SO_3H). The EL as a product in the reaction, demonstrated, the high efficiency of this

catalyst, it was able to de-polymerize the cellulose in D- glucose and to promote domino reaction according to Scheme 2.11.

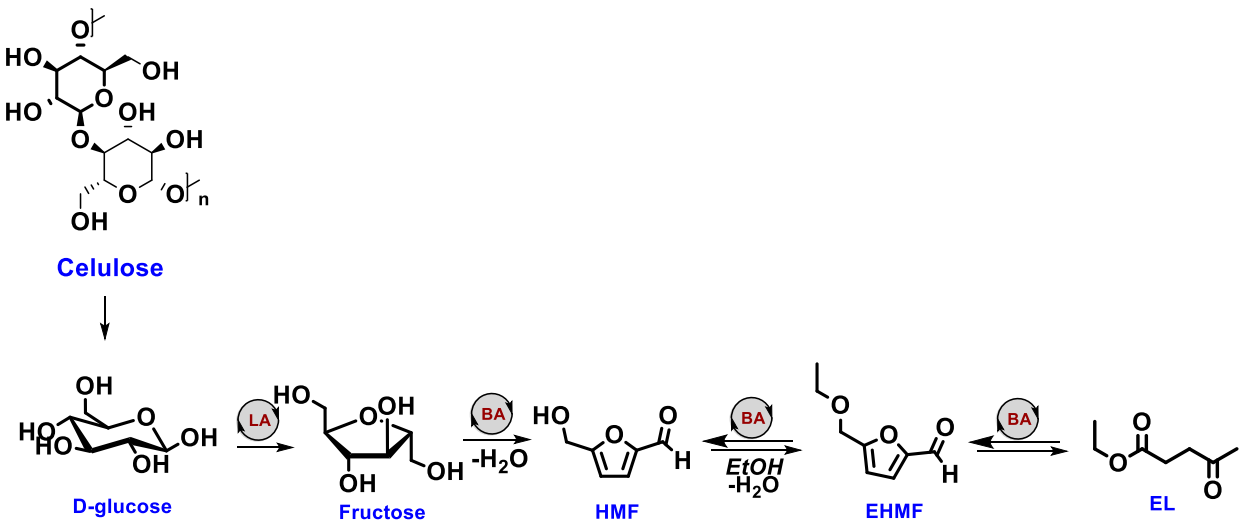

SCHEME 2.11-Conversion of cellulose to ethyl levulinate. HMF= ethyl levulinate, EHMF= 5- (ethoxy methyl) furan-2-carbaldehyde, EL = ethyl levulinate

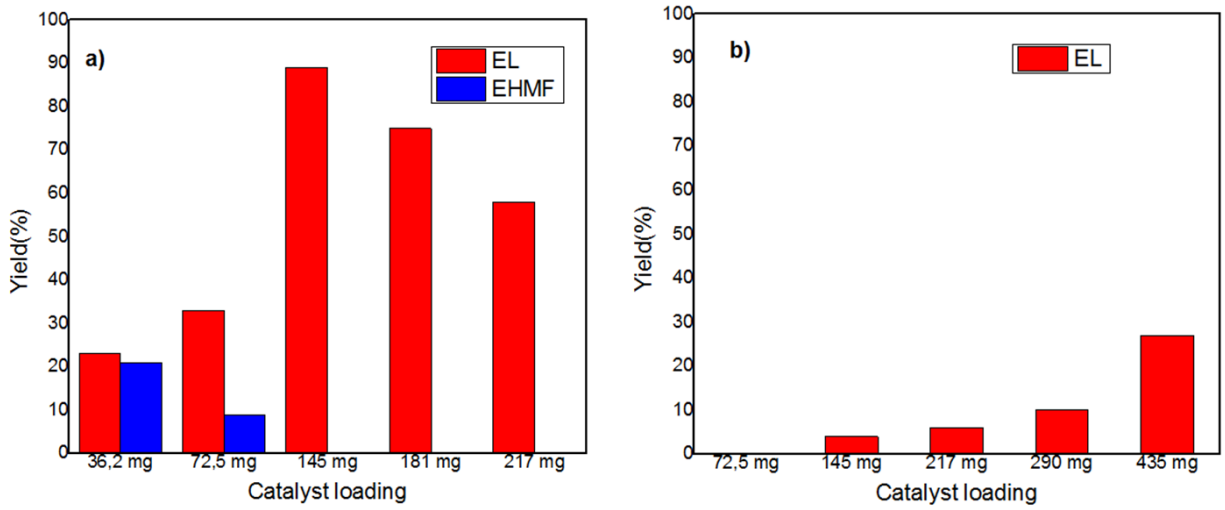

FIGURE 2.37- Evaluation of catalyst loading in the valorization of sucrose a) and cellulose b) using DMSi-SA catalyst. EL=ethyl levulinate, EHMF=5-(ethoxy methyl) furan-2-carbaldehyde.

2.2.3.5 Recyclability of the catalyst DMSi-SA in the conversion of glucose, fructose and sucrose to ethyl levulinate and xylose to furfural

To know if morphological changes occurred in the catalyst once it was used in the catalytic reactions, an HRTEM, EDS and an elemental analysis mapping were carried out to one of them. The one that is extracted from the conversion reaction of glucose to ethyl levulinate was chosen as the catalyst to be investigate. Figure 2.38 a, 2.38 b and 2.38 c show HR-TEM images of DMSi-SA catalyst after the reaction. It can be seen in the figure that the catalyst has not undergone appreciable morphological changes after being used in the reaction. It continues presenting the architecture of the dendritic particles with center-radial mesopore channels. The little sharpness of the particles may be due to the deposition on the surface of hemic. The HRTEM-EDS (Figure 2.38 d and 2.38 e) and chemical mapping (Figure 2.39) confirmed the presence of silicon, oxygen and sulfur atoms on the DMSi-SA catalyst after reaction. Confirming that the material has not changed because it keeps the sulfur attached to the entire surface of the material (Figure 2.39). It can also be seen that the oxygen and silicon atoms remain homogenously distributed in the DMSi-SA structure after having been used in the catalytic reactions.

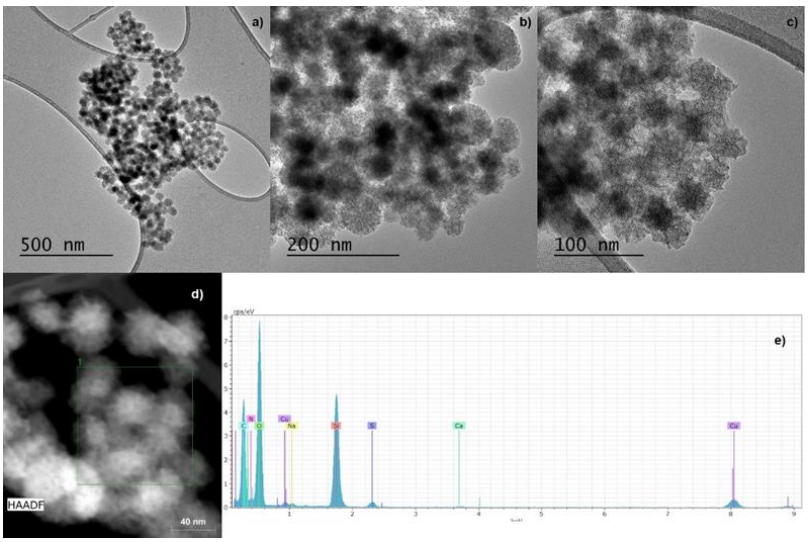

FIGURE 2.38- a), b), c) and d) HR-TEM images of DMSi-SA after reaction, e) EDS spectrum of DMSi-SA after reaction. Scale bar: a) 500 nm, b) 200 nm, c) 100 nm and d) 40 nm

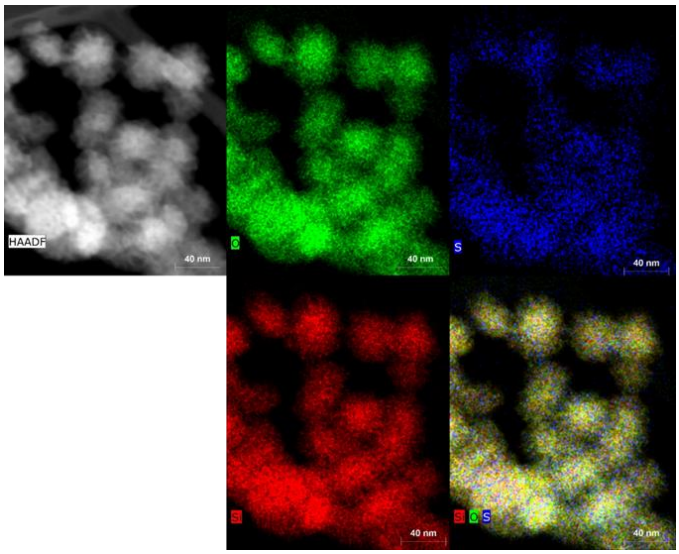

FIGURE 2.39- Chemical mapping of the DMSi-SA catalyst after reaction.

Subsequently, the recyclability of the DMSi-SA catalyst in the conversion of glucose, fructose and sucrose to ethyl levulinate and xylose to furfural was evaluated in the best obtained conditions (Figure 2.40 a – 2.40 d). When used as a starting material fructose and sucrose the catalyst could be recycled by two additional reaction cycles maintaining conversions above 58% to ethyl levulinate. In the case of using as starting material xylose and glucose the catalyst could be recycled by one additional reaction cycles maintaining conversions above 87% to furfural for xylose and about 42% to ethyl levulinate for glucose. For the four cases, after performing the next reaction cycle the conversion was significantly reduced. The conversion decreased after each reaction cycle probably due to the formation of hemins in the medium, which possibly blocked both the Lewis and Brönsted acids needed to promote the reaction of fructose to ethyl levulinate and xylose to furfural (Brönsted) as well as the of glucose and sucrose to ethyl levulinate (Lewis and Brönsted). The hemins can be organic material present in the reaction or polymeric material that has been produced. The polymeric material can come from the polymerization of furfural (FUR) or hidroximetilfulfural (HMF). When xylose is used as starting material, furfural is obtained as a product. Furfural can undergo a resignification reaction in an acid medium (reaction of

furfural with other furfural molecules). On the other hand, when glucose, fructose, sucrose is used as starting materials during the conversion process to EL, the HMF is the intermediate product. This material in an acidic medium can also polymerize through a self-condensation process.

The above corroborates that, as the reaction cycles are carried out, the conversion of the starting materials decreases. According to the spectroscopic analyzes carried out by Spange S. et al, the polymer of cross-linked FA that is grafted on the surface of the silica is bound to it by means of Si-O-C bonds, being strongly bound and its separation is very difficult [168] evidencing that probably the method used for the elimination of the hemins was not effective. In this case, unlike the procedure carried out in Section 2.1.3.3 for the zeolite, the presence of organic groups in the silica structure makes it impossible for the catalyst to be reactivated via calcination. Hence, it is necessary to conduct more studies to achieve better results in the recyclability of this material.

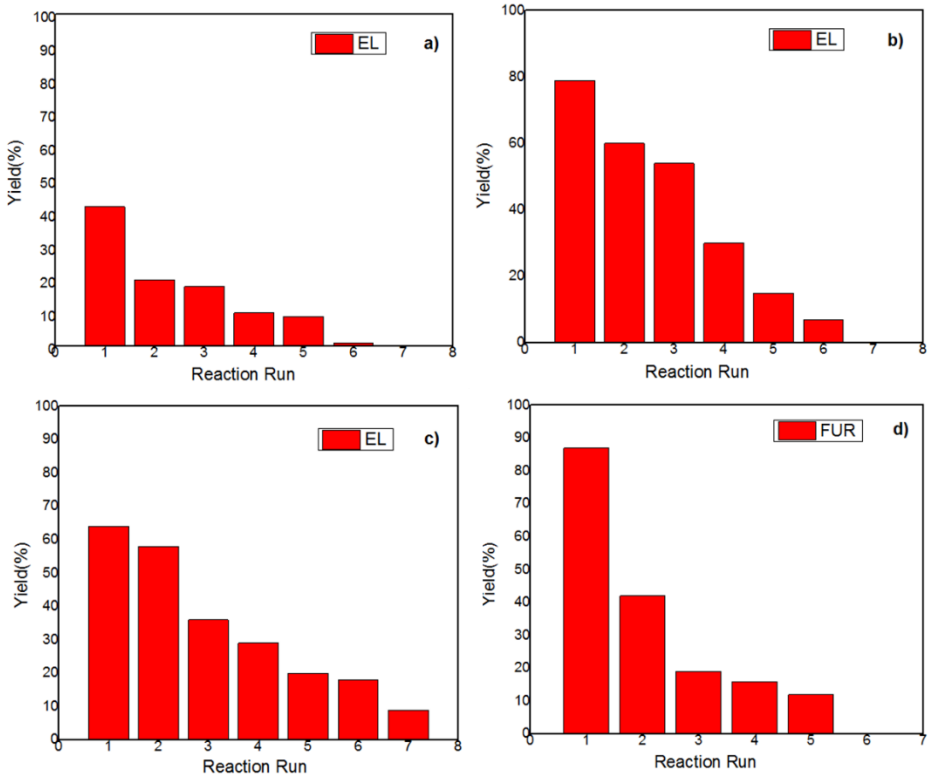

FIGURE 2.40- Evaluation of the recyclability of the DMSi catalyst in the upgrading of a) glucose, b) fructose, c) Sucrose to ethyl levulinates and d) xylose to furfural. EL= ethyl levulinate, FUR= furfural.

2.2.3.6 Comparison of the physicochemical properties of the DMSi-SA with other silicas functionalized with sulfonic acid

2.2.3.6.1 Synthesis and characterization

To verify that the DMSi is really a superior catalytic support, for its use in the valorization of compounds derived from the biomass in relation to other silicas, eight silicas were synthesized and functionalized (KCC, MCM-41, FDU-12, Stöber, silicate, SBA-15 and flash silica, the latter was acquired commercially). The methodologies for the synthesis and functionalization of each one of these silicas were described in the section: experimental procedure 3.2.1. Functionalization with sulfonic acid was performed by the same procedure described for the DMSi beforehand.

All the silicas were also characterized by X-ray diffraction (XRD), high-resolution transmission electron microscopy (HRTEM), chemical mapping, X-ray photoelectron spectroscopy (XPS), nitrogen sorption measurements, inductive coupled plasma-optical emission spectroscopy (ICP-OES), and Fourier transform infrared spectroscopy of adsorbed pyridine (FTIR-Pyr).

As in the case of the DMSi, the characterizations were performed for silicas functionalized with sulfonic acid (silicas-SA). The results obtained by HRTEM show that all the silicas show a consistent morphology and according to the one reported for each one of them in the literature[101, 169-185] (see Appendix). Unlike silicas which are amorphous materials and do not present diffraction patterns, silicate (dealuminated zeolite) shows a diffraction pattern. The XRD patterns of the silicate support were obtained, the characteristic and reported diffraction peaks are appreciated.[186, 187] (See Appendix)

The HRTEM-EDS and chemical mapping confirmed the presence of silicon, oxygen and sulfur atoms on the silicas-SA catalyst and show a very homogeneous distribution of sulfur atoms throughout the silica-SA structure (excepting the Stöber and FDU-12). For the Stöber-SA and FDU-12 the HRTEM-EDS technique confirmed the presence of silicon and oxygen but there is no evidence of sulfur indicating that the

functionalization of the material has not occurred or that the sulfur content is so small that it is below the limit of the equipment (see Appendix). The detection limit of EDS is typically about 1000 ppm (by weight). Because of this, if the concentration is lower, statistical errors and uncertainties in the background become dominant. Hence, for a concentration in the region of 100 ppm, the intensity measured at the peak consists mainly of the background (the element is not appreciated).[188] Probably, according to the same reason, the sulfur element was not appreciated in the elemental analysis mapping. However, by other techniques such as ICP-OES, FTIR of pyridine and by titration it was possible to verify the presence of sulfur in this samples.

TABLE 2.9- Values referring to the texture characterization of silica supports, and silica functionalized with sulfuric acid.

Silica	**$S_{B.E.T}$ (m^2g^{-1})**	**$A_{micropore}$ (m^2g^{-1})[a]**	**$V_{micropore}$ (cm^3g^{-1})[a]**	**Total pore volume (cm^3g^{-1})[b]**	**Pore diameter (nm)[b]**	**Pore size distribution (nm)***	**Isotherms Type/Hysteresis loop***
MCM-41	877.3			0.178	2.5	2.7	IV/n.d.
MCM-41- SA	345.3			0.0309	3.7	3.4	IV/n.d.
KCC	505.1	41.6	0.0166	1.399	10.8	3.6; 23.0	IV/H1
KCC-SA	439.0	19.9	0.00569	1.069	12.4	3.9; 6.4; 25.4	IV/H1
Silicalite	291.7	186.6	0.0929	0.0407	3.6	1.9; 3.8	I
Silicalite-SA	150.4	132.4	0.0667	0.0107	3.5	2.7	I
Flash	479.7			0.773	5.3	3.6; 5.9	IV/H2
Flash-SA	253.1			0.299	5.2	3.6; 6.4	IV/H2
FDU-12	580.9			0.589	3.9	3,8	IV/H2
FDU-12-SA	138.1			0.328	7.8	3.6; 6.9	IV/H2
Stöber	12.6			0.027	10.3	4.0; 10.5; 31.0	II/n.d.
Stöber-SA	5.7			0.00871	8.6	3.7; 5.4; 14.0	II/n.d.
SBA-15	578.8	105.2	0.0491	0.782	6.4	6.5	IV/H1
SBA-15-SA	327.7	74.1	0.0354	0,336	4	3.6	IV/H2

a Calculated using t-plot method; b Calculated using B.J.H. method; [n.d.] Hysteresis loop was not observed; *See Appendix

Subsequently, the texture characterization of silica supports as well as the final catalysts (silicas-SA) were conducted by nitrogen physisorption. The texture properties of all synthesized silica, as well as, the functionalized materials can be seen in Table 2.9. All the texture properties of the silica support towards functionalized material (catalyst) are diminished, the same behavior was presented by the DMSi. This behavior was equally expected and is due to the functionalization of silicas with organic groups, both on the surface and in the interior of the pores produced by blocking them too. On the other hand, the type of isotherm and slope of hysteresis is related to what has been reported for these materials in the literature. The type IV isotherms as mentioned above for the DMSi are characteristics of mesoporous materials. In the case of type II isotherms, they are characteristic of nonporous or microporous adsorbents, as Stober. On the other hand, those materials that present type I isotherms are microporous solids having relatively small external surfaces (silicate). Those adsorptive that present reversible type IV isotherm (not present hysteresis) possess mesoporous of a smaller width than those material present hysteresis. This is consistent with the results obtained in Table 2.9, where the MCM-41 has both, an average pore size as well as a smaller pore size distribution in relation to other materials that have this same type of isotherm. On the other hand, those materials that possess H1 hysteresis loops is characteristic of agglomerates or spherical particles arranged in a uniform way, cylindrical pore geometry, indicating relatively high pore size uniformity and facile pore connectivity. Hysteresis loops H2 type are given by more complex structures in which network effects are important.

To determine how sulfur is found in each of the functionalized samples, XPS analyzes were performed (See Appendix). The results showed that, as in the DMSi-SA, the sulfur is in the form of two species, -SH and -SO_3H (see Table 2.10).[110] Confirming the previously obtained in the elemental analysis mapping: the samples were functionalized, but also that the oxidation of the group -SH to -SO_3H was not complete. The total amount of sulfur was then quantified by ICP-OES and the number of groups in the form of Brönsted acid by aqueous titration, see Table 2.10. The results obtained by XPS have some correspondence with the results obtained by titration. The results obtained for the Stöber-SA by means of ICP-OES (0.04 $mmol \cdot g^{-1}$ which is the same as 1.2 $mg \cdot L^{-1}$) confirm the

results obtained by EDS and for the mapping of elemental analysis. It was not possible to detect the sulfur element for the Stöber-SA using these techniques since the concentration of this element in the sample is below the detection limit of the equipment (1000 ppm which is the same as 1000 $mg \cdot L^{-1}$).[188]

TABLE 2.10- Chemical properties of the organosulfonic acid-functionalized silica samples.

Silica-SA	–SH[a] (%)	$–SO_3H$[a] (%)	Sulfur total [b] (mmol/g)	$-SO_3H$[c] (mmol/g)
MCM-41	5.9	94.1	1.58	1.46
KCC	12.4	87.6	1.03	0.96
Silicate	18.9	81.1	0.49	0.12
Flash	14.1	89.5	1.41	1.48
FDU-12	6.3	93.7	0.95	1
Stöber	8.9	91.1	0.04	0.032
SBA-15	5.5	94.5	1.75	1.82

[a] Determined by XPS; [b] Determined by ICP-OES;[c] Determined by titration

On the other hand, the possible differences that exist between the results obtained by XPS, ICP-OES and titration is that the titration is a non-instrumental analytical technique and has a greater error than instrumental techniques. It is also a heterogeneous phase titration so the instrumental error in the test increases even more.

Finally, to determine the nature of the acidic sites present, infrared analysis of absorbed pyridine samples (see appendix) was performed. The results show that most of the samples present bands around 1630 cm^{-1} and 1550 cm^{-1} characteristic of Brönsted acid sites and a band around 1490 cm^{-1} characteristic of Brönsted and Lewis acid sites. In the case of the Stöber-SA only the band is appreciated at 1630 cm^{-1}.[168] The absence of the other two bands may be related to the small amount of sulfur element in the form of $-SO_3H$ in the sample (see Table 2.10).

2.2.3.6.2 Catalytic evaluation

Once the silica was synthesized and characterized they were tested in the xylose and glucose valorization reactions. This test was carried out with the objective of comparing the catalytic activity of the DMSi-SA synthesized with other silicas functionalized with sulfonic acid by the same methodology used for the DMSi. The xylose and glucose were chosen as starting materials because it allows to evaluate the response of both acid sites Brönsted (in the xylose recovery reaction) and Lewis-Brönsted (in the glucose recovery reaction) see outline of Sections 2.2.3.2 and Sections 2.2.3.3.

In all cases, ethanol was used as solvent and source of hydrogen, the working temperature was 170 ºC and the reaction time 24 h. To determine the different compounds both qualitatively and quantitatively that were obtained from the catalytic reactions, gas chromatography coupled to mass analysis was used. For the quantitative determination of the different compounds, the multiple point internal standard method was used. The experimental procedure used is described in Section 3.2.3.3 of the experimental section.

The analysis of the catalytic activities through the conversion of glucose into ethyl levulinate and xylose in furfural, reveals the superior activity of dendritic silica (DMSi) in comparison with the other silicas evaluated (see Table 2.11). This fact can be the result of a set of factors that contribute to the high activity. Among them are the pore generation system, the high surface area, the average pore diameter and the high functionalization with thiol and sulfuric groups. The system of generative pores is certainly the factor for the silica DMSi, since three different types of pores or three generations of pores are observed. According to the pore distribution curve (Figure 2.28 b), it was possible to verify the maximum of three pores in diameter, corroborating with the proposal of three different generations and pores. Therefore, the largest pores (third generation) have an average diameter of around 25 nm and these correspond to the outermost portion of the silica particles. Already the second generation and the first generation of pores have average diameters of 6.4 and 3.7 nm. Figure 2.41 illustrates a silica particle with three generations

of pores, as observed in the case of silica DMSi. This large pore size in not an impediment to the diffusion of the molecules, that is, the glucose and xylose molecules will be able to enter the pore to interact with the acidic sites and later the formed products will spread towards the outside of the pores without difficulty, not being so for the other silicas that have smaller pore size.

TABLE 2.11- Catalytic activities of the samples towards glucose and xylose.

Silica-SA	Reaction products		
	EL[a] (%)	EHMF[a] (%)	FUR[b] (%)
MCM-41	19	9	56
KCC	14	-	80
silicate	4	-	18
Flash	11	5	59
FDU-12	4	3	23
Stöber	-	-	7
SBA-15	18	5	72
DMSi	62	4	100

[a]1 mmol glucose, 170 ºC, 24 h reaction, ethanol as solvent, 5 mol% -SO_3H as catalyst; [b]1mmol of xylose, 170 ºC, 24 h of reaction, ethanol as solvent, 10mol% -SO_3H as catalyst. EHMF= 5- (ethoxy methyl) furan-2-carbaldehyde, EL = ethyl levulinate, FUR = furfural

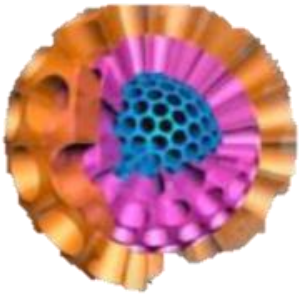

FIGURE 2.41 Dendritic silica with three generations of pores

Experimental Section

3. Experimental Section

3.1 Microporous materials: β-magnetic zeolite exchanged with transition metals

3.1.1. Synthesis

All solvents were dried prior to use by standard procedures. Reagents were purchased at the highest commercial quality and used without further purification.

3.1.1.1 Synthesis of the Fe_3O_4 microspheres

The magnetic Fe_3O_4 microspheres used as the support were prepared using a modified solvothermal method.[189] $FeCl_3 \cdot 6H_2O$ (3.9 g, 14.4 mmol), sodium citrate (1.2 g, 4.7 mmol), and sodic acetate (NaOAc, 7.2 g, 87.8 mmol) then were dispersed in ethylene glycol (60 ml) under magnetic stirring and the resulting suspension was transferred to a 200 ml Teflon-lined stainless-steel autoclave and placed in an oven at 200 ºC for 10 h. After cooling to room temperature, the obtained black product was isolated with the aid of a magnet and washed several times with deionized water and ethanol. The magnetite microspheres were dispersed and stored in distilled water for further use.

3.1.1.2 Functionalization of the Fe_3O_4 microspheres with PDDA

The functionalization of the magnetite microspheres was conducted using poly(dimethyldiallylammonium) chloride (PDDA) using the procedure described by Lv and co-workers.[121] In this approach, 1.0 g of wet magnetite nanospheres were added to an aqueous ammonia solution (2.0 wt%, 30.0 ml), magnetically stirred at room temperature for 30 min, followed by the addition of 5 ml of PDDA solution (20 wt% in H_2O). The mixture was then stirred at room temperature for 24 h. Subsequently, the ensuing PDDA-functionalized magnetite microspheres were magnetically separated from the reaction medium and kept in water for further functionalization with the zeolite.

3.1.1.3 Synthesis of the β zeolite in the sodic form (β-Na^+)

The β-zeolite in the sodic form was synthetized using the procedure described by Bhat et al.[122] In a typical procedure, 7.2 g (119.8 mmol) of silica gel were suspended in 44 ml of distilled water under magnetic stirring followed by the addition of 246 mg (6.2 mmol) of sodic hydroxide. Then, 7.35 g (49.9 mmol) of tetraethylammonium hydroxide were added to the mixture and stirred for 30 min. Next, a solution containing 465 mg (5.7 mmol) of sodium aluminate in 5.6 ml of distilled water was added and the resulting suspension was stirred for 1 h. The mixture was transferred to a Teflon-lined stainless-steel autoclave and placed in an oven at 150 ºC for 5 days. The former white power was filtered, washed with distilled water several times, and dried at 60 ºC for 12 h. Finally, the material was submitted to calcination at 550 ºC for 6 h under air atmosphere.

3.1.1.4 Preparation of the magnetically recoverable catalyst in the acid form (γ-Fe_2O_3-β-H^+)

300 mg of the PDDA-functionalized magnetite microspheres were dispersed in 50 ml of distilled water with the subsequent addition of 2.2 g of the zeolite β-Na^+ powder and stirring for 48 h at room temperature. The resulting composite Fe_3O_4-PDDA- β-Na^+ was magnetically separated from the aqueous mixture and dried at 60 ºC for 24 h under vacuum. The material was then calcinated under air atmosphere at 550 ºC for 5 h, producing the composite γ-Fe_2O_3-β-Na^+. To convert the sodic form of the material to its acid form (γ-Fe_2O_3-β-H^+), 1.0 g of the γ-Fe_2O_3-β-Na^+ magnetic zeolite was dispersed in 100 ml of an aqueous solution of NH_4NO_3 (1.0 mol/L) and the mixture was vigorously stirred (1000 rpm) at 80 ºC for 2 h. The material was separated from the media with the aid of an external magnet and resubmitted to this cationic exchange process twice more. The solid was then dried at 60 ºC under vacuum for 24 h and calcinated under air atmosphere at 500 ºC for 5 h, generating an orange-brown powder.

3.1.1.5 Preparation of the magnetically recoverable catalysts exchanged with Pd, Fe and Ir (γ-Fe_2O_3-β- Pd, γ-Fe_2O_3-β- Fe, γ-Fe_2O_3-β- Ir)

500 mg of the Fe_3O_4-PDDA- β-Na^+ were dispersed in 10 ml of distilled water followed by the addition of the metal salts [Pd $(NO_3)_2 \cdot H_2O$, $IrCl_3 \cdot H_2O$, Fe $(NO_3)_3 \cdot 6H_2O$ for Pd, Ir or Fe respectively] to attain a concentration of 0.01 mol·L^{-1} for Pd and Ir and 1 mol·L^{-1} for Fe. The mixture was stirred at room temperature for 6h, the solid was removed via magnetic decantation and dried at 60 ºC for 12 h. This ion exchange procedure was repeated twice more. Finally, the obtained powder was calcinated at 550 ºC for 5h.

3.1.1.6 Synthesis of pure beta zeolite

The synthesis of pure β zeolite was performed adapting of the procedure described by Camblor et al.[190] using TEAOH (40 wt.% in water) as template, fumed silica (Aerosol 200) as silica source and sodic aluminate as aluminum source. Firstly, a solution containing 5.94 ml of distilled water, 8.96 g (60.1 mmol) of TEAOH and 0.053 g (0.9 mmol) of sodium chloride was prepared, followed by the addition of 2.95 g (49.1 mmol) of Aerosol 200 silica and stirring for 20 min. Next, a solution containing 10.0 ml of distilled water, 0.033 g (0.8 mmol) of sodium hydroxide and 0.179 g (2.2 mmol) of sodium aluminate was prepared and added to the previously prepared silica mixture. A thick gel with theoretical molar composition of 1.97 Na_2O:1.00 K_2O:12.5$(TEA)_2O$:Al_2O_3:50 SiO_2:750 H_2O:2.9HCl was obtained, stirred for 30 min and transferred to a 100 ml Teflon-lined autoclave. The gel was hydrothermally treated at 140 ºC for 5 days and the resulting powder was filtrated and washed thoroughly with distilled water, dried at 80 ºC for 12 h and calcined in air atmosphere at 550 ºC for 6 h.

3.1.1.7 Synthesis of pure ZSM-12 zeolite

The synthesis of pure ZSM-12 zeolite was performed according the procedure described by Gopal et al,[124] using TEAOH (40 wt.% in water) as template, colloidal silica LUDOX (40 wt.%) as silica source and sodic aluminate as aluminum source. For the preparation of the gel, 8.75 ml (60 mmol) of TEAOH were mixed with 8.5 ml of distilled water and 0.343 g (4.2 mmol) of sodium aluminate, and this mixture was stirred until the sodic

aluminate was dissolved. Next, a solution containing 19.2 ml of colloidal silica and 10.0 ml of distilled water was added to the above solution and stirred for 30 min. After that, the gel with a theoretical composition of Na_2O:Al_2O_3:80SiO_2:12. 7TEAOH:104H2O was transferred to a 100 ml Teflon-lined autoclave and hydrothermally treated at 160 ºC for 5.5 days. The solid was then filtrated and washed thoroughly with distilled water and dried at 80 ºC for 12 h, followed by calcination in air at 600 ºC for 6 h.

3.1.1.8 Preparation of the catalyst with the pure β zeolite (γ-Fe_2O_3-βp-Pd) and pure ZSM-12 zeolite (γ-Fe_2O_3-ZSM-12-Pd)

70 mg of the PDDA-functionalized magnetite microspheres were dispersed in 12 ml of distilled water with the subsequent addition of 500 mg of pure β zeolite or pure ZSM-12 zeolite powder and stirred for 48 h at room temperature. The resulting composite Fe_3O_4-PDDA-βp-Na^+ or Fe_3O_4-PDDA-ZSM-12-Na^+ was magnetically separated from the aqueous mixture and dried at 60 ºC for 24 h under vacuum. The material was then calcinated under air atmosphere at 550 ºC for 5 h, affording the composite γ-Fe_2O_3-β(p)-Na^+ or Fe_3O_4-PDDA-ZSM-12-Na^+. 250 mg of the γ-Fe_2O_3-β(p)-Na^+ or Fe_3O_4-PDDA-ZSM-12-Na^+ were dispersed in 5 ml of distilled water followed by the addition of Pd $(NO_3)_{2.H2O}$ to attain a Pd concentration of 0,01 mol/L. The mixture was stirred at room temperature for 6h, the solid was removed via magnetic decantation and dried at 60 ºC for 12 h. This ion exchange procedure was repeated twice more. Finally, the obtained powder was calcinated at 550 ºC for 5h.

3.1.1.9 Preparation of the catalyst with the physical mixture of β and ZSM-12 zeolites - γ-Fe_2O_3-(β+ZSM-12)-Pd

Approximately 70 mg of the PDDA-functionalized magnetite microspheres were dispersed in 12 ml of distilled water with the subsequent addition of a mixture of 320 mg of pure β zeolite and 180 mg of ZSM-12 zeolite, followed by stirring for 48 h at room temperature. The resulting composite Fe_3O_4-PDDA-(β+ZSM-12)-Na^+ was magnetically separated from the aqueous mixture and dried at 60 ºC for 24 h under vacuum. The material was then calcinated under air atmosphere at 550 ºC for 5 h, affording the composite *γ* -

Fe_2O_3-PDDA-(β+ZSM-12)-Na^+. 250 mg of *γ*-Fe_2O_3-PDDA-(β+ZSM-12)-Na+ were dispersed in 5 ml of distilled water followed by the addition of Pd $(NO_3)_{2.H2O}$ to attain a Pd concentration of 0,01 mol/L. The mixture was stirred at room temperature for 6h, and the solid was removed via magnetic decantation and dried at 60 ºC for 12 h. This ion exchange procedure was repeated twice more. Finally, the obtained powder was calcinated at 550 ºC for 5h.

3.1.2. Characterization of the support, the magnetically recoverable catalysts exchanged with Ir, Fe or Pd and catalysts made from the pure zeolites (β and ZSM-12) and their physical mixture

The particle size and morphological studies of the Fe_3O_4 microspheres used as support and all the catalysts were performed by Transmission Electron Microscopy (TEM), which was carried out using a FEI TECNAI G2 F20 microscope. For the TEM analyses, the powder samples were dispersed in ethanol and -sonicated for 5 min. One drop of this solution was placed on a 400-mesh copper grid with carbon film and the sample was dried at room temperature.

The XRD measurements were performed in a Rigaku Miniflex Diffractometer using the Kα radiation of a Cu source (λ=1,54187 Å), 40 kV, 30 mA and 2θ in the range of 5° to 80° and a rate of 2°/min.

The Rietveld refinement[191] was performed in order to quantify the different crystalline phases present in the beta zeolite samples. For that, the diffractogram of the sodic form of magnetic beta zeolite was obtained using a Rigaku Geiger-Flex diffractometer with a graphite monochromator in the 2θ range of 5° to 100° using a CuKα source and a step scan of 0.02° and 6 s by step. The Rietveld refinement was carried out using the space groups P4122 for beta zeolite [JCPDS 48-0074], C12/m1 for ZSM-12 zeolite [JCPDS 86-2364], and P213 for maghemite [JCPDS 04-0755] and using the software GSAS,[192] which uses the least-squares method to reach the best agreement between the experimental and the calculated diffraction profiles. The quality of the Rietveld refinement was accessed through the R values and χ^2.

The experimental content of aluminum and silicon were determined by x-ray fluorescence (XRF) analyses in a PANalytical MiniPal 4 spectrometer equipped with a Rh X-ray tube operating at 4 kW.

TPD measurements were conducted in a Micromeritics Autochem II 2920 Chemisorption Analyzer equipment with a TCD (Thermal Conductivity Detector) detector. For this, 50 mg of the sample were pre-treated thermally under 30 ml·min^{-1} helium flow at a heating rate of 10 ºC min^{-1} until 600 ºC and kept at this temperature for 30 min. After this period, the reactor was cooled to 120 ºC, and the He flow was kept for 60 min. Next, the adsorption of ammonia was performed through the passing of a 15% mixture of NH_3 in He for 30 min over the sample. After saturation, the sample was purged with He for 1 hour to remove the excess of ammonia. Finally, the temperature desorption was initiated under a 30 ml·min^{-1} He flow in a 15 ºC·min^{-1} heating rate until 600 ºC. To quantify the acid sites, the area under the curve of the graph of TCD signal x temperature was calculated.

The infrared spectrum of absorbed pyridine was recorded on a Fourier Transform Infrared spectrophotometer model Prestigi-21 in the range of 1800–1400 cm^{-1}. For the qualitative acidity determination, 50 mg of sample were subjected to a heat treatment in a tubular furnace at 300 ºC and 100 ml·min^{-1} N_2 flow for 1 h. Gaseous pyridine was then adsorbed on the samples for 1 h at 150 ºC with a N_2 gas carrier flow at 100 ml/min. Next, the N_2 flow was kept constant for 1 h at 150 ºC for the removal of the physically adsorbed pyridine.

ICP-OES measurements were conducted in a Thermo Fisher Scientific, iCAP 6300 Duo, with a CID (Charge Injection Device) detector.

The XPS analyses were conducted in a UNI-SPECS UHV spectrometer with a base pressure below 5x10-7 Pa. The Al Kα line was used (hv = 1486.6 eV) as ionization source, and the analyzer pass energy was set to 10 eV. The inelastic noise of the high-resolution spectra Fe2p, Ir4f and Pd3d, was subtracted using the Shirley method. The composition was determined from the relative areas corrected using the Scofield atomic sensitivity factor with a ± 5% precision. The spectra were deconvoluted using a Voight-type function, combined with Gaussian and Lorentz. The FWHM varied between 1,4 eV and 2,1 eV, and the position of the peaks was determined with a ± 0,1 eV precision.[193]

The nitrogen sorption measurements were performed using a Micromeritics equipment model ASAP 2020. Before the measurements, the powdered samples were previously treated at 200 ºC for 2 h under vacuum aiming to remove adsorbed water. After that, the powders were analyzed with gaseous nitrogen adsorption at -196 ºC and the volume of micropores and the external area were determined using the t-plot method. [194]

The magnetic measurements were carried out using and apparatus combining a superconducting quantum interference device and a vibrating sample magnetometer model Quantum Design MPMS SQUID-VSM. The magnetization was measured as function of the applied magnetic field (MxH) at room temperature and up to 70 kOe.

The Mössbauer characterization were carried out using a standard spectrometer at room temperature and a ^{57}Co as radioactive source dissolved in Rh matrix. The measurements were carried out using a transmission geometry without external magnetic field.

3.1.3. Catalytic application

3.1.3.1 Preparation of isopropyl levulinates from furfural, furfuryl alcohol and ethyl levulinate using the catalysts (γ-Fe_2O_3-β-Pd, γ-Fe_2O_3-β-Fe, γ-Fe_2O_3-β-Ir, γ-Fe_2O_3-β-H^+) using oil bath

In a typical catalytic test, 0.3 mmol of the starting material (furfural, furfuryl alcohol or ethyl levulinate), 750 µL of isopropyl alcohol for the reaction with furfural or ethyl levulinate or 230 µL for the reaction with furfuryl alcohol and 75 mg of the magnetically recoverable catalyst were added to a glass vial containing a magnetic stir bar. The vial was sealed and immersed in a pre-heated oil bath at 130 ºC and magnetically stirred at 700 rpm for 24 h for the reaction with furfural or ethyl levulinate or for 21 h for the reaction with furfuryl alcohol. The test was carried out in triplicate.

For the reactions under microwave irradiation, the reaction mixture was stirred in a 10 ml microwave tube at 130 ºC for 1 h for the reaction with furfural or for 30 min for the reaction. The reaction was carried out in triplicate too.

After the completion of the reaction, the vial was cooled to room temperature and the catalyst was separated with the aid of a magnet and a small amount of the reaction

liquid (50 μL) was removed from the vial, diluted in isopropyl alcohol and the products were analyzed using GC-MS; the retention times of the products were compared to those of commercial standards.

3.1.3.2 Preparation of isopropyl levulinates from furfural or furfuryl alcohol using the γ-Fe_2O_3-(β+ZSM-12)-Pd, γ-Fe_2O_3- βp-Pd and γ-Fe_2O_3-ZSM-12-Pd catalysts

0.3 mmol of the starting material (furfural or furfuryl alcohol), 750 μL of isopropyl alcohol for the reaction with furfural or 230 μL for the reaction with furfuryl alcohol and 75 mg of the magnetically recoverable catalyst were added to a glass vial containing a magnetic stir bar. The vial was sealed and immersed in a pre-heated oil bath at 130 ºC and magnetically stirred at 700 rpm for 24 h for the reaction with furfural or for 21 h for the reaction with furfuryl alcohol. The reaction was carried out in triplicate. After completion of the reaction, the vial was cooled to room temperature and the catalyst was separated with the aid of a magnet and a small amount of the reaction liquid (50 μL) was removed from the vial, diluted in isopropyl alcohol and the products were analyzed using GC-MS; the retention times of the products were compared to those of commercial standards.

3.1.3.3 Preparation of furfuryl alcohol from furfural or using the γ-Fe_2O_3-β- Pd catalyst

In a typical catalytic test, 0.15 mmol of furfural, 1 ml of water, 204 mg (3 mmol) of sodium formats and 32.5 mg of the magnetically recoverable catalyst were placed in a glass vial containing a magnetic stir bar. The vial was sealed and immersed in a pre-heated oil bath at 60 ºC and magnetically stirred at 700 rpm for 24 h. The reaction was carried out in triplicate.

After the completion of the reaction, the vial was cooled to room temperature and the catalyst was separated with the aid of a magnet. A small amount of the reaction liquid (50 μL) was removed from the vial, diluted in isopropyl alcohol and the products were analyzed using GC-MS; the retention times of the products were compared to those of commercial standards.

3.1.3.4 Recyclability of γ-Fe_2O_3-β- Pd catalyst

0.6 mmol of furfural or FA, 150 mg of catalyst, and 920 µL of isopropyl alcohol or 460 µL for the reaction with FA at 130 ºC for 24 h or 21 h for FA. After each reaction run, the catalyst was removed from the reaction medium with the aid of an external magnet, dried for at least 12 h at 100 ºC and reused in a new reaction cycle. For the determination of the reaction products was followed the same procedure as described in the previous tests.

3.1.4. Analyses of the reaction products

Samples were analyzed using a Shimadzu GCMS-QP2010S Gas Chromatograph coupled to a mass spectrometry (MS) detector equipped with a Zebron ZB5-MS capillary column (30 m x 0.32 mm, 0.25 µm) under the operation parameters. The inlet temperature was 250 °C, the interface temperature was 300 °C, the temperature ramp of the oven was from 50 to 250 °C at a rate of 10 °C·min^{-1}.

3.2 Mesoporous materials: sulfonic acid- functionalized dendritic silica

3.2.1. Synthesis

All solvents were dried prior to use by standard procedures. Reagents were purchased at the highest commercial quality and used without further purification.

3.2.1.1 Synthesis of dendritic mesoporous silica (DMSi) nanospheres

The DMSi nanospheres used as support for the catalyst was synthesized following a procedure described by Yang and co-workers.[94] A solution containing 72 ml of distilled water, 48 ml (145.2 mmol) of cetyltrimethylammonium chloride (CTAC, 25 wt% aqueous solution) and 360 µL (2.7 mmol) of triethanolamine (TEA) was stirred at 500 rpm for 1 h at 60 ºC. A solution containing 8 ml (36.1 mmol) of tetraethyl orthosilicate (TEOS) and 32 ml (296.2 mmol) of cyclohexane was then added dropwise to the CTAC solution. The mixture was kept under reflux at 60 ºC for 20 h under slow magnetic stirring (200 rpm). The resultant material was cooled to room temperature and centrifuged at 13000 rpm for 20 min, followed by washing with distilled water several times. Next, the white material was

dried at 60 ºC for 24 h followed by trituration and calcination at 600 ºC in air atmosphere for 3 h.

3.2.1.2 Synthesis of mesoporous silica KCC

The KCC used as support for the catalyst was synthesized following a procedure described by Yu and co-workers.[195] A solution containing 0.5 g (1.3 mmol) of hexadecyl pyridinium bromide (CPB), 0.75 ml (6.5 mmol) of n-pentanol and 15 ml (138.8 mmol) of cyclohexane was added to a solution having 0.3 g (5 mmol) of urea and 15 ml of water under stirring and room temperature. Then 1.25 ml (5.6 mmol) of ethyl silicate (TEOS) was added, then the mixture was transferred to a 50 ml Teflon-lined autoclave and heated at 120 ºC for 4 h. The obtained materials were washed with ethanol and dried at 60 ºC for 12 h. Finally, the materials were calcined at 550 ºC for 5 h.

3.2.1.3 Synthesis of mesoporous silica MCM-41 materials

The MCM-41 used as support for the catalyst was synthesized following a procedure described by Grün and co-workers.[196] A solution containing 13.2 g of aqueous ammonia (32 wt.%, 0.25 mol) and 60.0 g of absolute ethanol (EtOH, 1.3 mol) were added to a solution containing 2.5 g of n-hexadecyltrimethylammonium bromide (C_{16}TMABr, 0.007 mol) dissolved in 50 g of deionized water. The solution was stirred for 15 min (250 rpm) and posteriorly 4.7 g of TEOS (0.022 mol) was added. The mixture was stirred for 2 h. The resultant material was cooled to room temperature and filtered, followed by washing with distilled water and methanol several times. Next, the white material was dried at 60 ºC for 24 h followed by trituration and calcination at 550 ºC in air atmosphere for 5 h.

3.2.1.4 Synthesis of large-pore silica FDU-12 materials

The FDU-12 used as support for the catalyst was synthesized following a procedure described by Kruk and co-workers[197] with some modifications. A solution containing three grams of Pluronic F127 copolymer and 185 ml of 1.97 M HCl was placed in a water bath set to 15.0 ºC and stirred until total homogenization. Then, 4.7 ml (3.6 g, 26.8 mmol) of cymene and 15.0 g (201.2 mmol) of KCl were introduced. After 2 h of constant

stirring, 13.3 ml (12.5 g, 60 mmol) of TEOS was added and the mixture was stirred for a day in an open container at 15 ºC. Afterwards, the reaction mixture was closed and was refluxed at 100 ºC for 1 day. The samples were recovered by filtration without washing and were dried in the air. Then the dried as-synthesized material was subjected to an additional hydrothermal treatment in an acid solution. 0.5 g of the as-synthesized sample was placed in 30 ml of 1.97 M HCl solution and heated at 100 ºC in a Teflon-lined autoclave for 24 h. The resultant material was cooled to room temperature and filtered, followed by washing with distilled water several times. Next, the white material was dried at 60 ºC for 24 h followed by trituration and calcination at 550 ºC in air atmosphere for 5 h.

3.2.1.5 Synthesis of spherical silica particles by Stöber process

The Stöber used as support for the catalyst was synthesized following a procedure described by Wang and co-workers[198] with some modifications. First, 10.8 ml of deionized H_2O, 9.8 ml (42 mmol) of NH_3 and 73.8 ml of ethanol were blended for 10 min, and then 5.6 ml (25.3 mmol) of TEOS was added into the previous solution at room temperature under magnetic stirring for 12 h. The resultant material was cooled to room temperature and centrifuged at 5000 rpm for 15 min, followed by washing with water and ethanol several times. Then, the white material was dried at 150 ºC for 5 h.

3.2.1.6 Synthesis of microporous silica, silicate

The silicate used as support for the catalyst was synthesized following a procedure described by Zhou and co-workers.[199] A solution containing 11.16 ml (50.4 mmol) of TEOS, 27 ml of water and 3 ml (14.9 mmol) of tetra propylammonium hydroxide (TPAOH, 40 wt% aqueous solution) was stirred for 24 h at room temperature. Then was added a solution of 0.08 g (2 mmol) of NaOH, 27 ml of water and 3 ml (14.9 mmol) of TPAOH, this mixture was stirred for 2 h at room temperature. The new solution was stirred for 10 min and they were transferred to a 50 mL Teflon-lined autoclave, maintaining the stirring and the heating in a sand bath at 150 ºC for 24h. Then, the white material was washed with water several times and dried at 60 ºC for 24 h, followed by trituration and calcination at 500 ºC in air atmosphere for 16 h.

3.2.1.7 Synthesis of SBA-15

The silicate used as support for the catalyst was synthesized following a procedure described by Zhau and co-workers.[200] A solution containing 4 g (0.7 mmol) of Pluronic P123 and 30ml of distillate water was stirred and heated at 50 ºC. Then, was added a solution of 120ml of HCL 2.0 mol/L. The mixture was stirred and heated to 50 ºC for 30 min. It was added 10 ml of TEOS, the mixture was refluxed at 50 ºC for 24 h, and the stirring was kept all the time. Then, the mixture was refluxed at 80 ºC for 24 h in static condition. The white material was washed with water several times and dried at 60 ºC for 24 h, followed by trituration and calcination at 550 ºC in air atmosphere for 5 h.

3.2.1.8 Functionalization of silicas with sulfonic acid groups (Silicas-SA)

The procedure to functionalize silica (KCC, MCM-41, silicate, Stöber, FDU-12, SBA-15, silica flash) with sulfonic acid, is the same procedure described below for the functionalization of DMSi nanospheres. All silicas were previously synthesized with the exception of silica flash that was obtained commercially.

The sulfonic acid functionalized DMSi nanospheres were obtained following a two-step procedure recently described by Pirez and co-workers.[161] 1 g of the calcined DMSi nanospheres was added to a solution containing 30 mL of distilled water and 200 mg (3.4 mmol) of sodium chloride under vigorous stirring at room temperature for 30 min. Then, 1 mL (5.4 mmol) of 3-mercaptopropyl trimethoxy silane (MPTMS) was added to the mixture, which was refluxed at 100 ºC under magnetic stirring (600 rpm) for 24 h. The mercaptopropyl functionalized material (DMSi-MP) was filtered under vacuum and washed several times with distilled water followed by drying at 50 ºC under vacuum overnight. The thiol groups were then converted into sulfonic groups by a mild oxidation process using hydrogen peroxide as oxidant. For this step, the dried and triturated DMSi-MP (~1.6 g) was added into 30 mL of a 30% hydrogen peroxide solution and vigorously stirred (1000 rpm) at room temperature for 24 h. The resultant material was filtered under vacuum and washed several times with methanol, followed by drying at 50 ºC under vacuum for 24 h. The dendritic mesoporous silica functionalized with sulfonic acid groups was named as DMSi-SA.

3.2.2. Characterization of the silicas support and the silicas-SA catalysts

The particle size and morphological studies of the silica's catalyst were performed by TEM (Transmition Electron Microscopy). The TEM analyses were conducted using JEOL JEM 2010F at 160 kV of accelerating voltage.

Microscopic images were obtained for all sulfonated catalysts by HRTEM TITAN 60-300 with X-FEG type emission gun, operating at 80 kV; this microscope is equipped with a Cs image corrector and a TEM high-angle annular dark-field detector (HAADF). The point resolution is 0.06 nm in HRTEM mode. The elemental mappings were obtained by STEM-Energy Dispersive X-ray Spectroscopy (EDS) with an acquisition time of 20 min. For HRTEM analyses, the powder samples were dispersed in ethanol and ultrasonicated for 5 min. One drop of this solution was placed on a copper grid with a holey carbon film. The sample was then dried at room temperature.

Low angle x-ray diffraction patterns were recorded with a PANalytical X'Pert PRO MPD (PANalytical, Netherlands) diffractometer in the Bragg-Brentano geometry, Co-Kα radiation (40 kV, 30 mA, λ = 0.1789 nm) equipped with an X'Celerator detector and programmable divergence and diffracted beam anti-scatter slits. The measurement range was 2θ:0° - 5° with a step size of 0.017°.

The nitrogen desorption analyses were conducted at a Micromeritics equipment (ASP-2420). The samples were treated under vacuum at 200 ºC for 240 minutes for the elimination of water and physically adsorbed gases. Then, the samples were transferred to the adsorption unit, were liquid nitrogen is fed to the sample at varying relative pressures (p/p_0).

The infrared spectrum of absorbed pyridine was recorded on a Bruker Fourier Transform Infrared spectrophotometer model Vertex-70. For the qualitative acidity determination, the samples were previously heated at 250 ºC for 2h under nitrogen flow (100 $mL \cdot min^{-1}$). The application of pyridine over the samples conducted using a pyridine/nitrogen flow (30 $mL \cdot min^{-1}$) at 150 ºC for 10 min. Next, the N_2 flow was kept constant (100 $mL \cdot min^{-1}$) at 200 ºC for 1 h for the removal of the physically adsorbed pyridine. The materials were

then analyzed by DRIFTS in the 1800-1400 cm^{-1} wavenumber range using a spectral resolution of 4 cm^{-1} with the collection of 32 scans for each spectrum.

The infrared spectrum of absorbed pyridine was recorded on a Fourier Transform Infrared spectrophotometer model Prestigi-21 in the range of 1800 cm^{-1} –1400 cm^{-1} wavenumber. For the qualitative acidity determination, 50 mg of sample were subjected to a heat treatment in a tubular furnace at 300 ºC and 100 $mL \cdot min^{-1} N_2$ flow for 1 h. Gaseous pyridine was then adsorbed on the samples for 1 h at 150 ºC with a N_2 gas carrier flow at 100 $mL \cdot min^{-1}$. Next, the N_2 flow was kept constant for 1 h at 150 ºC for the removal of the physically adsorbed pyridine.

XPS surface investigation has been performed on the PHI 5000 VersaProbe II XPS system (Physical Electronics) with monochromatic Al-Kα source (15 kV, 50 W) with photon energy of 1486.7 eV. Dual beam charge compensation was used for all measurements. All the spectra were measured in the vacuum at 1.4 x 10^{-7} Pa and the room temperature of 22 ºC. For the high-resolution spectra was the pass energy set up to 23.500 eV and step size 0.200 eV. The spectra were evaluated with the MultiPak (Ulvac - PHI, Inc.) software. All binding energy (BE) values were referenced to the C1s peak at 284.80 eV.

The total Brönsted acid site of the samples was determined by aqueous titration using thymol blue as indicator. The samples were previously submitted to an ionic exchange with KCl and the resulting HCl was titrated with a NaOH solution previously standardized using potassium hydrogen phthalate ($KHC_8H_4O_4$). All analyses were performed as triplicates and with different batches of the materials.

3.2.3. Catalytic application

3.2.3.1 Preparation of ethyl levulinates from fructose and furfural from xylose using the DMSi-SA catalyst using conventional heating

In a typical catalytic test, 1 mmol of the starting material (fructose and xylose), 2 ml of ethanol and 72.5 mg of the catalyst were added to the vial containing a magnetic stir bar. The vial was sealed and immersed in a pre-heated oil bath at 130 ºC and magnetically stirred at 700 rpm for 24 h.

After the completion of the reaction, the vial was cooled to room temperature and 1.4 mmol of the internal standard (para-nitrophenol) is added. Subsequently the catalyst was separated with the aid of centrifuge (5 min, 5000 rpm), a small amount of the reaction liquid (14 µL for the xylose and 12 µL for the fructose test) was removed from the vial, diluted in 1ml of ethanol, and the products were analyzed using GC-MS. The retention times of the products were compared to those of commercial standards and the quantification was done using para-nitrophenol as internal standard. The reaction was carried out in triplicate.

3.2.3.2 Preparation of ethyl levulinates from glucose, sucrose, cellulose using the DMSi-SA catalyst using conventional heating

In a typical catalytic test, 1 mmol of the starting material (glucose and cellulose) and 0.5 mmol for sucrose, 3 ml of ethanol and 72.5 mg of the catalyst were added to the vial containing a magnetic stir bar. The vial was sealed and immersed in a pre-heated oil bath at 170 ºC and magnetically stirred at 700 rpm for 24 h.

After the completion of the reaction, the vial was cooled to room temperature and 1.4 mmol of the internal standard (para-nitrophenol) is added. Subsequently the catalyst was separated with the aid of a centrifuge (5 min, 5000 rpm), a small amount of the reaction liquid (12 µL) was removed from the vial, diluted in 1ml of ethanol, and the products were analyzed using GC-MS. The retention times of the products were compared to those of commercial standards and the quantification was done using para-nitrophenol as internal standard. The reaction was carried out in triplicate.

3.2.3.3 Preparation of ethyl levulinates from glucose and furfural from xylose using the silicas-SA catalyst (KCC-SA, MCM-41-SA, silicate-SA, Stöber-SA, FDU-12-SA, TUD-1-SA, SBA-15-SA, silica flash-SA)) using conventional heating

1 mmol of the starting material (xylose and glucose), 3 ml of ethanol and 5 mol% of -SO_3H of the catalyst for xylose or 10 mol% of -SO_3H of the catalyst for glucose were added to the vial containing a magnetic stir bar. The vial was sealed and immersed in a pre-heated oil bath at 170 ºC and magnetically stirred at 700 rpm for 24 h.

After the completion of the reaction, the vial was cooled to room temperature and 1.4 mmol of the internal standard (para-nitrophenol) is added. Subsequently the catalyst was separated with the aid of a centrifuge (5 min, 5000 rpm), a small amount of the reaction liquid (14 µL for the xylose and 12 µL for the glucose test) was removed from the vial, diluted in 1ml of ethanol, and the products were analyzed using GC-MS. The retention times of the products were compared to those of commercial standards and the quantification was done using para-nitrophenol as internal standard. The reaction was carried out in triplicate.

3.2.3.4 Recyclability of DMSi-SA catalyst

1 mmol of xylose or fructose or glucose or sucrose, 72.5 mg of catalyst for xylose or fructose or 145mg for glucose or sucrose, and 3 ml of ethanol at 170 ºC for 24 h. After each reaction run, the catalyst was removed from the reaction medium with the aid with the aid of centrifuge (5min, 5000 rpm). The catalyst is then washed three times with a 10% solution of sulfuric acid in DMSO, then twice with ethanol.[201] The separation of the catalyst from the washing solutions was by centrifugation (10,000 rpm for 10 min). Afterwards, the samples are subjected to a drying process for 24 h in an oven at 60 ºC and reused in a new reaction cycle. For the determination of the reaction products was followed the same procedure as described in the previous tests.

3.2.4. Analyses of the reaction products

The yield of the reactions was determined using GC-MS with 4-nitrophenol as an internal standard. Calibration curves were acquired in triplicates for each of the expected products. The samples were analyzed using Shimadzu GCMS-QP2010S Gas Chromatograph coupled to a MS detector equipped with a ZB-5MS column (30 m x 0.25 mm x 0.25 µm) under the operation parameters. The inlet temperature was 250 °C and the temperature ramp of the oven was from 100 to 250 °C at a rate of 10 °C·min^{-1}

Conclusions

4. Conclusions

From the results obtained in the work, it can be concluded that bifunctional catalysts, both microporous and mesoporous, capable of promoting cascade reactions of lignocellulosic biomass-derived compounds, were synthesized. In the first part of the work were designed, synthesized and fully characterized a series of new catalysts comprising magnetically recoverable β-zeolites exchanged with transition metals that displayed immense potential in the catalytic valorization of lignocellulosic biomass-derived compounds. The Pd-exchanged catalyst, especially, has shown remarkable efficiency in the conversion of both furfural and furfuryl alcohol to isopropyl levulinate, to platform chemical with broad potential applications. Additionally, the same catalyst was also very promising in the environmentally friendly reduction of furfural to furfuryl alcohol using sodium formate as a hydrogen source in aqueous medium. The use of an unconventional heating source (microwave) permit obtain the same results for the conversion of furfural and furfuryl alcohol to propyl levulinate in significantly lower times. Still, recyclability studies have shown that the Pd-exchanged catalyst was only deactivated after the 4th reaction run when starting from furfural, or in the 3rd reaction run, when starting from furfuryl alcohol; however, the catalyst could be re-activated by a simple calcination step which bodes well for its application.

In the second part of the work a new catalyst that displays both Lewis and Brönsted acid sites (DMSi-SA) was prepared and thoroughly characterized. The catalyst showed exceptional activity in the conversion of fructose, glucose, sucrose and cellulose to ethyl levulinate and xylose to furfural. However, the obtention of EL from cellulose with good yields and the role of sulfur as Lewis acid still remains a challenge. The DMSi-SA does not show good recyclability for the tested substrates because was not possible to eliminate the humins that form on the surface of the catalyst during the reaction; this will be aims of future studies. . In spite of this the DMSi-SA experienced the best catalytic responses, in comparison with the other tested silicas, for conversion of glucose to fructose to propyl levulinate which could be related to its characteristic morphology and pore size.

References

5. References

1. Wrigh, L., et al., *Biomass Energy Data Book*. 2006: United States.
2. McKendry, P., *Energy production from biomass (part 1): overview of biomass.* Bioresource Technology, 2002. **83**: p. 37-46.
3. *Biomass—renewable energy from plants and animals*. 2018; Available from: https://www.eia.gov/energyexplained/index.php?page=biomass_home.
4. Vassilev, S.V., et al., *An overview of the chemical composition of biomass.* Fuel, 2010. **89**: p. 913–933.
5. Saxena, R.C., D.K. Adhikari, and H.B. Goyal, *Biomass-based energy fuel through biochemical routes: A review.* Renewable and Sustainable Energy Reviews 2009. **13**: p. 167–178.
6. Akhtar, J. and N.A.S. Amin, *A review on process conditions for optimum bio-oil yield in hydrothermal liquefaction of biomass.* Renewable and Sustainable Energy Reviews 2011. **15**: p. 1615–1624.
7. Alonso, D.M., S.G. Wettstein, and J.A. Dumesic, *Gamma-valerolactone, a sustainable platform molecule derived from lignocellulosic biomass.* Green Chem., 2013. **15**: p. 584–595.
8. Lima, C.G.d.S., *"NANOSTRUCTURED CATALYSTS FOR ORGANIC REACTIONS: DESIGN, SYNTHESIS AND APPLICATIONS"*, in *Chemistry Department*. 2016, UNIVERSIDADE FEDERAL DE SÃO CARLOS: SÃO CARLOS.
9. Demolis, A., N. Essayem, and F. Rataboul, *Synthesis and Applications of Alkyl Levulinates.* ACS Sustainable Chem. Eng., 2014. **2**: p. 1338-1352.
10. Galbe, M. and G. Zacchi, *Pretreatment of Lignocellulosic Materials for Efficient Bioethanol Production.* Adv Biochem Engin / Biotechnol 2007. **108**: p. 41–65.
11. Faith, W.L., *Development of the Scholler Process in the United States.* Ind. Eng. Chem., 1945. **37**(1): p. 9-11.
12. Bergius, F., *Conversion of Wood To Carbohydrates.* Ind. Eng. Chem., 1937. **29**(3): p. 247–253.
13. Antonoplis, R.A., et al., *Production of sugars from wood using high-pressure hydrogen chloride.* Biotechnology and Bioengineering, 1983. **25**(11): p. 2757-2773.
14. Erckel, R., et al., *Process for hydrolyzing cellulose-containing material with gaseous hydrogen fluoride* 1985: UNITED STATES OF AMERICA.
15. Rinaldi, R. and F. Schüth, *Acid Hydrolysis of Cellulose as the Entry Point into Biorefinery Schemes.* ChemSusChem, 2009. **2**(12): p. 1096-1107.
16. Rinaldi, R. and F. Schuth, *Design of solid catalysts for the conversion of biomass.* Energy Environ. Sci. , 2009. **2**: p. 610 –626.
17. Nagorski, R.W. and J.P. Richard, *Mechanistic Imperatives for Aldose−Ketose Isomerization in Water: Specific, General Base- and Metal Ion-Catalyzed Isomerization of Glyceraldehyde with Proton and Hydride Transfer.* J. Am. Chem. Soc., 2001. **123**(5): p. 794–802.
18. Román-Leshkov, Y., et al., *Mechanism of Glucose Isomerization Using a Solid Lewis Acid Catalyst in Water.* Angewandte Chemie, 2010. **122**(47): p. 9138-9141.
19. Gilkey, M.J. and B. Xu, *Heterogeneous Catalytic Transfer Hydrogenation as an Effective Pathway in Biomass Upgrading.* ACS Catal. , 2016. **6**(3): p. 1420-1436.
20. Dias, A.S., et al., *Modified versions of sulfated zirconia as catalysts for the conversion of xylose to furfural.* Catalysis Letters, 2007. **114**(3-4): p. 151-160.
21. Dias, A.S., et al., *Exfoliated titanate, niobate and titanoniobate nanosheets as solid acid catalysts for the liquid-phase dehydration of d-xylose into furfural.* Journal of Catalysis, 2006. **244**(2): p. 230-237.
22. Dias, A.S., et al., *Acidic cesium salts of 12-tungstophosphoric acid as catalysts for the dehydration of xylose into furfural.* Carbohydrate Research, 2006. **341**(18): p. 2946-2953.
23. Dias, A.S., et al., *Liquid-phase Dehydration of d-xylose over Microporous and Mesoporous Niobium Silicates.* Catalysis Letters, 2006. **108**(3-4): p. 179-186.
24. Dias, A.S., M. Pillinger, and A. A.Valente, *Dehydration of xylose into furfural over micro-mesoporous sulfonic acid catalysts.* Journal of Catalysis, 2005. **229**(2): p. 414-423.

25. Moliner, M., Y. Román-Leshkov, and M.E. Davis, *Tin-containing zeolites are highly active catalysts for the isomerization of glucose in water.* PNAS, 2010. **107**(4): p. 6164 – 6168.
26. Lew, C.M., N. Rajabbeigi, and M. Tsapatsis, *One-Pot Synthesis of 5-(Ethoxymethyl)furfural from Glucose Using Sn-BEA and Amberlyst Catalysts.* Ind. Eng. Chem. Res., 2012. **51**: p. 5364 - 5366.
27. Saravanamurugan, S., et al., *Efficient Isomerization of Glucose to Fructose over Zeolites in Consecutive Reactions in Alcohol and Aqueous Media.* J.Am.Chem.Soc., 2013. **135**: p. 5246 −5249.
28. Yomaira J. Pagan-Torres, et al., *Production of 5-Hydroxymethylfurfural from Glucose Using a Combination of Lewis and Brønsted Acid Catalysts in Water in a Biphasic Reactor with an Alkylphenol Solvent.* ACS Catal, 2012. **2**: p. 930 - 934.
29. Vinke, P. and H. van Bekkum, *The Dehydration of Fructose Towards 5-Hydroxymethylfurfural Using Activated Carbon as Adsorbent.* Starch - Stärke, 1992. **44**(3): p. 90-96.
30. Rac, V., et al., *Hierarchical ZSM-5, Beta and USY zeolites: Acidity assessment by gas and aqueous phase calorimetry and catalytic activity in fructose dehydration reaction.* Microporous and Mesoporous Materials, 2014. **194**: p. 126-134.
31. Bui, L., et al., *Domino Reaction Catalyzed by Zeolites with Brønsted and Lewis Acid Sites for the Production of γ-Valerolactone from Furfural.* Angewandte Chemie, 2013. **125**(31): p. 8180-8183.
32. Alonso, D.M., et al., *Direct conversion of cellulose to levulinic acid and gamma-valerolactone using solid acid catalysts.* Catal. Sci. Technol., 2013. **3**: p. 927-931.
33. Koehle, M. and R.F. Lobo, *Lewis acidic zeolite Beta catalyst for the Meerwein–Ponndorf–Verley reduction of furfural* Catal. Sci. Technol., 2016. **6**: p. 3018-3026
34. Satterfield, C.N., *Heterogeneous Catalysis in Industrial Practice*. second edition ed. 1996 Malabar, Florida: Krieger publishing company.
35. Sing, K.S.W., et al., *Reporting Physisorption data for Gas/Solid System with Special Reference to the Determination of Surface Area and Porosity.* Pure & Appl. Chem., 1985. **57**(4): p. 603—619.
36. M.Csicsery, S., *Shape-selective catalysis in zeolites.* Zeolites, 1984. **4**(3): p. 202-213.
37. AvelinoCorma, *State of the art and future challenges of zeolites as catalysts.* Journal of Catalysis, 2003. **216**(1-2): p. 298-312.
38. Auerbach, S.M., K.A. Carrado, and P.K. Dutta, *Handbook of Zeolite Science and Technology*. 1 ed. 2003, NEW 'YORK BASEL: Marcel Dekker.
39. Xu, R., et al., *Chemistry of Zeolites and Related Porous Materials: Synthesis and Structure*. 1 ed. 2007 John Wiley & Sons.
40. Weitkamp, J., *Zeolites and catalysis.* Solid State Ionics 2000. **131**: p. 175–188.
41. Kamimura, Y., et al., *Crystallization Behavior of Zeolite Beta in OSDA-Free, Seed-Assisted Synthesis.* J. Phys. Chem. C, 2011. **115**(3): p. 744–750.
42. Ennaert, T., et al., *Potential and challenges of zeolite chemistry in the catalytic conversion of biomass.* Chem. Soc. Rev., 2016. **45**: p. 584-611.
43. Taarning, E., et al., *Zeolite-catalyzed biomass conversion to fuels and chemicals* Energy Environ. Sci., 2011. **4**: p. 793-804
44. Xiao, F.-S. and X. Meng, *Zeolites in Sustainable Chemistry: Synthesis, Characterization and Catalytic Applications*. 1 ed. Green Chemistry and Sustainable Technology. 2015: Springer.
45. Nadgeri, J.M., et al., *Liquid phase hydrogenation of methyl levulinate over the mixture of supported ruthenium catalyst and zeolite in water.* Applied Catalysis A: General, 2014. **470**: p. 215-220.
46. Cai, J., et al., *Gold Nanoclusters Confined in a Supercage of Y Zeolite for Aerobic Oxidation of HMF under Mild Conditions.* Chemistry – A European Journal, 2013. **19**(42): p. 14215-14223.
47. Cao, Q., et al., *Solid acid-catalyzed conversion of furfuryl alcohol to alkyl tetrahydrofurfuryl ether.* Catalysis Communications, 2015. **58**: p. 76-79.
48. Mellmer, M.A., et al., *Selective Production of Levulinic Acid from Furfuryl Alcohol in THF Solvent Systems over H-ZSM-5.* ACS Catal., 2015. **5**: p. 3354 − 3359.
49. Mohan, V., et al., *Ni/H-ZSM-5 as a promising catalyst for vapour phase hydrogenation of levulinic acid at atmospheric pressure* RSC Adv., 2014. **4**: p. 9660-9668
50. Lima, T.M., et al., *Magnetic ZSM-5 zeolite: a selective catalyst for the valorization of furfuryl alcohol to γ-valerolactone, alkyl levulinates or levulinic acid* Green Chemistry, 2016. **18**(20): p. 5586-5593
51. Newsam, J.M., et al., *Structural characterization of zeolite beta.* Proceedings of the Royal Society of London. A. Mathematical and Physical Sciences, 1988. **420**(1859): p. 375-405.

52. Borade, R.B. and A. Clearfield, *Preparation of aluminum-rich Beta zeolite.* Microporous Materials 1996. **5**: p. 289 297.
53. Baerlocher, C., L.B. McCusker, and D.H. Olson, *Atlas of Zeolite Framework Types*. Sixth revised edition ed. 2007.
54. Mihalcik, D.J., C.A. Mullen, and A.A. Boateng, *Screening acidic zeolites for catalytic fast pyrolysis of biomass and its components.* Journal of Analytical and Applied Pyrolysis 2011. **92**(1): p. 224–232.
55. Nikolla, E., et al., *"One-Pot" Synthesis of 5-(Hydroxymethyl)furfural from Carbohydrates using Tin-Beta Zeolite.* ACS Catal., 2011. **1**(4): p. 408–410.
56. Wang, J., S. Jaenickea, and G.-K. Chuah, *Zirconium–Beta zeolite as a robust catalyst for the transformation of levulinic acid to γ-valerolactone via Meerwein–Ponndorf–Verley reduction* RSC Adv., 2014. **4**: p. 13481-13489
57. Li, H., et al., *Direct conversion of biomass components to the biofuel methyl levulinate catalyzed by acid-base bifunctional zirconia-zeolites.* Applied Catalysis B: Environmental, 2017. **200**: p. 182-191.
58. Dijkmans, J., et al., *Cooperative Catalysis for Multistep Biomass Conversion with Sn/Al Beta Zeolite.* ACS Catal. , 2015. **5**(2): p. 928-940.
59. Shu, Q., et al., *Synthesis of biodiesel from soybean oil and methanol catalyzed by zeolite beta modified with La3+.* Catalysis Communications, 2007. **8**(12): p. 2159-2165.
60. Yan, B., et al., *Sustainable Production of Acrylic Acid: Alkali-Ion Exchanged Beta Zeolite for Gas-Phase Dehydration of Lactic Acid.* ChemSusChem, 2014. **7**(6): p. 1568-1578.
61. Baeza, A., G. Guillena, and D.J. Ramón, *Magnetite and Metal-Impregnated Magnetite Catalysts in Organic Synthesis: A Very Old Concept with New Promising Perspectives.* ChemCatChem, 2016. **8**(1): p. 49-67.
62. Rossi, L.M., et al., *Magnetic nanomaterials in catalysis: advanced catalysts for magnetic separation and beyond* Green Chem., 2014. **16**: p. 2906-2933.
63. Wang, D. and D. Astruc, *Fast-Growing Field of Magnetically Recyclable Nanocatalysts.* Chem. Rev., 2014. **114**(14): p. 6949–6985.
64. Gawande, M.B., P.S. Branco, and R.S. Varma, *Nano-magnetite (Fe_3O_4) as a support for recyclable catalysts in the development of sustainable methodologies* Chem. Soc. Rev., 2013. **42**: p. 3371-3393
65. Polshettiwar, V., et al., *Magnetically Recoverable Nanocatalysts.* Chem. Rev. , 2011. **111**(5): p. 3036-3075.
66. Shylesh, S., V. Schünemann, and W.R. Thiel, *Magnetically Separable Nanocatalysts: Bridges between Homogeneous and Heterogeneous Catalysis.* Angewandte Chemie International Edition, 2010. **49**(20): p. 3428-3459.
67. Chaudhuri, R.G. and S. Paria, *Core/Shell Nanoparticles: Classes, Properties, Synthesis Mechanisms,Characterization, and Applications.* Chem. Rev. , 2012. **112**: p. 2373–2433.
68. Lu, A.-H., E.L. Salabas, and F. Schth, *Magnetic Nanoparticles: Synthesis, Protection, Functionalization, and Application.* Angew. Chem. Int. Ed. , 2007. **46**: p. 1222 – 1244.
69. Liu, B. and Z. Zhang, *Catalytic Conversion of Biomass into Chemicals and Fuels over Magnetic Catalysts.* ACS Catal. , 2016. **6**(1): p. 326-338.
70. Zhang, X., et al., *Nanocoating of magnetic cores with sulfonic acid functionalized shells for the catalytic dehydration of fructose to 5-hydroxymethylfurfural.* Chin. J. Catal., 2014. **35**(5): p. 703-708.
71. Martínez, J.J., et al., *Dehydration of Xylose to Furfural and Its Valorization via Different Multicomponent Reactions Using Sulfonated Silica with Magnetic Properties as Recyclable Catalyst.* Catalysis Letters, 2014. **144**(7): p. 1322–1331.
72. Galvis, H.M.T., et al., *Supported Iron Nanoparticles as Catalysts for Sustainable Production of Lower Olefins.* Science 2012. **335**(6070): p. 835-838.
73. Yan, Q., et al., *Iron nanoparticles in situ encapsulated in biochar-based carbon as an effective catalyst for the conversion of biomass-derived syngas to liquid hydrocarbons.* Green Chem., 2013. **15**: p. 1631-1640
74. Aho, A., et al., *Catalytic upgrading of woody biomass derived pyrolysis vapours over iron modified zeolites in a dual-fluidized bed reactor.* Fuel, 2010. **89**(8): p. 1992-2000.
75. Deng, J., et al., *Conversion of Carbohydrate Biomass to γ-Valerolactone by using Water-Soluble and Reusable Iridium Complexes in Acidic Aqueous Media.* ChemSusChem, 2013. **6**(7): p. 1163-1167.

76. Wei, Y., et al., *Highly efficient transformation of levulinic acid into pyrrolidinones by iridium catalysed transfer hydrogenation.* Chem. Commun., 2013,49, , 2013. **49**: p. 5408-5410
77. Du, X., et al., *Catalytic conversion of biomass-derived levulinic acid into γ-valerolactone using iridium nanoparticles supported on carbon nanotubes.* Chinese Journal of Catalysis, 2013. **34**(5): p. 993-1001.
78. Xu, X., et al., *Synthesis of Palladium Nanoparticles Supported on Mesoporous N-Doped Carbon and Their Catalytic Ability for Biofuel Upgrade.* J. Am. Chem. Soc., 2012. **134**(41): p. 16987–16990.
79. Zhang, Z., et al., *Selective aerobic oxidation of the biomass-derived precursor 5-hydroxymethylfurfural to 2,5-furandicarboxylic acid under mild conditions over a magnetic palladium nanocatalyst* Green Chem., 2015. **17**: p. 1308-1317
80. Huang, Y.-B., et al., *Heterogeneous Palladium Catalysts for Decarbonylation of Biomass-Derived Molecules under Mild Conditions.* ChemSusChem, 2013. **6**(8): p. 1348-1351.
81. Kresge, C.T., et al., *Ordered mesoporous molecular sieves synthesized by a liquid-crystal template mechanism.* Nature, 1992. **359**: p. 710-712.
82. Gómez-Romero, P. and C. Sanchez, *Functional Hybrid Materials* 6ed. 2004. 434
83. Rahmat, N., A.Z. Abdullah, and A.R. Mohamed, *A Review: Mesoporous Santa Barbara Amorphous-15, Types, Synthesis and Its Applications towards Biorefinery Production* American Journal of Applied Sciences, 2010. **7**(12): p. 1579-1586.
84. Gu, D. and F. Schüth, *Synthesis of non-siliceous mesoporous oxides.* Chem. Soc. Rev., 2014. **43**: p. 313-344.
85. Zhanga, Q., et al., *Facile general strategy toward hierarchical mesoporous transition metal oxides arrays on three-dimensional macroporous foam with superior lithium storage properties.* Nano Energy, 2015. **13**: p. 77-91.
86. Liang, h., Z. Li, and S. Dai, *Mesoporous Carbon Materials: Synthesisand Modification.* Angew.Chem.Int.Ed., 2008. **47**: p. 3696 – 3717.
87. Miller, C.A. and P. Neogi, *Interfacial Phenomena: Equilibrium and Dynamic Effects, Second Edition (Surfactant Science)*. 2 ed, ed. M.J. Schick and A.T. Hubbard. 2007.
88. Hoffmann, F., et al., *Silica-based mesoporous organic-inorganic hybrid materials.* Angew Chem Int Ed Engl, 2006. **45**(20): p. 3216-3251.
89. Seddon, J.M. and M.E. Raimondi., *Liquid crystal templating of mesoporous materials.* Mol. Cryst. Liquid Cryst. , 2000. **347**: p. 221-229.
90. Monnier, A., et al., *Cooperative formation of inorganic-organic interfaces in the synthesis of silicate mesostructures. .* Science, 1993. **261**: p. 1299-1303.
91. Patarin, J., B. Lebeau, and R. Zana., *Recent advances in the formation mechanisms of organized mesoporous materials.* Curr. Opin. Colloid Interf. Sci., 2002. **7**: p. 107-115.
92. Wan, Y. and D. Zhao, *On the Controllable Soft-Templating Approach to Mesoporous Silicates.* Chemical Reviews, 2007. **107**(7): p. 2822-2860.
93. Du, X. and S.Z. Qiao, *Dendritic Silica Particles with Center-Radial Pore Channels: Promising Platforms for Catalysis and Biomedical Applications.* small, 2015. **11**(4): p. 392–413.
94. Shen, D., et al., *Biphase Stratification Approach to Three-Dimensional Dendritic Biodegradable Mesoporous Silica Nanospheres.* Nano Lett., 2014. **14**(2): p. 923–932.
95. Cortright, R.D., M. Sanchez-Castillo, and J.A. Dumesic, *Conversion of biomass to 1,2-propanediol by selective catalytic hydrogenation of lactic acid over silica-supported copper.* Applied Catalysis B: Environmental, 2002. **39**: p. 353–359.
96. Dias, A.S., et al., *Acidic cesium salts of 12-tungstophosphoric acid as catalysts for the dehydration of xylose into furfural.* Carbohydrate Research 2006. **341**: p. 2946–2953.
97. Shi, X., et al., *Catalytic conversion of xylose to furfural over the solid acid SO_4^{2-}/ZrO_2–Al_2O_3/SBA-15 catalysts.* Carbohydrate Research 2011. **346**: p. 480–487.
98. Shi, X., et al., *Selective Preparation of Furfural from Xylose over Sulfonic Acid Functionalized Mesoporous Sba-15 Materials.* Energies 2011. **4**: p. 669-684.
99. Atsushi, T., et al., *Hydrolysis of Sugars Using Magnetic Silica Nanoparticles with Sulfonic Acid Groups* Chem. Lett., 2011. **40**(10): p. 1195 -1197.
100. Chermahini, A.N., et al., *Production of 5-hydroxymethylfurfural from fructose using spherically fibrous KCC-1 silica catalyst.* RSC Adv., 2016. **6**: p. 33804-33810.

101. Margolese, D., et al., *Direct Syntheses of Ordered SBA-15 Mesoporous Silica Containing Sulfonic Acid Groups.* Chem. Mater. , 2000. **12**: p. 2448-2459.
102. Wang, X., et al., *Preparation of ordered large pore SBA-15 silica functionalized with aminopropyl groups through one-pot synthesis.* Chem. Commun. , 2004: p. 2 7 6 2 – 2 7 6 3.
103. Stein, A., B.J. Melde, and R.C. Schroden, *Hybrid Inorganic-Organic Mesoporous Silicates-Nanoscopic Reactors Coming of Age.* Adv. Mater. , 2000. **12**(19): p. 1403-1419.
104. Yang, Q., et al., *Synthesis, characterization, and catalytic activity of sulfonic acid-functionalized periodic mesoporous organosilicas.* Journal of Catalysis 2004. **228**: p. 265–272.
105. Rhijn, W.M.V., et al., *Sulfonic acid functionalised ordered mesoporous materials as catalysts for condensation and esterification reactions.* Chem. Commun., 1998: p. 317-318.
106. Wilson, K., et al., *Structure and reactivity of sol–gel sulphonic acid silicas.* Applied Catalysis A: General, 2002. **228**: p. 127–133.
107. Hamoudi, S. and S. Kaliaguine, *Sulfonic acid-functionalized periodic mesoporous organosilica.* Microporous and Mesoporous Materials 2003. **59**: p. 195–204.
108. Hamoudi, S. and S. Kaliaguine, *Sulfonic acid-functionalized periodic mesoporous organosilica.* Microporous and Mesoporous Materials, 2003. **59**: p. 195–204.
109. Gill, C.S., B.A. Price, and C.W. Jones, *Sulfonic acid-functionalized silica-coated magnetic nanoparticle catalysts.* Journal of Catalysis 2007. **251**: p. 145–152.
110. Cano-Serrano, E., J.M. Campos-Martin, and J.L.G. Fierro, *Sulfonic acid-functionalized silica through quantitative oxidation of thiol groups.* CHEM. COMMUN., 2003: p. 246–247.
111. Morales, G., et al., *Efficient production of 5-ethoxymethylfurfural from fructose bysulfonic mesostructured silica using DMSO as co-solvent.* Catalysis Today, 2017. **279**(2,1): p. 305-316.
112. Agirrezabal-Telleria, I., et al., *Dehydration of d-xylose to furfural using selective and hydrothermally stable arenesulfonic SBA-15 catalysts.* Applied Catalysis B: Environmental, 2014. **145**: p. 34-42.
113. Agirrezabal-Telleria, I., et al., *Pore size tuning of functionalized SBA-15 catalysts for the selective production of furfural from xylose.* Applied Catalysis B: Environmental 2012. **115-116**: p. 169– 178.
114. Hua, D., et al., *Preparation of solid acid catalyst packing AAO/SBA-15-SO3H and application for dehydration of xylose to furfural.* Journal of Industrial and Engineering Chemistry 2013. **19**: p. 1395–1399.
115. Jackson, D.H.K., et al., *Amine Catalyzed Atomic Layer Deposition of (3-Mercaptopropyl)trimethoxysilane for the Production of Heterogenous Sulfonic Acid Catalysts.* Chem. Mater. , 2013. **25**(19): p. 3844–3851.
116. Upare, P.P., et al., *Chemical conversion of biomass-derived hexose sugars to levulinic acid over sulfonic acid-functionalized graphene oxide catalysts†.* Green Chem., 2013. **15**: p. 2935–2943.
117. Weingarten, R., et al., *Design of solid acid catalysts for aqueous-phase dehydration of carbohydrates: The role of Lewis and Brønsted acid sites.* Journal of Catalysis 2011. **279**: p. 174-182.
118. Hamoudi, S. and S. Kaliaguine, *Sulfonic acid-functionalized periodic mesoporous organosilica.* Microporous and Mesoporous Materials, 2003. **59**: p. 195–204.
119. Hua, W., Y. Yue, and Z. Gao, *Acidity enhancement of SBA mesoporous molecular sieve by modification with SO_4^{2-}/ZrO_2.* Journal of Molecular Catalysis A: Chemical 2001. **170**: p. 195–202.
120. Liu, J., et al., *Highly Water-Dispersible Biocompatible Magnetite Particles with Low Cytotoxicity Stabilized by Citrate Groups.* Angewandte Chemie International Edition, 2009. **48**(32): p. 5875-5879.
121. Lv, Q., et al., *Preparation of magnetic zeolite γ-Fe_2O_3/TS-1 with core/shell structure and application in photocatalytic degradation.* Microporous and Mesoporous Materials, 2015. **203**: p. 202–207.
122. Bhat, R.N. and R. Kumar, *Synthesis of zeolite beta using silica gel as a source of SiO2.* Journal of Chemical Technology & Biotechnology, 1990. **48**(4): p. 453-466.
123. Loiha, S., et al., *Synthesis of zeolite beta with pretreated rice husk silica and its transformation to ZSM-12.* Materials Chemistry and Physics, 2009. **115**(2-3): p. 637-640.
124. Gopal, S., K. Yoo, and P.G. Smirniotis, *Synthesis of Al-rich ZSM-12 using TEAOH as template.* Microporous and Mesoporous Materials, 2001. **49**(1-3): p. 149-156.
125. LaPierre, R.B., et al., *The framework topology of ZSM-12: A high-silica zeolite.* Zeolites, 1985. **5**(6): p. 346-348.

126. Pu, S.-B. and T. Inui, *Synthesis of 2,6-dimethylnaphthalene by methylation of methylnaphthalene on various medium and large-pore zeolite catalysts.* Applied Catalysis A: General, 1996. **146**(2): p. 305-316.
127. Li, J., et al., *Synthesis, characterization of Al-rich ZSM-12 zeolite and their catalytic performance in liquid-phase tert-butylation of phenol.* Catalysis Communications, 2014. **50**: p. 97-100.
128. Carvalho, K.T.G. and E.A. Urquieta-Gonzalez, *Microporous-mesoporous ZSM-12 zeolites: Synthesis by using a soft template and textural, acid and catalytic properties.* Catalysis Today, 2014. **243**: p. 92-102.
129. JP, L., v.d.G. WD, and H. RJ., *Conversion of furfuryl alcohol into ethyl levulinate using solid acid catalysts.* ChemSusChem, 2009. **2**(5): p. 43-441.
130. Chen, N.Y. and J.N. Miale, *Process for preparing organic fuels and chemicals from biomass*. 1987. p. Medium: X; Size: Pages: v.
131. *International Zeolite Association Database*. Available from: http://www.iza-online.org/.
132. Niwa, M., N. Katada, and K. Okumura, *Characterization and Design of Zeolite Catalysts: Solid Acidity, Shape Selectivity and Loading Properties*. Springer Series in Materials 2010, New York.
133. Boss, C.B. and K.J. Fredeen, *Concepts, Instrumentation and Techniques in Inductively Coupled Plasma Optical Emission Spectrometry*. Third Edition ed. 2004, USA: PerkinElmer Life and Analytical Sciences.
134. Hattori, H. and Y. Ono, *Solid Acid Catalysis, From Fundamentals to Applications*. 2015: Pan Stanford.
135. Corma, A., M.E. Domine, and S. Valencia, *Water-resistant solid Lewis acid catalysts: Meerwein–Ponndorf–Verley and Oppenauer reactions catalyzed by tin-beta zeolite.* Journal of Catalysis 2003. **215**: p. 294–304.
136. Vimont, A., F. Thibault-Starzyk, and J.C. Lavalley, *Infrared Spectroscopic Study of the Acidobasic Properties of Beta Zeolite.* J. Phys. Chem. B 2000. **104**(2): p. 286–291.
137. Lercher, J.A., et al., *Infra-red studies of the surface acidity of oxides and zeolites using adsorbed probe molecular.* Catalysis today, 1996. **27**(27): p. 353-376.
138. Skoog, D.A., F.J. Holler, and S.R. Crouch, *Principios de Análisis Instrumental*. 6ª ed, ed. C. Learning. 2008
139. Neyestanaki, A.K., et al., *Application of metal-exchanged zeolites in removal of emissions from combustion of biofuels.* Applied Catalysis A: General 2000. **196**: p. 233–246.
140. Voskoboinikov, T.V. and E.S. Shpiro, *IRIDIUM IN PENTASIL: REDOX BEHAVIOR AND REACTIVITY.* Stud. Surf. Sci. Catal., , 1997. **105**: p. 2027–2034.
141. Chalamala, B.R., Y. Wei, and R.H. Reuss, *Effect of growth conditions on surface morphology and photoelectric work function characteristics of iridium oxide thin films* Appl. Phys. Lett. , 1999. **74**: p. 1394–1396.
142. Willis, A.L., N.J. Turro, and S. O'Brien, *Spectroscopic Characterization of the Surface of Iron Oxide Nanocrystals.* Chem. Mater., 2005. **17**(24): p. 5970-5975.
143. Mills, P. and J.L. Sullivan, *A study of the core level electrons in iron and its three oxides by means of X-ray photoelectron spectroscopy.* Journal of Physics D: Applied Physics, 1983. **16**(5).
144. Yang, Z. and K. Yao, *Effects of several kinds of anisotropy on the coercivity behaviors of iron oxides* Journal of Applied Physics 73, 6665 (1993), 1993. **73**(10): p. 6665-6667.
145. Dar, M.I. and S.A. Shivashankar, *Single crystalline magnetite, maghemite, and hematite nanoparticles with rich coercivity.* RSC Advances, 2014. **4**(8): p. 4105 – 4113.
146. Yoshida, Y. and G. Langouche, *Mössbauer Spectroscopy*. 2013: Springer, Berlin, Heidelberg.
147. *Mössbauer Spectroscopy: Applications in chemistry, biology, and nanotechnology.*, ed. P.D. Virender K. Sharma, G. Klingelhöfer, and T. Nishida. 2013: John Wiley & Sons, Inc., Hoboken, New Jersey.
148. Tuček, J., R. Zboril, and D. Petridis, *Maghemite Nanoparticles by View of Mössbauer Spectroscopy.* Journal of Nanoscience and Nanotechnology, 2006. **6**(4): p. 926-947.
149. Bingfeng Chen, F.L. and G.Y. Zhijun Huang, *Hydrogen-transfer conversion of furfural into levulinate esters as potential biofuel feedstock.* Journal of Energy Chemistry, 2016. **25**(2): p. 888-894.
150. Zhu, S., et al., *One-pot conversion of furfural to alkyl levulinate over bifunctional Au-$H_4SiW_{12}O_{40}/ZrO_2$ without external H_2.* Green Chem., 2016. **18**(20): p. 5667-5675
151. Chen, B., et al., *Integrated Catalytic Process to Directly Convert Furfural to Levulinate Ester with High Selectivity.* ChemSusChem, 2014. **7**(1): p. 202-209.

152. Robinson, J., et al., *Microwave Pyrolysis of Biomass: Control of Process Parameters for High Pyrolysis Oil Yields and Enhanced Oil Quality.* Energy Fuels, 2015. **29**(3): p. 1701–1709.
153. Choi, M., et al., *High Catalytic Activity of Palladium(II)-Exchanged Mesoporous Sodalite and NaA Zeolite for Bulky Aryl Coupling Reactions: Reusability under Aerobic Conditions.* Angewandte Chemie International Edition, 2009. **48**(20): p. 3673-3676.
154. H.L.Tidahy, et al., *Influence of the exchanged cation in Pd/BEA and Pd/FAU zeolites for catalytic oxidation of VOCs.* Applied Catalysis B: Environmental, 2007. **70**(1-4): p. 377-383.
155. Djakovitch, L. and K. Koehler, *Heterogeneously catalysed Heck reaction using palladium modified zeolites.* Journal of Molecular Catalysis A: Chemical, 1999. **142**(2): p. 275-284.
156. Gelin, P., et al., *Catalytic properties of palladium exchanged ZSM-5 catalysts in the reduction of nitrogen monoxide by methane in the presence of oxygen. Nature of the active sites*. 1998: Elsevier Science Publishers, Amsterdam (Netherlands);. Medium: X; Size: pp. 275-284.
157. Mehdi, H., et al., *Integration of Homogeneous and Heterogeneous Catalytic Processes for a Multi-step Conversion of Biomass: From Sucrose to Levulinic Acid, γ-Valerolactone, 1,4-Pentanediol, 2-Methyl-tetrahydrofuran, and Alkanes.* Topics in Catalysis, 2008. **48**(1-4): p. 49–54.
158. Jumde, V.R., et al., *Domino Hydrogenation–Reductive Amination of Phenols, a Simple Process To Access Substituted Cyclohexylamines.* Org. Lett. , 2015. **17**(16): p. 3990-3993.
159. A.Cortez, N., et al., *Ruthenium(II) and rhodium(III) catalyzed asymmetric transfer hydrogenation (ATH) of acetophenone in isopropanol and in aqueous sodium formate using new chiral substituted aromatic monosulfonamide ligands derived from (1R,2R)-diaminocyclohexane.* Tetrahedron: Asymmetry, 2008. **19**(11): p. 1304-1309.
160. Zoran, A., Y. Sasson, and J. Blum, *Catalytic transfer hydrogenation of unsaturated compounds by solid sodium formate in the presence of palladium on carbon.* Journal of Molecular Catalysis, 1984. **26**(3): p. 321-326.
161. Pirez, C., et al., *Hydrothermal saline promoted grafting: a route to sulfonic acid SBA-15 silica with ultra-high acid site loading for biodiesel synthesis* Green Chem., 2014,16, , 2014. **16**: p. 4506-4509
162. Ebnesajjad, S., *Chapter 4 - Surface and Material Characterization Techniques*, in *Surface Treatment of Materials for Adhesive Bonding*, S. Ebnesajjad, Editor. 2014, William Andrew Publishing. p. 39-75.
163. Thommes, M., et al., *Physisorption of gases, with special reference to the evaluation of surface area and pore size distribution (IUPAC Technical Report).* Pure Appl. Chem. , 2015.
164. SING, K.S.W., et al., *REPORTING PHYSISORPTION DATA FOR GAS/SOLID SYSTEMS with Special Reference to the Determination of Surface Area and Porosity.* Pure & Appl. Chem., 1984. **57**(4): p. 603-619.
165. ALOthman, Z.A., *A Review: Fundamental Aspects of Silicate Mesoporous Materials.* Materials, 2012. **5**: p. 2874-2902.
166. Ribeiro, E.S., et al., *Princípios básicos de XAS e XPS.* Chemkeys, 2018. **2**: p. 1-23.
167. Jr, S.F., *Caracterización Química de Nanosuperficies. Introducción a la Espectroscopía Fotoelectrónica de Rayos X (XPS).* CENIM, 2010. **356**: p. 838-842.
168. Wang, Y., et al., *Intermolecular condensation of ethylenediamine to 1,4-diazabicyclo[2,2,2]octane over TS-1 catalysts.* Journal of Catalysis, 2009. **266**: p. 258–267.
169. Heikkilä, T., et al., *Mesoporous silica material TUD-1 as a drug delivery system.* International Journal of Pharmaceutics, 2007. **331**(1): p. 133-138.
170. Hamdy, M.S., et al., *TiO_2 Nanoparticles in Mesoporous TUD-1: Synthesis, Characterization and Photocatalytic Performance in Propane Oxidation.* Chem. Eur. J., 2006. **12**.
171. Li, H., et al., *Water-medium isomerization of homoallylic alcohol over a Ru(II) organometallic complex immobilized on FDU-12 support.* Green Chem., 2007. **9**: p. 500–505.
172. Ersen, O., et al., *3D-TEM characterization of nanometric objects.* Solid State Sciences, 2007. **9**: p. 1088-1098.
173. Ersen, O., et al., *Direct Observation of Stacking Faults and Pore Connections in Ordered Cage-Type Mesoporous Silica FDU-12 by Electron Tomography.* J. AM. CHEM. SOC., 2008. **130**: p. 16800–16806.
174. Dodd, B.M., H.V. Tafreshi, and G.C. Tepper, *Flow-enhanced kinetics of uranyl (UO2) transport into nano-porous silica gel.* Materials and Design, 2016. **106**: p. 330–335.

175. Qureshi, Z.S., et al., *Gold Nanoparticles Supported on Fibrous Silica Nanospheres (KCC-1) as Efficient Heterogeneous Catalysts for CO Oxidation.* ChemCatChem 2016. **8**: p. 1671 –1678.
176. Bouhrara, M., et al., *Nitridated Fibrous Silica (KCC-1) as a Sustainable Solid Base Nanocatalyst.* ACS Sustainable Chem. Eng. , 2013. **1**: p. 1192−1199.
177. Pauwels, B., et al., *Structure Determination of Spherical MCM-41 Particles.* Adv. Mater., 2001. **13**(17): p. 1317-1320.
178. Szegedi, Á., et al., *Spherical mesoporous MCM-41 materials containing transition metals: synthesis and characterization.* Applied Catalysis A: General 2004. **272**: p. 257–266.
179. Mathew, A., et al., *Hydrophobically modified spherical MCM-41 as nanovalve system for controlled drug delivery.* Microporous and Mesoporous Materials 2014. **200**: p. 124–131.
180. Martins, A.R., et al., *Highly ordered spherical SBA-15 catalysts for the removal of contaminants from the oil industry.* Chemical Engineering Journal, 2017. **318**: p. 189-196.
181. Zhao, D., et al., *Morphological Control of Highly Ordered Mesoporous Silica SBA-15.* Chem. Mater. , 2000. **12**: p. 275-279.
182. Ramanan, H. and E.K.u.M. Tsapatsis, *On the TEM and AFM Evidence of Zeosil Nanoslabs Present during the Synthesis of Silicalite-1.* Angew. Chem. , 2004. **116**: p. 4658 –4661.
183. Bonilla, G., et al., *Zeolite (MFI) Crystal Morphology Control Using Organic Structure-Directing Agents.* Chem. Mater. , 2004. **16**: p. 5697-5705.
184. Costa, C.A.R., C.A.P. Leite, and F. Galembeck, *ESI-TEM Imaging of Surfactants and Ions Sorbed in Stober Silica Nanoparticles.* Langmuir 2006. **22**: p. 7159-7166.
185. Ibrahim, I.A.M., A.A.F. Zikry, and M.A. Sharaf, *Preparation of spherical silica nanoparticles: Stober silica.* Journal of American Science, 2010. **6**(11): p. 985-989.
186. Kabalan, I., et al., *Synthesis of purely silica MFI-type nanosheets for molecular decontamination.* RSC Adv., 2014. **4**: p. 37353–37358.
187. Rigo, R.T., M.T. Rodriguez, and S.B.C. Pergher, *Synthesis Of Nano-Crystalline Silicalite Zeolite.* Erechim. . **38**(143): p. 81-87.
188. *Introduction to Energy Dispersive X -ray Spectrometry (EDS)*. Available from: https://cfamm.ucr.edu/documents/eds-intro.pdf.
189. Liu, J., et al., *Highly Water-Dispersible Biocompatible Magnetite Particles with Low Cytotoxicity Stabilized by Citrate Groups.* Angew. Chem. Int. Ed, 2009. **48**: p. 5875-5879.
190. M.A.CamblorJ and Pérez-Pariente, *Crystallization of zeolite beta: Effect of Na and K ions.* Zeolites, 1991. **11**(3): p. 202-2010.
191. Rietveld, H.M., *A profile refinement method for nuclear and magnetic structures.* Journal of Applied Crystallography, 1969. **2**(2): p. 65-71.
192. Toby, B.H., *EXPGUI, a graphical user interface for GSAS.* Journal of Applied Crystallograph, 2001. **34**: p. 210-213.
193. Naumkin, A., et al., *NIST X-ray Photoelectron Spectroscopy Database*.
194. B.C.Lippens and J.H.d. Boer, *Studies on pore systems in catalysts: V. The t method.* Journal of Catalysis, 1985. **4**(3): p. 319-323.
195. Yu, K., et al., *Synthesis of fibrous monodisperse core–shell Fe3O4/SiO2/KCC-1.* Materials Letters, 2013. **106**: p. 151-154.
196. Grün, M., et al., *Novel pathways for the preparation of mesoporous MCM-41 materials: control of porosity and morphology.* Microporous and Mesoporous Materials, 1999. **27**(2-3): p. 207-216.
197. Kruk, M. and C. MingHui, *Synthesis and characterization of large-pore FDU-12 silica.* Microporous and Mesoporous Materials, 2008. **14**(1-3): p. 64-73.
198. Wang, X.-D., et al., *Preparation of spherical silica particles by Stöber process with high concentration of tetra-ethyl-orthosilicate.* Journal of Colloid and Interface Science, 2010. **341**(1): p. 23-29.
199. Zhou, M., A.A. Rownaghi, and J. Hedlund, *Synthesis of mesoporous ZSM-5 zeolite crystals by conventional hydrothermal treatment* RSC Adv., 2013. **3**: p. 15596-15599
200. Zhao, D., et al., *Nonionic Triblock and Star Diblock Copolymer and Oligomeric Surfactant Syntheses of Highly Ordered, Hydrothermally Stable, Mesoporous Silica Structures.* J. Am. Chem. Soc., 1998. **124**(24): p. 6024–6036.
201. Zandvoort, I.v., *Towards the Valorization of Humin By-products: Characterization, Solubilization and Catalysis*. 2015, Universiteit Utrecht.

Appendices

6. Appendices

Appendix 1: Selected chromatograms of standards and reactions

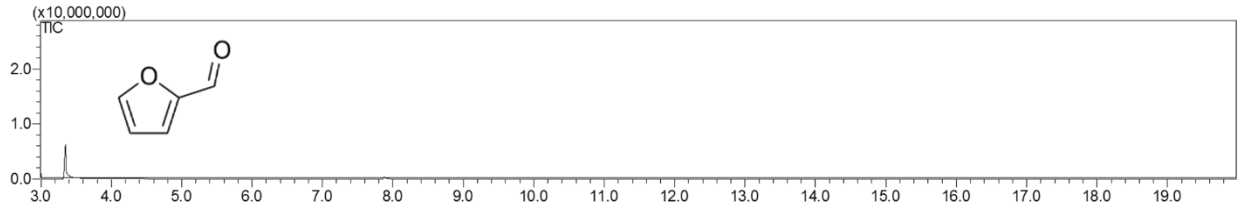

FIGURE A1- GC-MS chromatogram of the furfural standard.

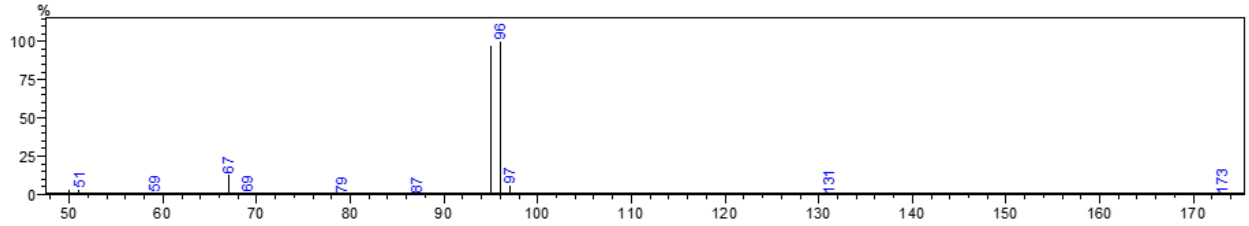

FIGURE A2- GC-MS of peak of the furfural standard.

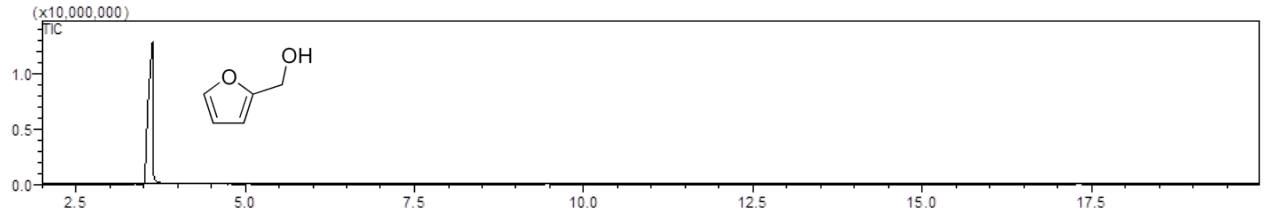

FIGURE A3- GC-MS chromatogram of the furfuryl alcohol standard.

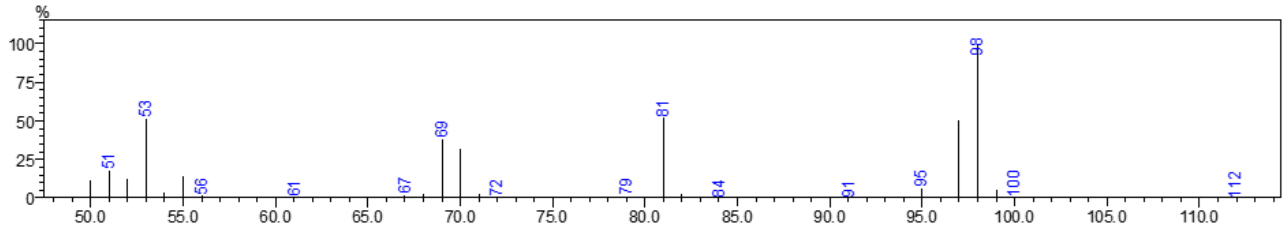

FIGURE A4- GC-MS of peak of the furfuryl alcohol standard.

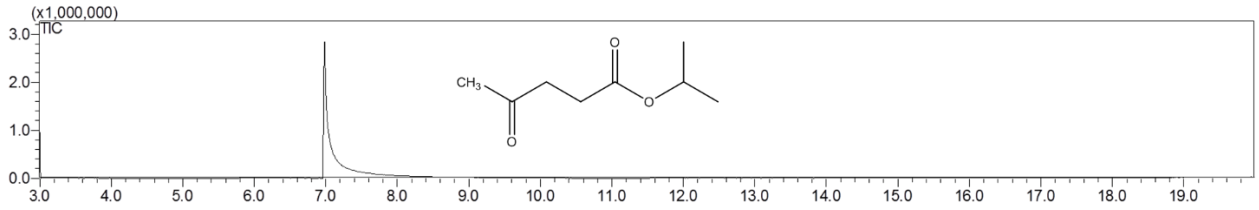

FIGURE A5- GC-MS chromatogram of the isopropyl levulinate standard.

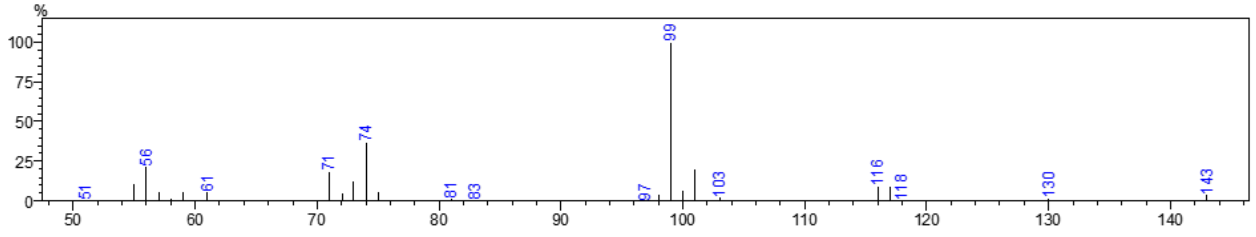

FIGURE A6- GC-MS of peak of the isopropyl levulinate standard.

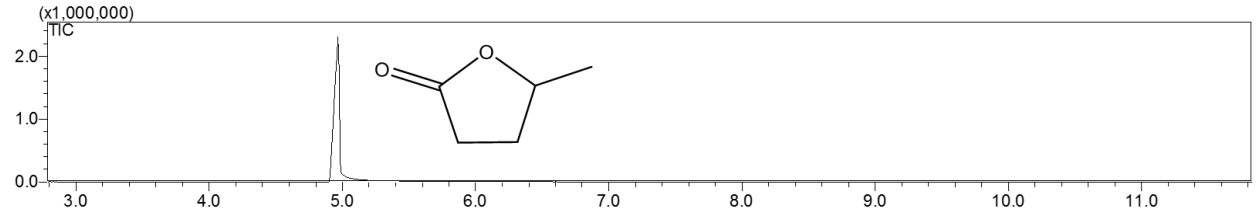

FIGURE A7- GC-MS chromatogram of valerolactone standard.

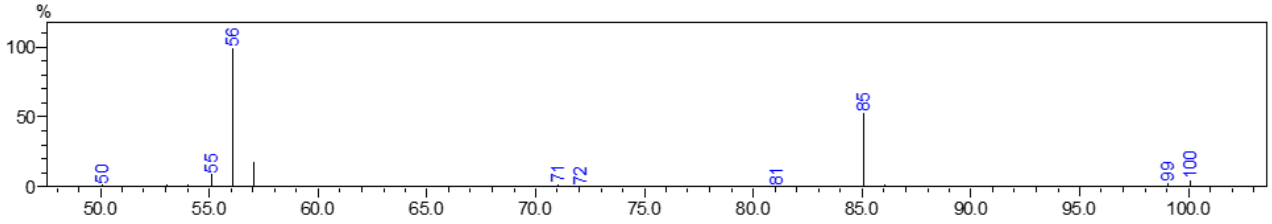

FIGURE A8- GC-MS of peak of the valerolactone standard.

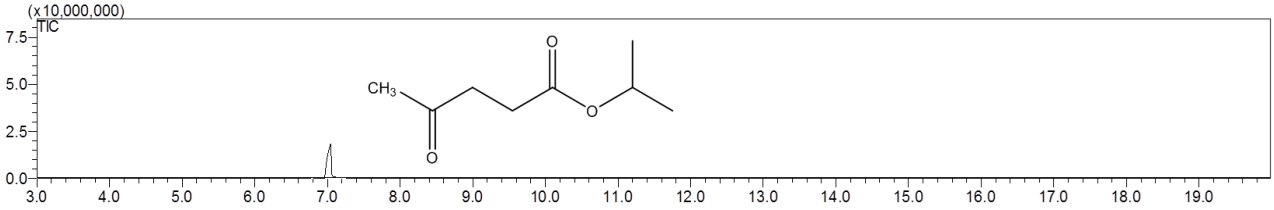

FIGURE A9- GC-MS chromatogram of the reaction of valorization of furfural using a magnetically recoverable Pd-exchanged β zeolite catalyst in optimized conditions.

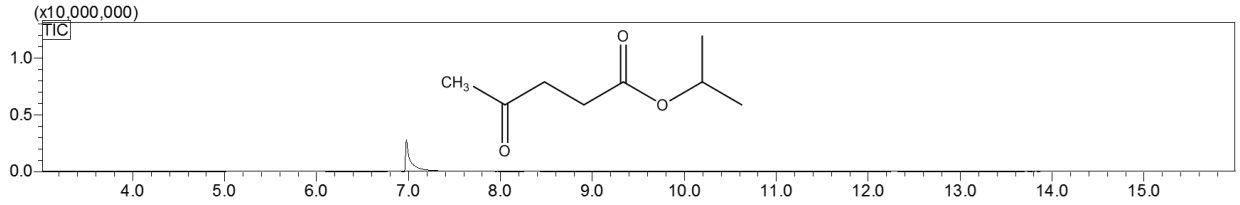

FIGURE A10- GC-MS chromatogram of the reaction of valorization of furfuryl alcohol using a magnetically recoverable Pd-exchanged β zeolite catalyst in optimized conditions.

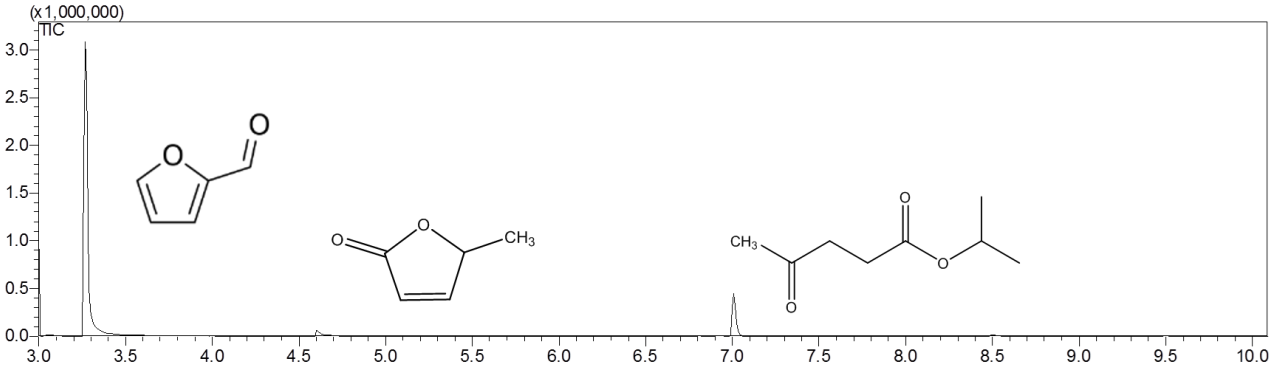

FIGURE A11- GC-MS chromatogram of the reaction of valorization of furfural using a magnetically recoverable Pd-exchanged β zeolite catalyst in optimized conditions to 3 h of reaction.

TABLE A1 - Data extracted from GC-MS chromatogram of the reaction of valorization of furfural using a magnetically recoverable Pd-exchanged β zeolite catalyst in optimized conditions to 3 h of reaction.

Peak #	Initial time	End time	Ret. time	Peak Area	% Area
1	3.24	3.61	3.27	5132857	87.22
2	4.58	4.68	4.60	115546	1.96
3	6.98	7.07	7.01	636493	1082

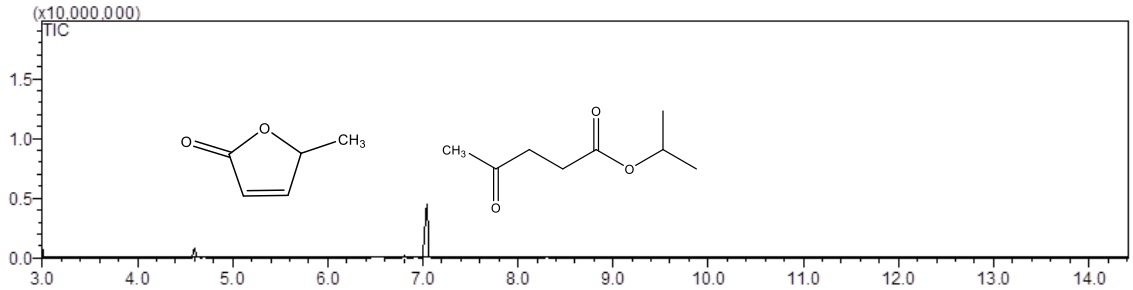

FIGURE A12- GC-MS chromatogram of the reaction of valorization of furfural alcohol using a magnetically recoverable Pd-exchanged β zeolite catalyst in optimized conditions to 15 h of reaction

TABLE A2 - Data extracted from GC-MS chromatogram of the reaction of valorization of furfural using a magnetically recoverable Pd-exchanged β zeolite catalyst in optimized conditions to 3 h of reaction.

Peak #	Initial time	End time	Ret. time	Peak Area	% Area
1	4.53	4.65	4.60	1288500	11.67
2	6.97	7.11	7.04	9748910	88.33

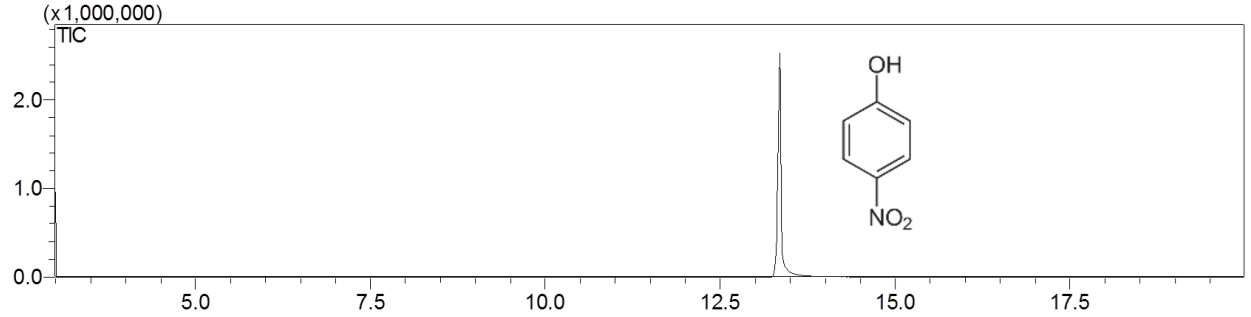

FIGURE A13- GC-MS chromatogram of the para-nitrophenol internal standard.

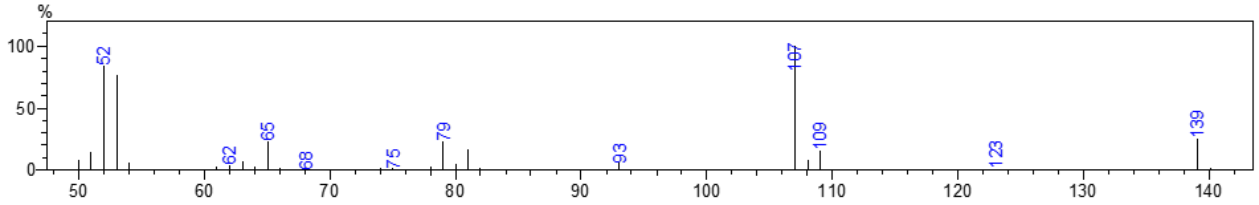

FIGURE A14- GC-MS of peak of the para-nitrophenol internal standard.

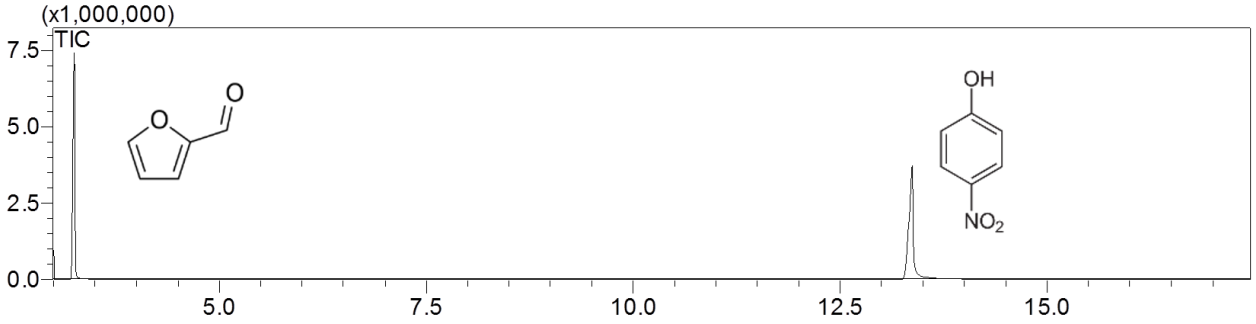

FIGURE A15- GC-MS chromatogram of the para-nitrophenol internal standard in the presence of furfural standard.

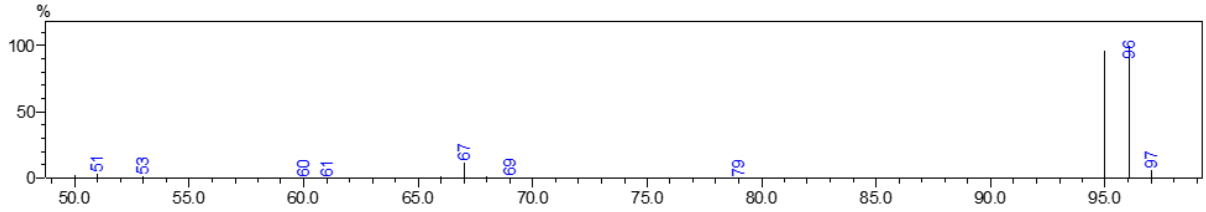

FIGURE A16- GC-MS of peak #1 of the GC-MS chromatogram of the para-nitrophenol internal standard in the presence of Furfural standard.

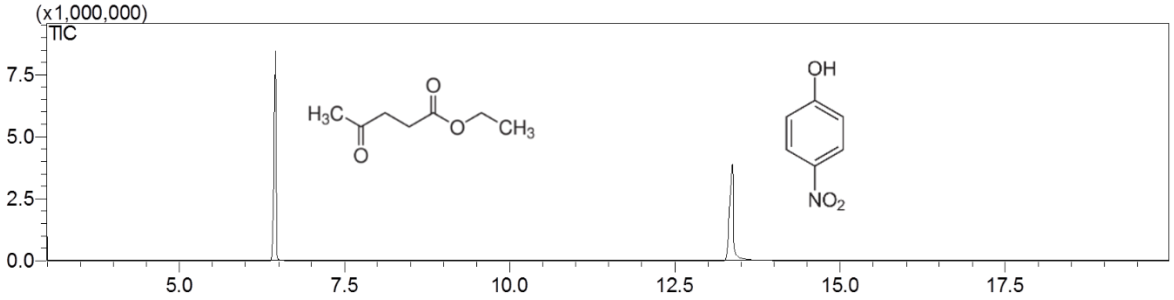

FIGURE A17- GC-MS chromatogram of the para-nitrophenol internal standard in the presence of ethyl levulinate standard.

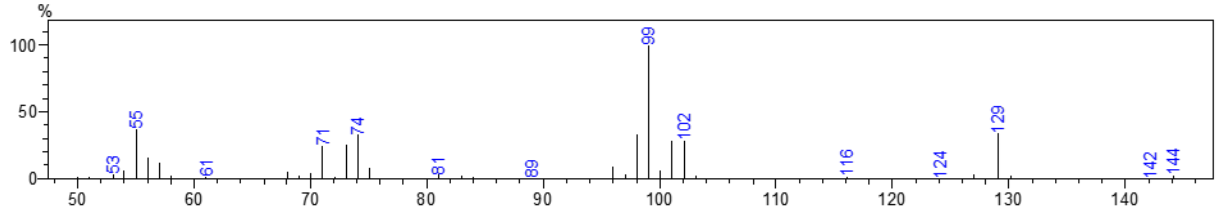

FIGURE A18- GC-MS of peak #1 of the GC-MS chromatogram of the para-nitrophenol internal standard in the presence of ethyl levulinate standard.

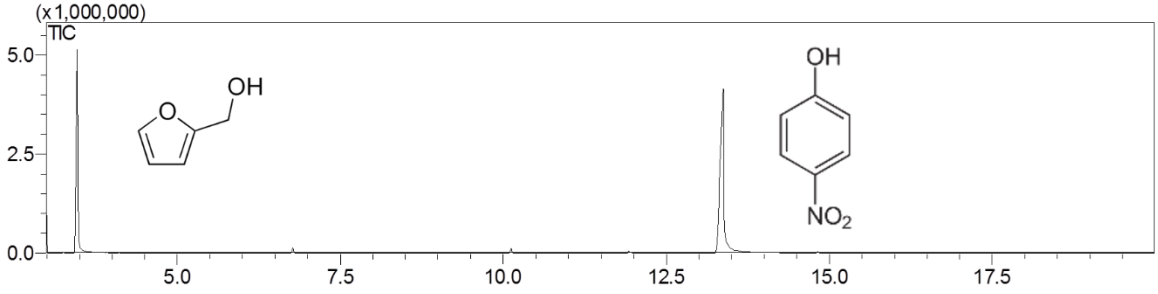

FIGURE A19- GC-MS chromatogram of the para-nitrophenol internal standard in the presence of furfuryl alcohol standard.

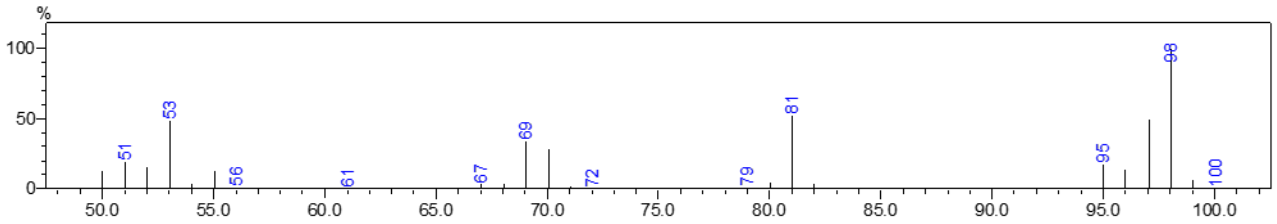

FIGURE A20- GC-MS of peak #1 of the GC-MS cromatogram of the para-nitrophenol internal standard in the presence of furfuryl alcohol standard.

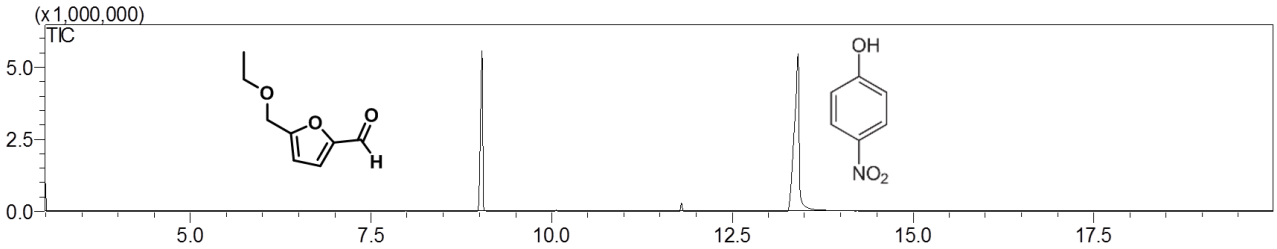

FIGURE A21- GC-MS chromatogram of the para-nitrophenol internal standard in the presence of 5-(ethoxymethyl)furan-2-carbaldehyde standard.

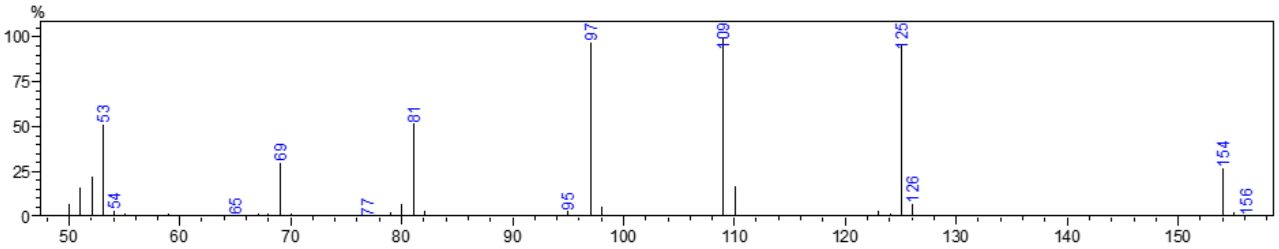

FIGURE A22- GC-MS of peak #1 of the GC-MS chromatogram of the para-nitrophenol internal standard in the presence of 5-(ethoxymethyl)furan-2-carbaldehyde standard.

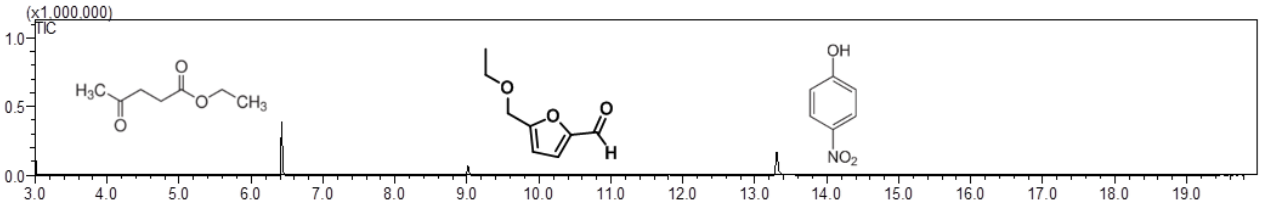

FIGURE A23- GC-MS chromatogram of the reaction of valorization of fructose using sulfonic acid-functionalized dendritic mesoporous silica catalyst (DMSi-SA) in optimized conditions.

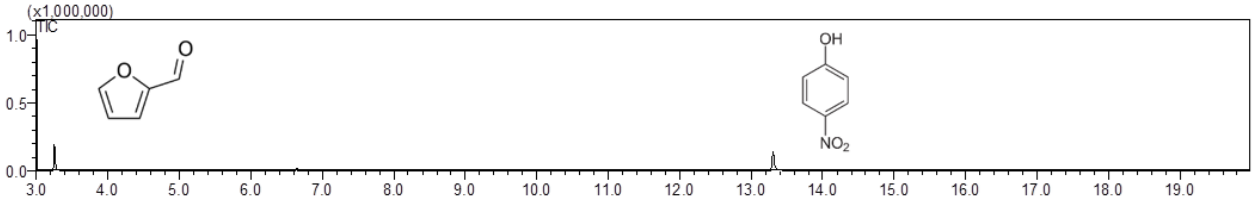

FIGURE A24- GC-MS chromatogram of the reaction of valorization of xylose using sulfonic acid-functionalized dendritic mesoporous silica catalyst (DMSi-SA) in optimized conditions.

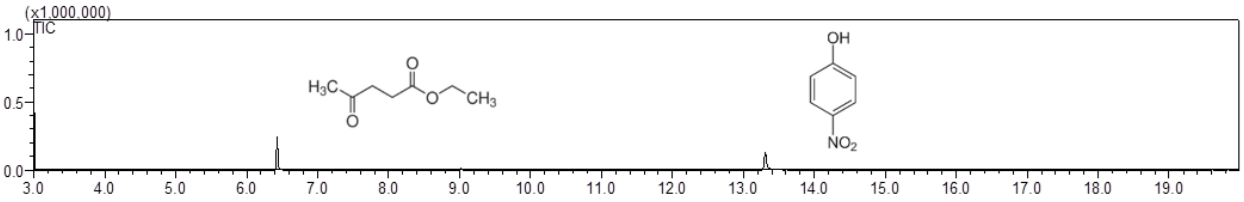

FIGURE A25- GC-MS chromatogram of the reaction of valorization of glucose using sulfonic acid-functionalized dendritic mesoporous silica catalyst (DMSi-SA) in optimized conditions.

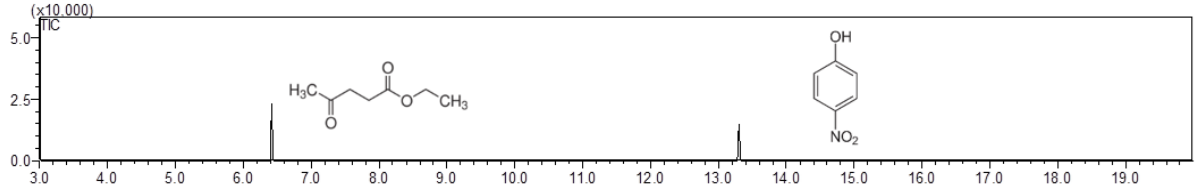

FIGURE A26- GC-MS chromatogram of the reaction of valorization of saccharose using sulfonic acid-functionalized dendritic mesoporous silica catalyst (DMSi-SA) in the best conditions tested.

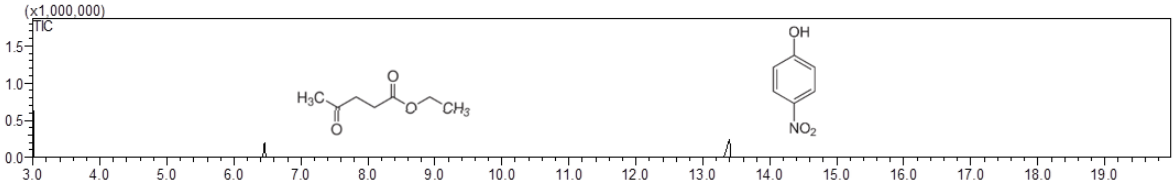

FIGURE A27- GC-MS chromatogram of the reaction of valorization of cellulose using sulfonic acid-functionalized dendritic mesoporous silica catalyst (DMSi-SA) in the best conditions tested.

Appendix 2: Calibration curve

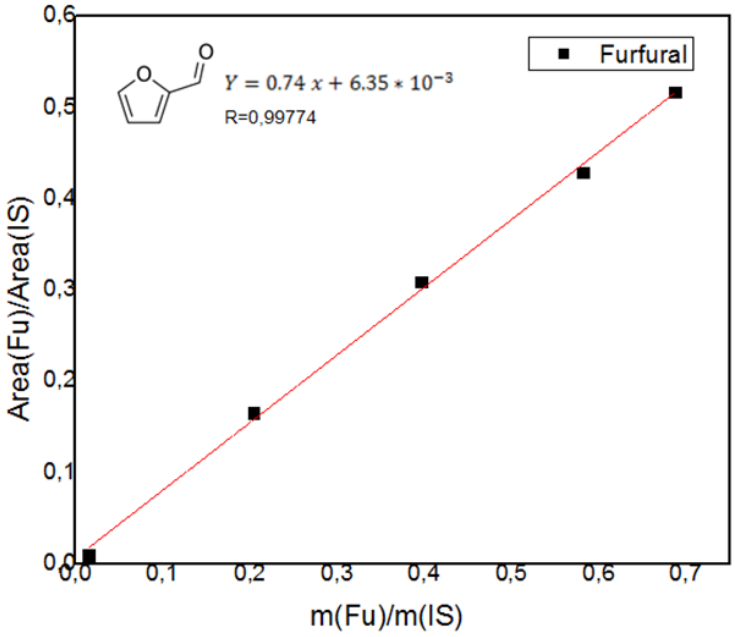

FIGURE A26- Calibration curve of furfural in presence of the para-nitrophenol internal standard (IS).

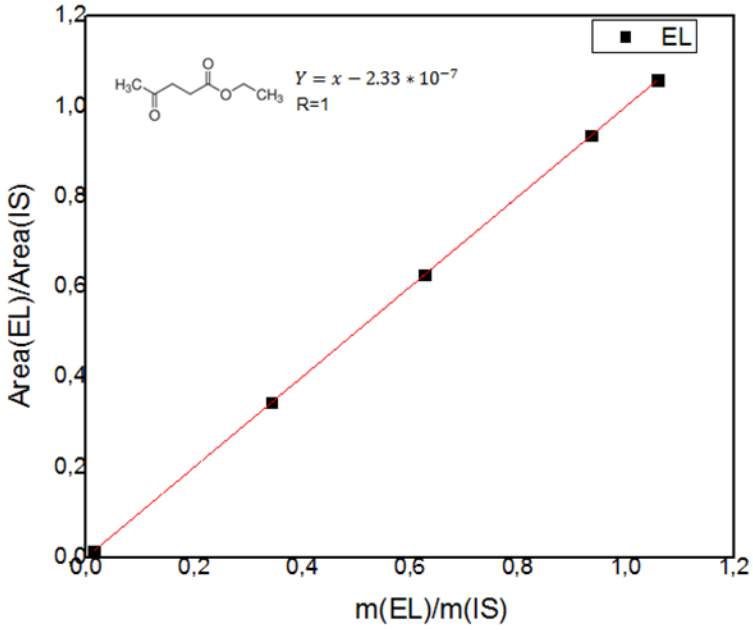

FIGURE A27- Calibration curve of ethyl levulinate (EL) in presence of the para-nitrophenol internal standard.

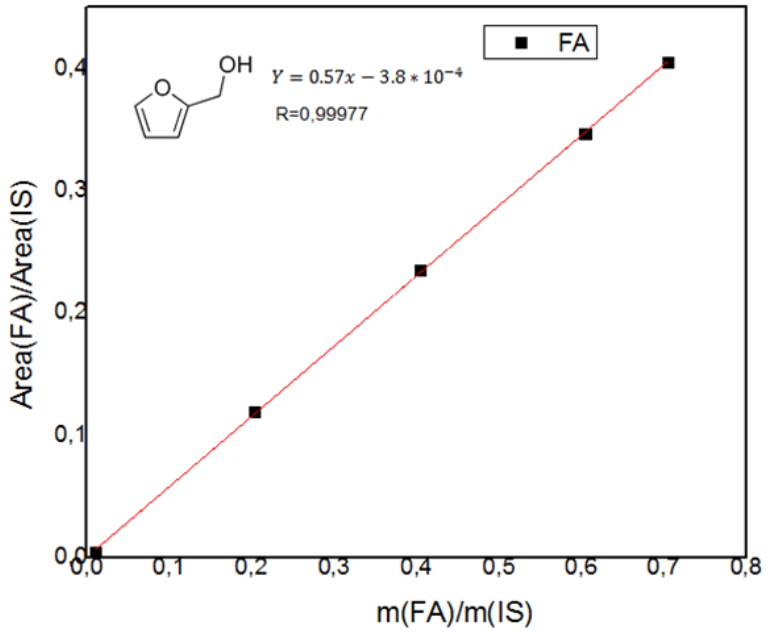

FIGURE A28- Calibration curve of furfuryl alcohol(FA) in presence of the para-nitrophenol internal standard.

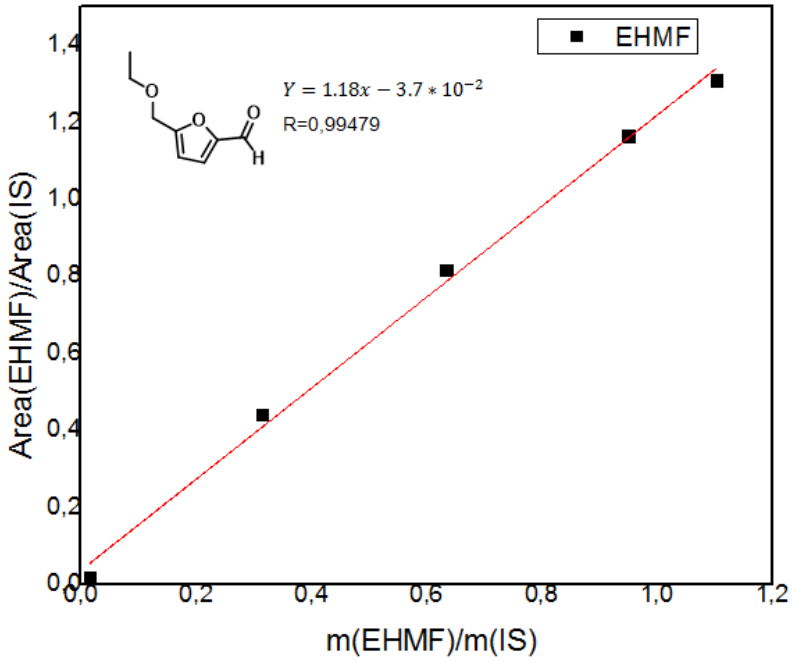

FIGURE A29- Calibration curve of 5-(ethoxymethyl)furan-2-carbaldehyde (EHMF) in presence of the para-nitrophenol internal standard.

Appendix 3: Characterization of silica

DRX

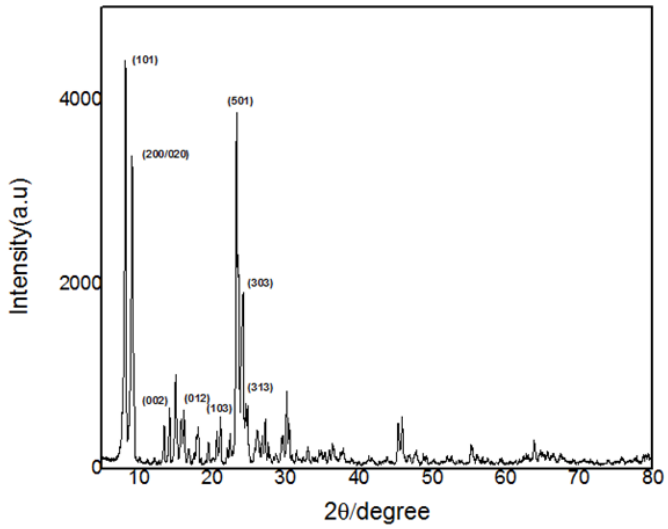

FIGURE A30- DRX patterns of calcined silicate.

HR-TEM and EDS

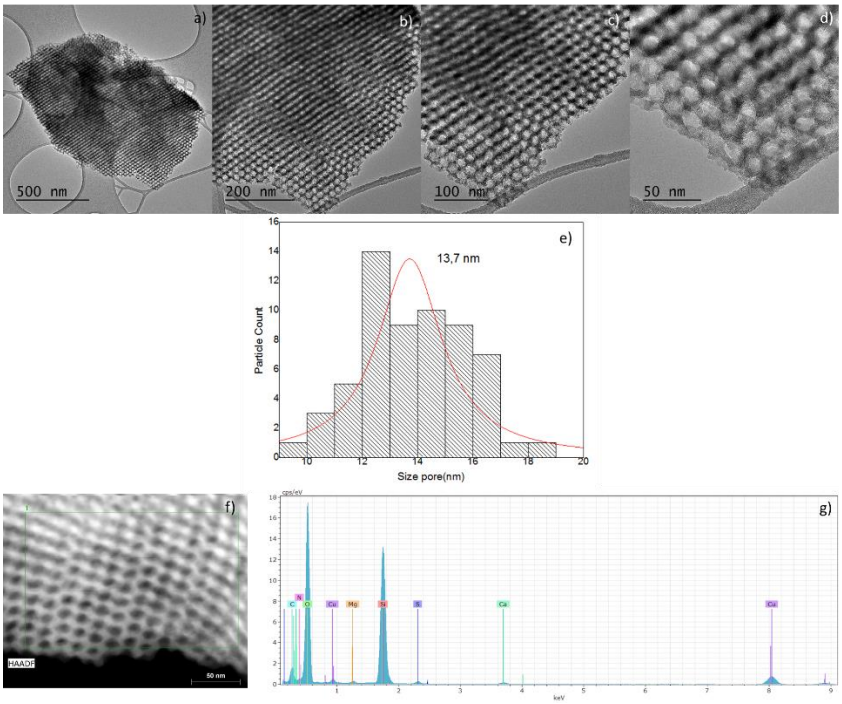

FIGURE A31- a), b), c), d) and f) HR-TEM images of MCM-41-SA catalyst, e) pore size distribution analysis of particle of Figure c) and g) EDS spectrum of MCM-41-SA catalyst. Scale bar: a) 500 nm, b) 200 nm, c) 100 nm, d) 50 nm and f) 50 nm

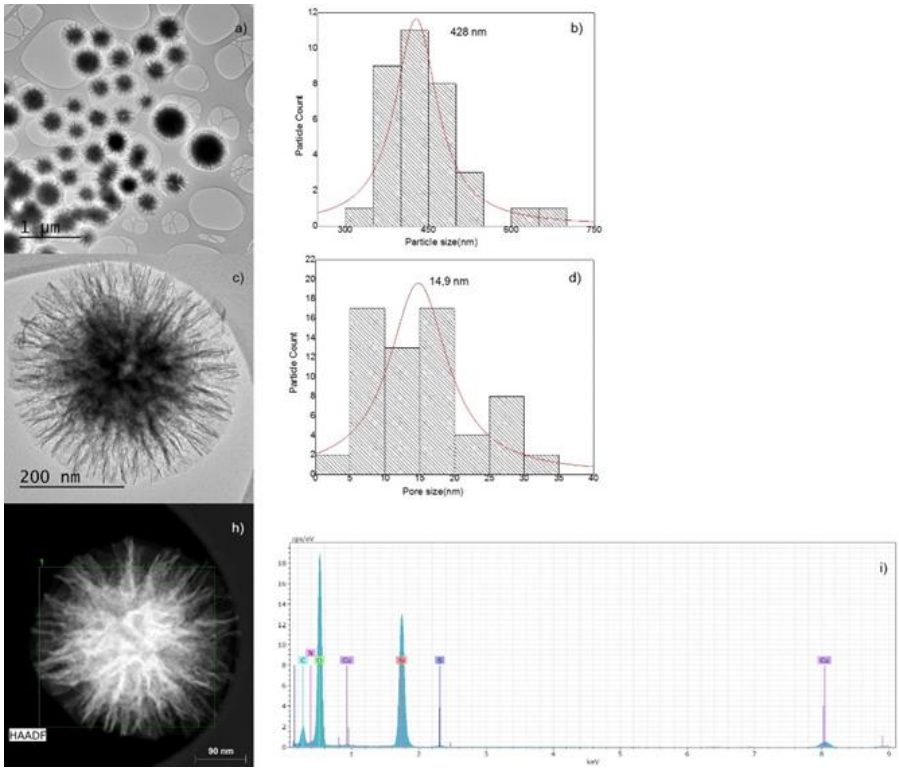

FIGURE A32- a), c) and h) HR-TEM images of KCC-SA catalyst, b) particle size distribution analysis from particle of Figure a), d) pore size distribution analysis of particle of Figure c) and i) EDS spectrum of MCM-41-SA catalyst. Scale bar: a) 1µm, c) 200 nm and d) 90 nm

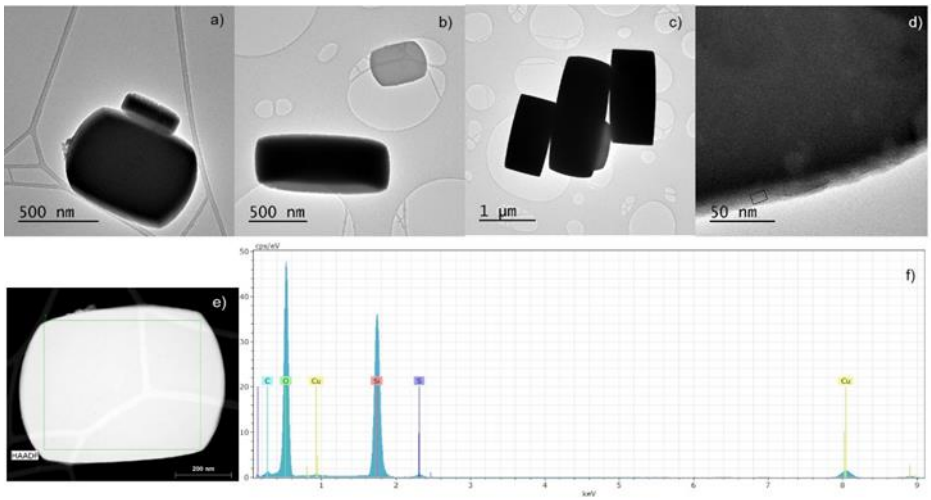

FIGURE A33- a), b), c), d) and e) HR-TEM images of silicate-SA catalyst, f) EDS spectrum of silicate-SA catalyst. Scale bar: a) 500 nm, b) 500 nm, c) 1µm, d) 50 nm and e) 200 nm

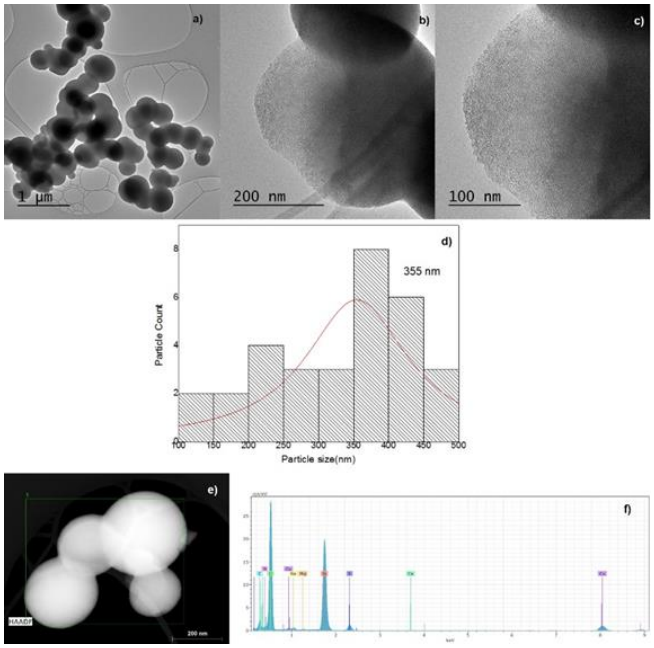

FIGURE A34- a), b), c) and e) HR-TEM images of flash-SA catalyst, d) particle size distribution analysis from particle of Figure a) and f) EDS spectrum of flash-SA catalyst. Scale bar: a) 1µm, b) 200 nm, c) 100 nm and d) 200 nm

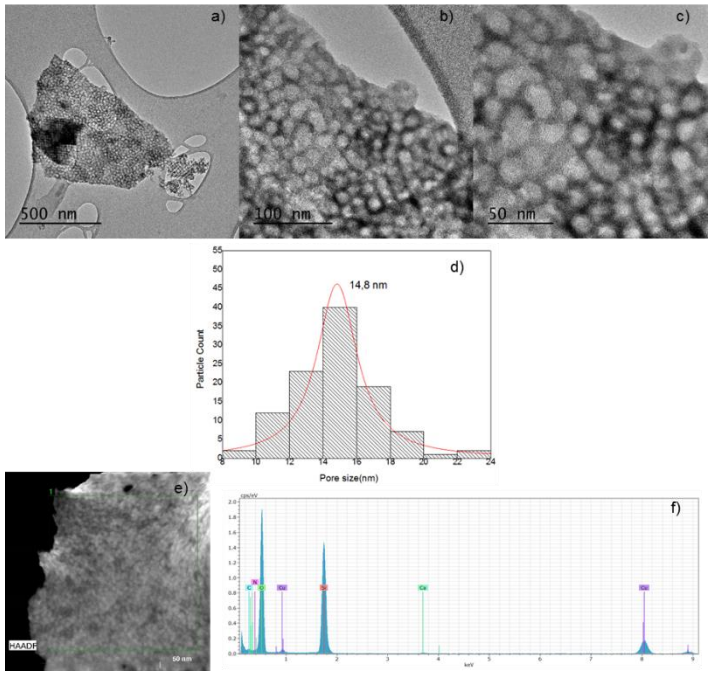

FIGURE A35- a), b), c) and e) HR-TEM images of FDU-12-SA catalyst, d) pore size distribution analysis of particle of Figure a) and f) EDS spectrum of FDU-12-SA catalyst. Scale bar: a) 500 nm, b) 50 nm, e) 50 nm

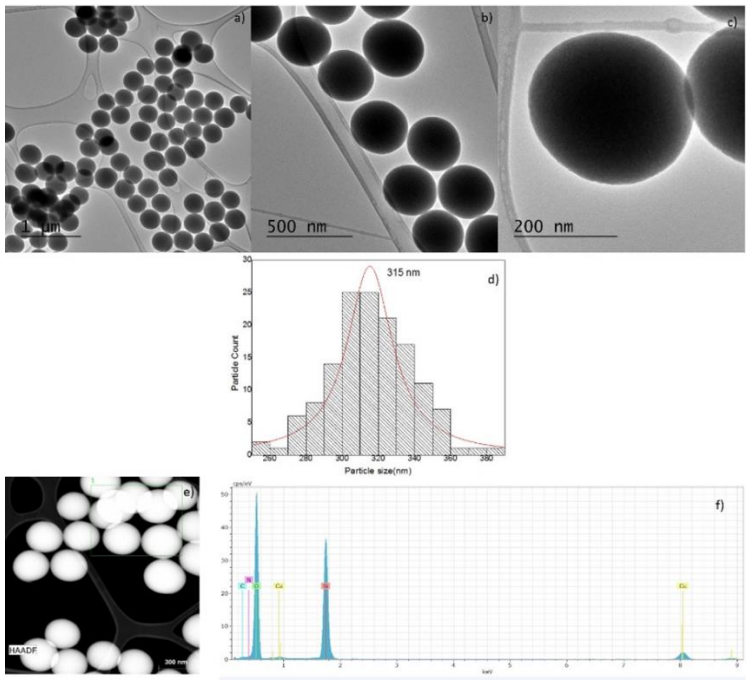

FIGURE A36- a), b), c) and e) HR-TEM images of Stöber-SA catalyst, h) particle size distribution analysis of FIGURE a), f) EDS spectrum of Stöber-SA catalyst. Scale bar: a) 1 µm, b) 500 nm, c) 200 nm and e) 300 nm

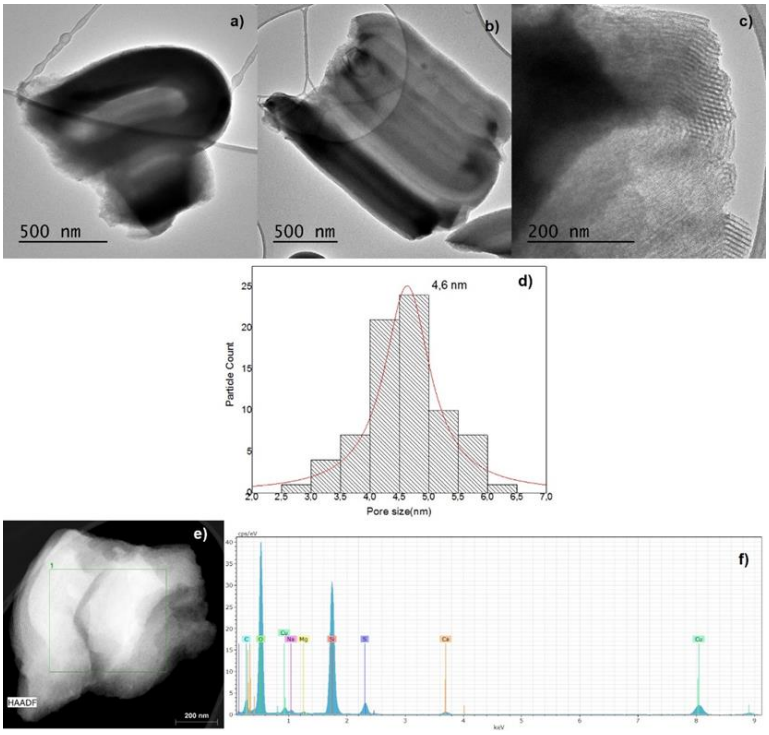

FIGURE A37. a), b), c) and e) HR-TEM images of SBA-15-SA catalyst, d) pore size distribution analysis of FIGURE a), f) EDS spectrum of SBA-15-SA catalyst. Scale bar: a) 500 nm, b) 500 nm, c) 200 nm and e) 200 nm

Chemical mapping

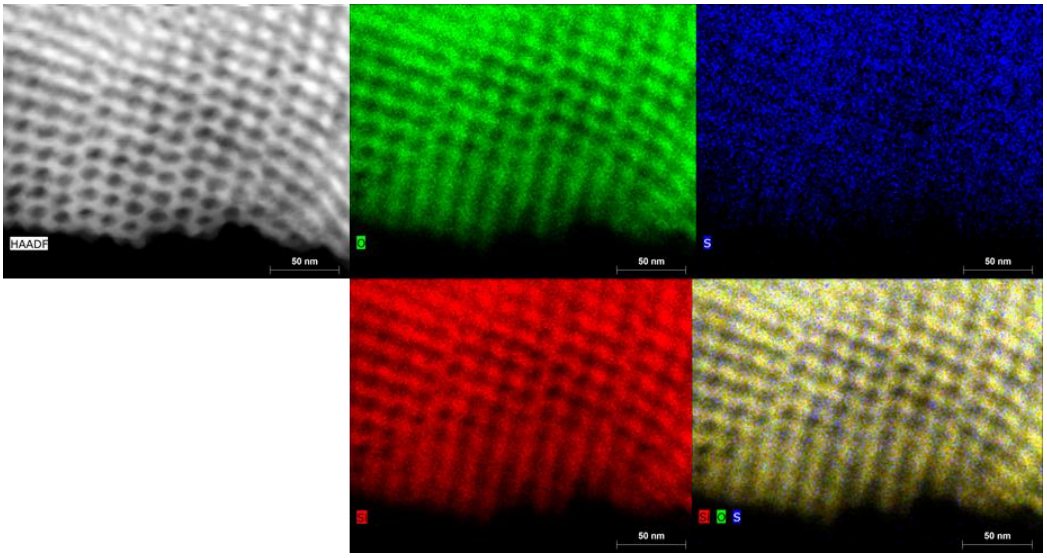

FIGURE A38- Chemical mapping of the MCM-41-SA catalyst.

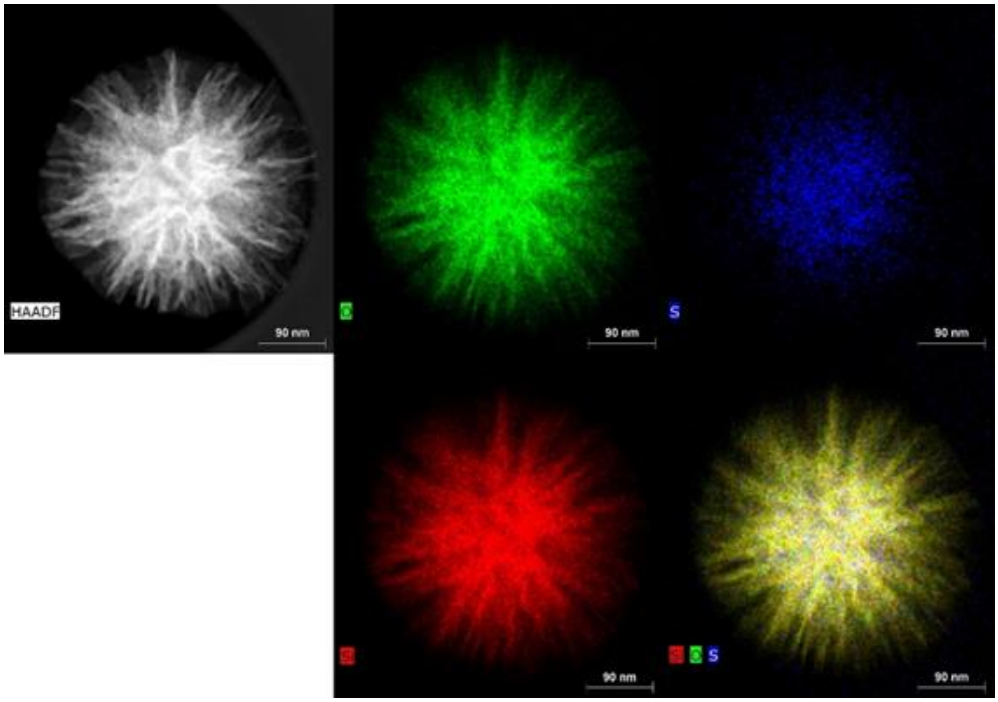

FIGURE A39- Chemical mapping of the KCC-SA catalyst.

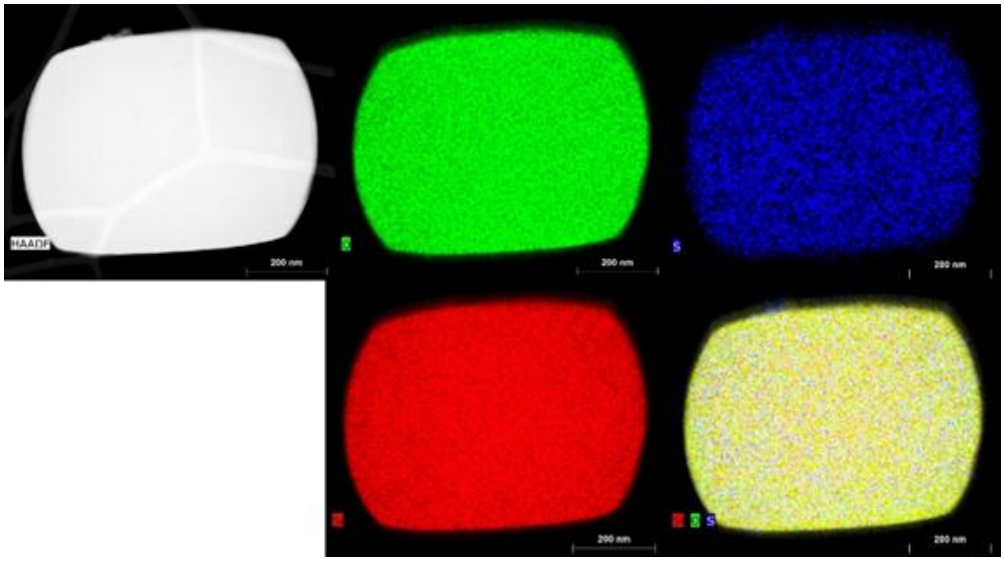

FIGURE A40- Chemical mapping of the silicate-SA catalyst.

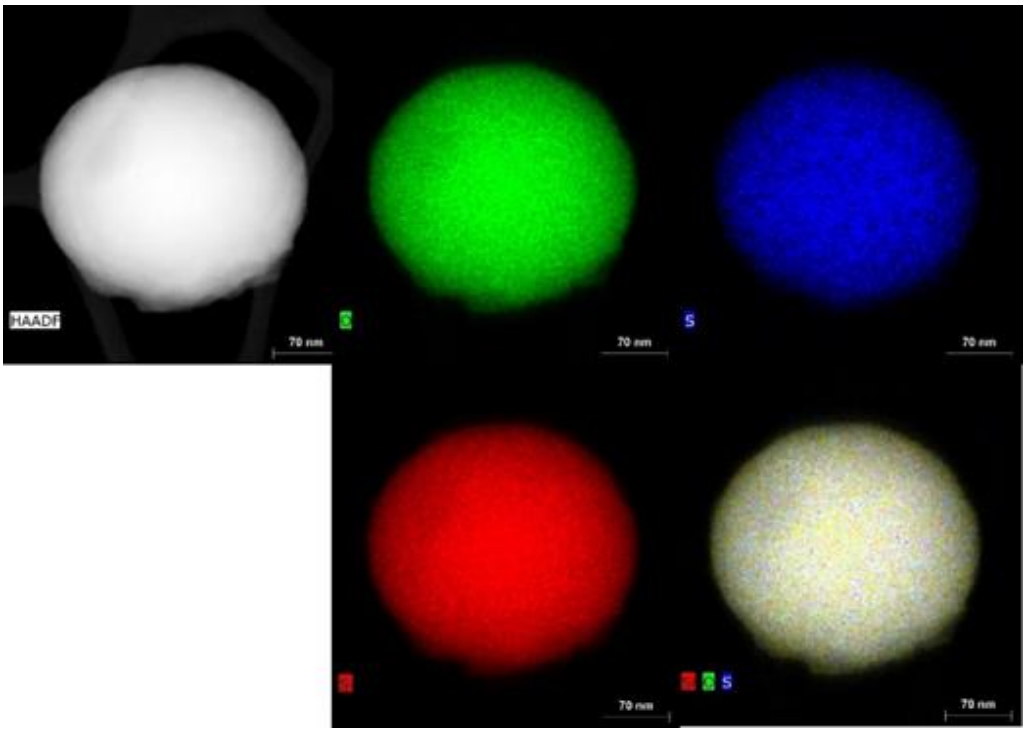

FIGURE A41- Chemical mapping of the Flash-SA catalyst.

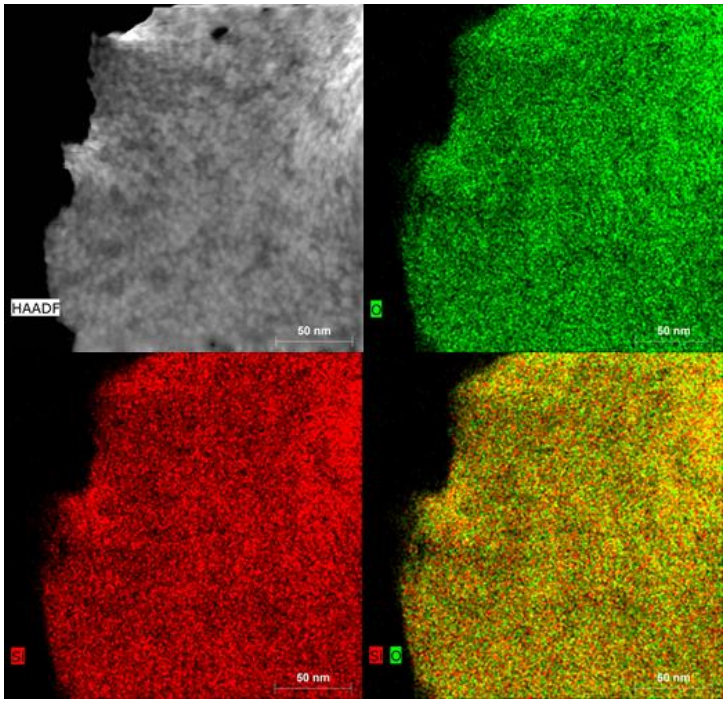

FIGURE A42- Chemical mapping of the FDU-12-SA catalyst.

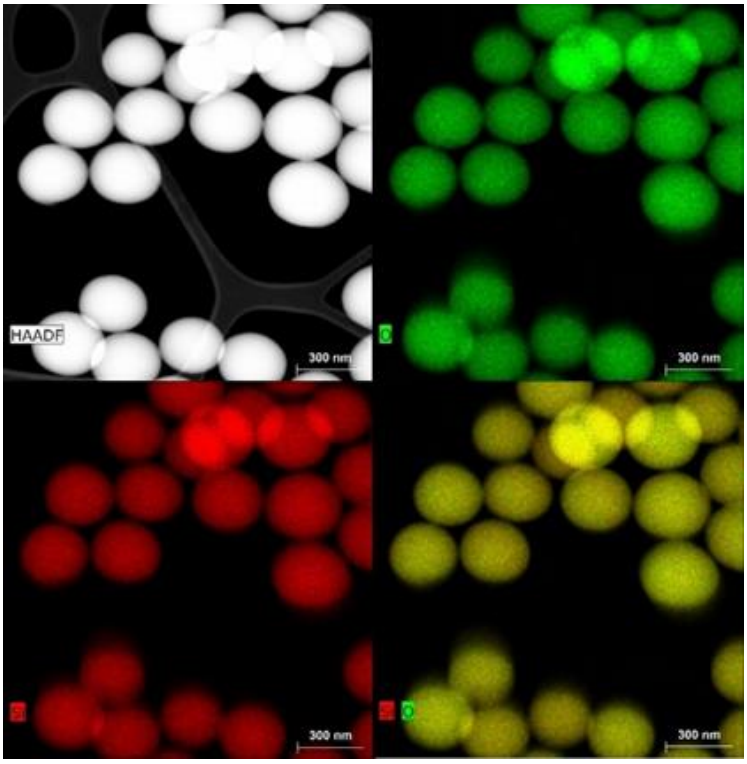

FIGURE A43- Chemical mapping of the Stöber-SA catalyst.

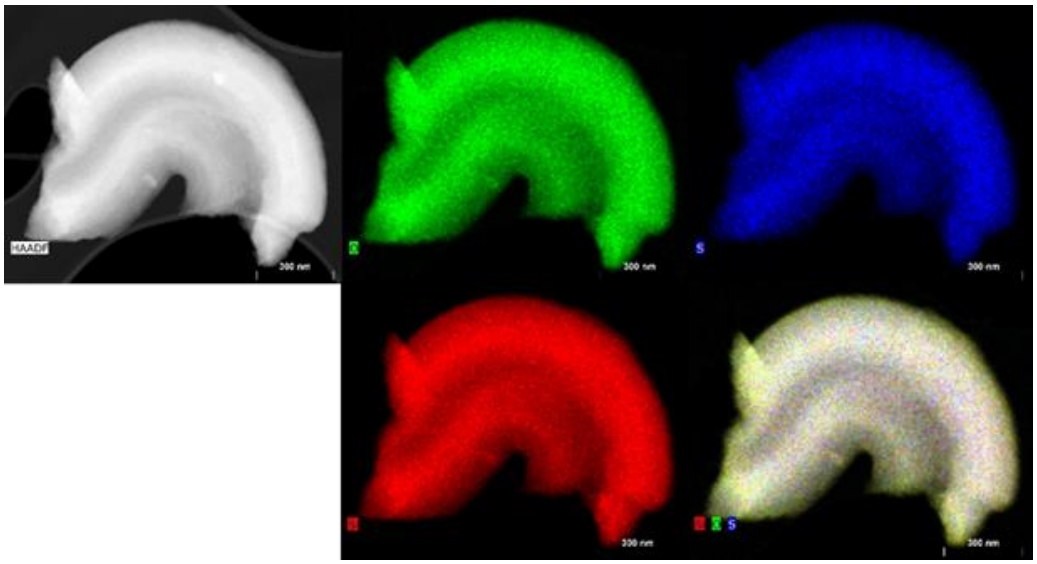

FIGURE A44- Chemical mapping of the SBA-SA catalyst.

Nitrogen adsorption/desorption isotherms

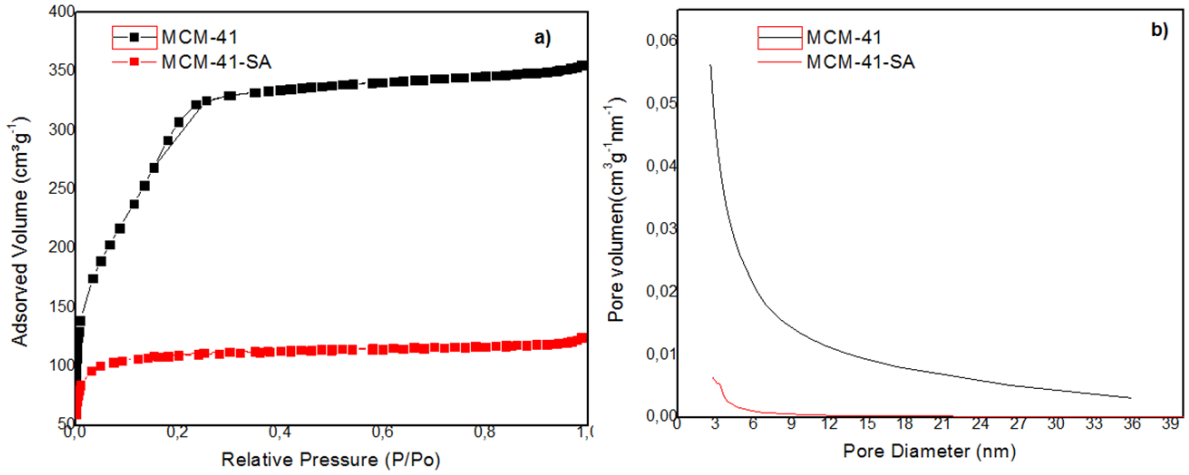

FIGURE A45- Textural characterization of MCM-41 support (black line) and MCM-41 functionalized with sulfuric acid (red line) (a) isotherms of adsorption / desorption of N_2 and (b) pore distribution.

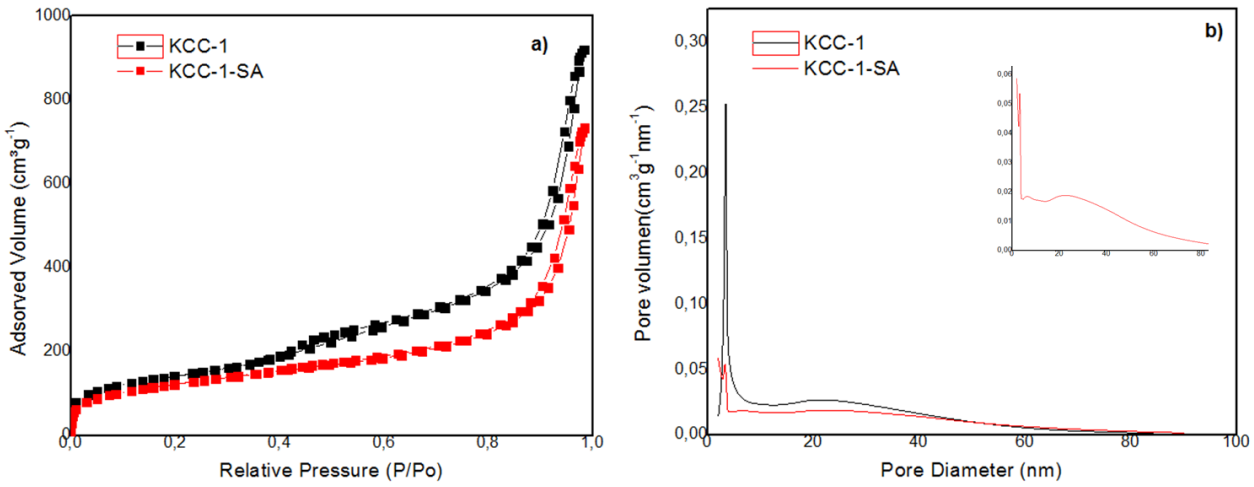

FIGURE A46- Textural characterization of KCC support (black line) and KCC functionalized with sulfonic acid (red line) (a) isotherms of adsorption / desorption of N_2 and (b) pore distribution.

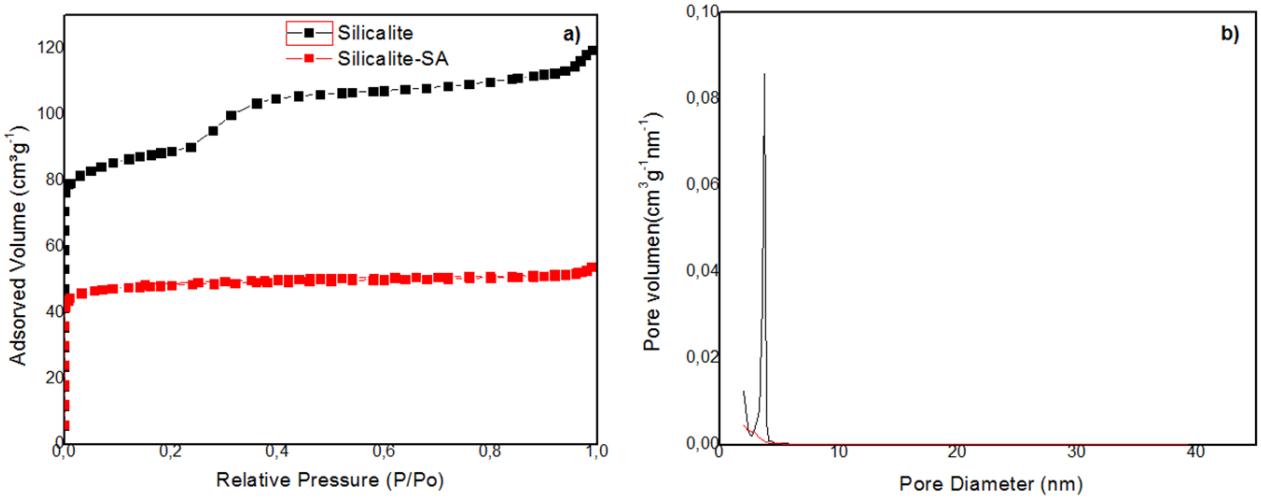

FIGURE A47- Textural characterization of silicate support (black line) and silicate functionalized with sulfonic acid (red line) (a) isotherms of adsorption / desorption of N_2 and (b) pore distribution.

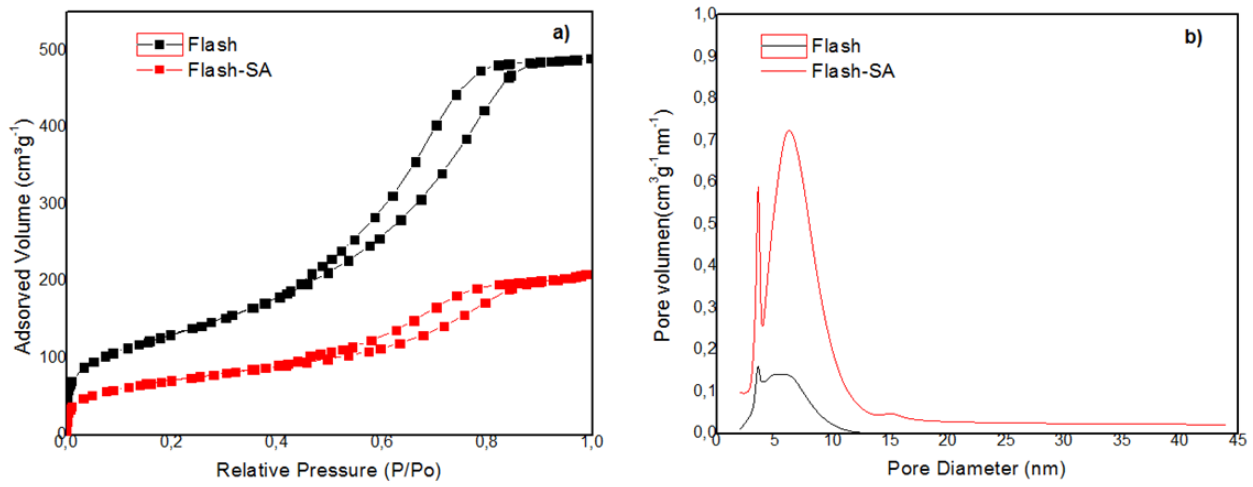

FIGURE A48- Textural characterization of Flash support (black line) and Flash functionalized with sulfonic acid (red line) (a) isotherms of adsorption / desorption of N_2 and (b) pore distribution.

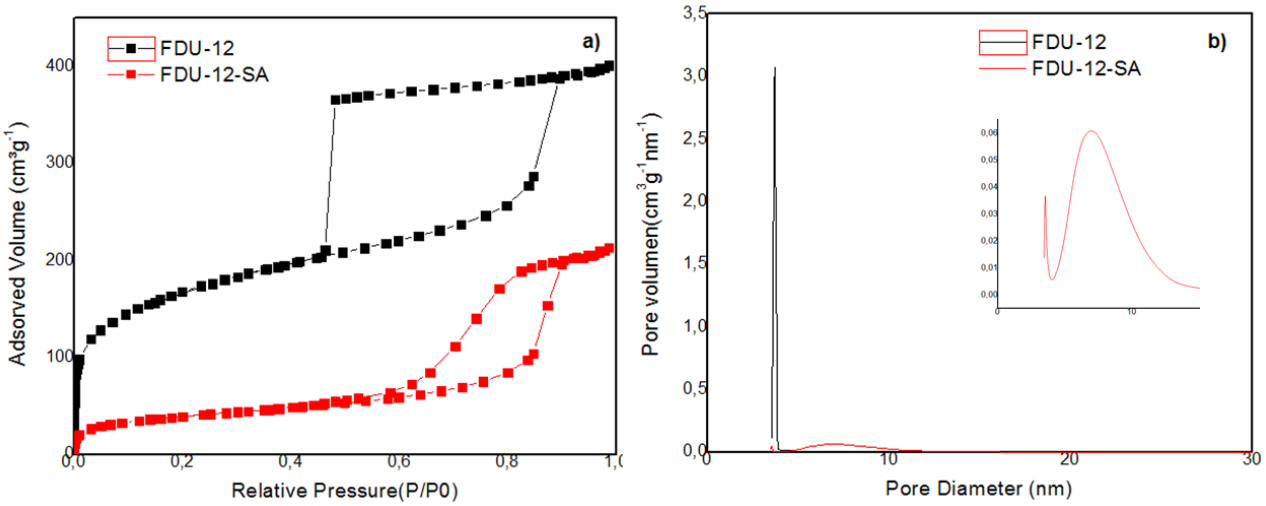

FIGURE A49- Textural characterization of FDU-12 support (black line) and FDU-12 functionalized with sulfonic acid (red line) (a) isotherms of adsorption / desorption of N_2 and (b) pore distribution

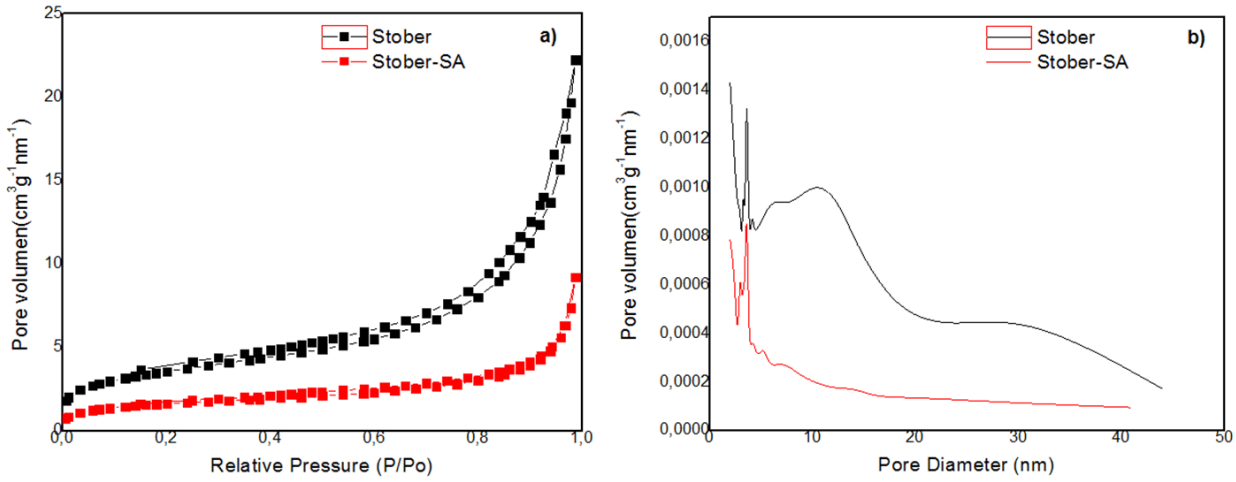

FIGURE A50- Textural characterization of Stöbert support (black line) and Stöbert functionalized with sulfonic acid (red line) (a) isotherms of adsorption / desorption of N_2 and (b) pore distribution.

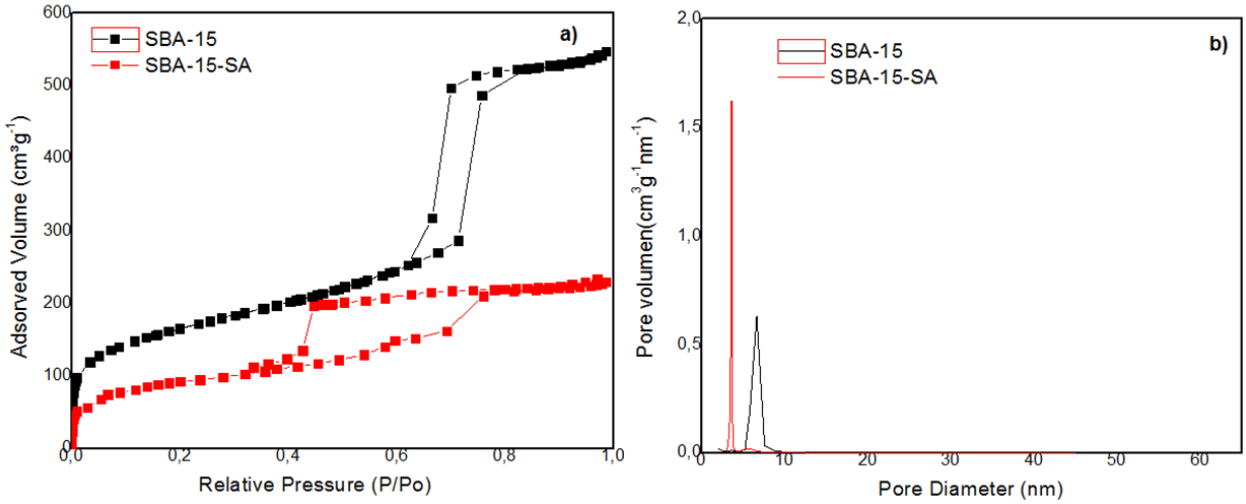

FIGURE A51. Textural characterization of SBA-15 support (black line) and SBA-15 functionalized with sulfonic acid (red line) (a) isotherms of adsorption / desorption of N_2 and (b) pore distribution.

FT-IR of Pyridine

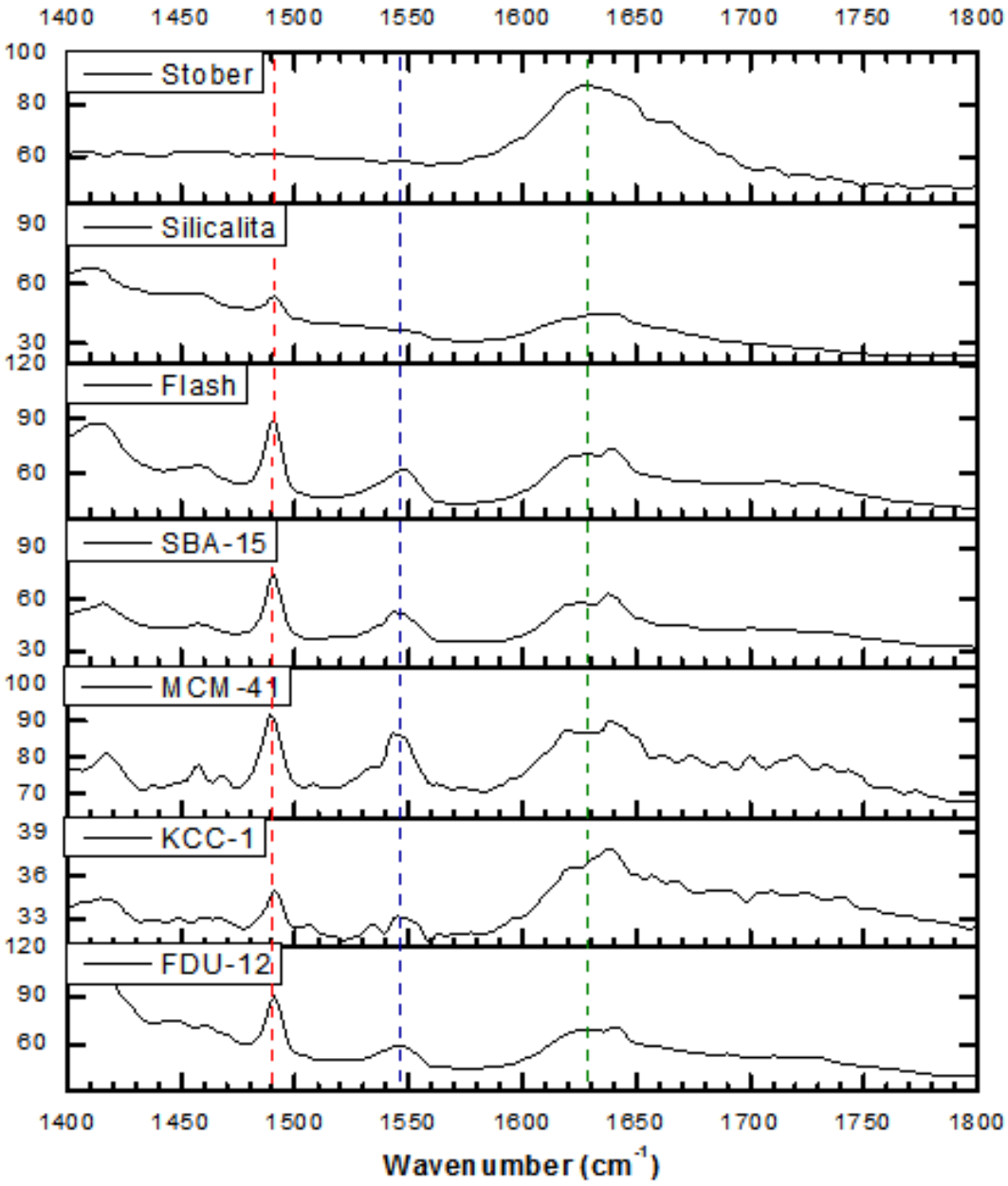

FIGURE A52- Infrared of adsorbed pyridine of the sulfonic-acid functionalized silica.

XPS

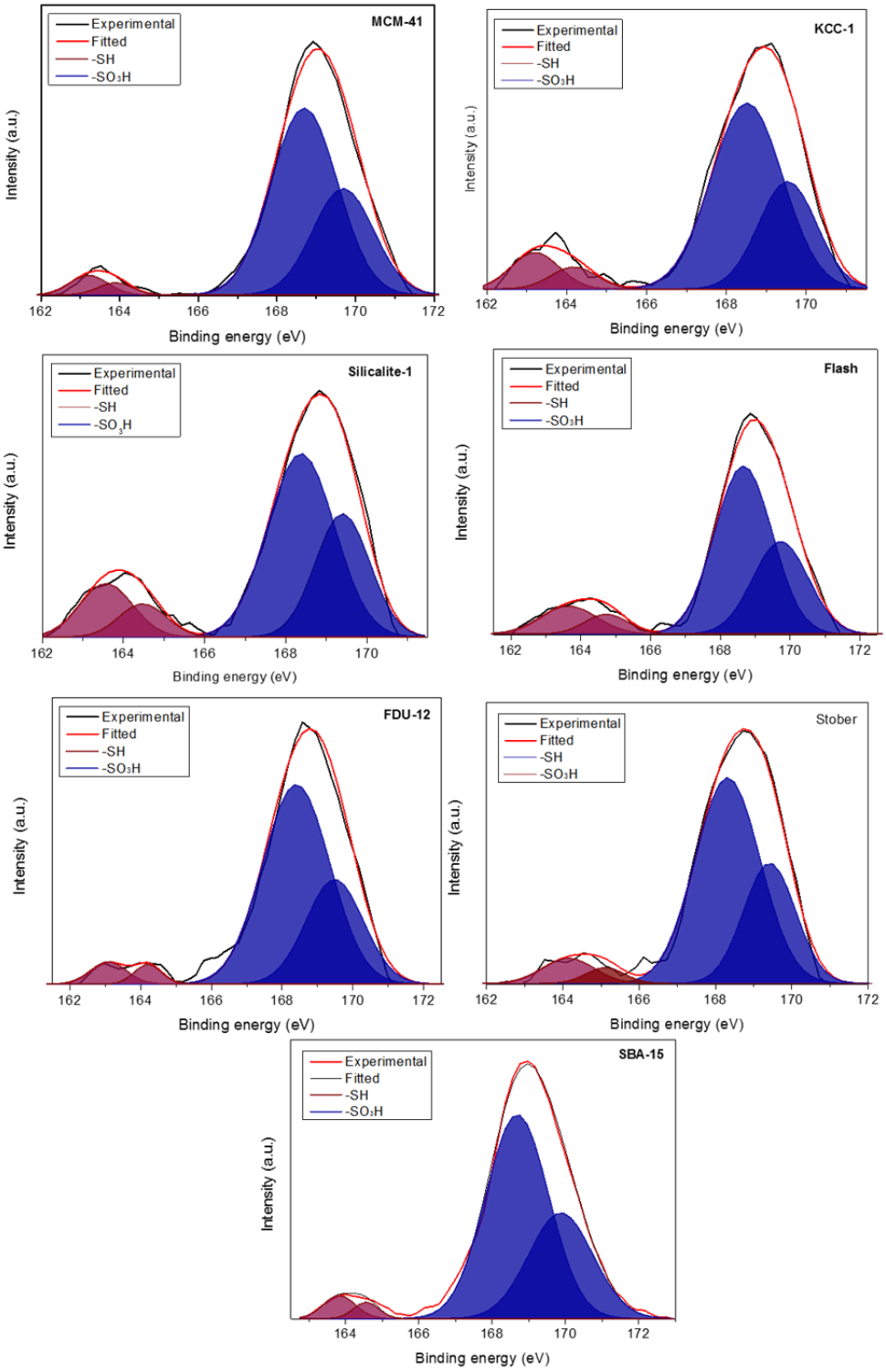

FIGURE A53. XPS spectra for the sulfonic-acid functionalized silica.